

Direct Use of Low Temperature Heat in District Heating Networks with Booster Heat Pumps

Dissertation Submitted in Partial Satisfaction
of the Requirements for the Degree Doctor of Philosophy in Engineering

Al Dipartimento di Ingegneria Industriale (DII)
Corso di Dottorato In Ingegneria Industriale
Curriculum Energetica, XXX Ciclo

UNIVERSITÀ DEGLI STUDI DI PADOVA

Jacopo Vivian

Supervisor: Prof. Michele De Carli

Co-supervisor : Dott. Angelo Zarrella



Acknowledgements

The PhD has been a long journey, a strenuous path full of obstacles but also of unexpected satisfactions. In a few words, the main result of this experience is having reached the ability to independently develop new ideas and at the same time the tools to defend them. What I hope (but I can not be sure of), is to have never abandoned that good companion called Doubt. Looking instead at the journey itself rather than at the destination, it comes clear that the best thing of doing a PhD is by far the opportunity one has to meet great people!

So, first of all I want to thank my supervisors: Michele for always believing in my skills and supporting my proposals, and also for the relaxed atmosphere one can breathe in our group of colleagues and friends. Thanks to Angelo, that was always there to support me with precious advices and with patience during all the PhD and particularly during the exhausting sessions of modelling.. this Thesis would not have been possible without your valuable guidance! Thanks to Beppe, for the help you gave me in almost every activity I've carried out, for the House&Dad "rent" in Sicily and most of all for being such a good "old brother"! Thanks to Samantha, for being there when it was needed and for your patience that helped us go on day by day! .. and thanks to Giulia, Alberto and Laura for your positive attitude and help! Thanks also to Dirk and Ursula, that gave me precious feedbacks and guidance during my stay in Germany. A special thanks goes to Prof. Johann Hurink, for the incredible hospitality and knowledge-transfer I received during the week in Twente! I also want to thank the reviewers of the thesis, and in particular Mr. Donal Finn for the valuable feedbacks that contributed to improve the work! I also want to thank other two great persons that supported me at the beginning of this journey: Prof. Andrea Lazzaretto for pushing me to apply for the PhD position and for the unconditioned help given during the first months, and Wilmer for your hints and for the funny atmosphere you managed to create in that cozy and noisy office!

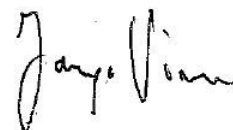
A particular thank goes to the guys of LEDS.. I am always astonished when I see how you managed to make our project grow bigger and bigger, without changing the principles that inspired it!

The PhD would not have been such a good time without the love and support of so many good friends outside the University. Going back to the beginning, I have to thank Nicolò, for bearing me during the endless phone calls before the PhD, and the restless and confused months of the first year. But thanks also for the inspiration you gave me with your ideas and attitude of always aiming high. I am very grateful to my friend and “shoulder” Marcon, with whom I’ve let half of my salary to the bars of Padova and shared so much. Thanks to Giacomo, for sharing the happiest but also the difficult moments both here and during our stay in the cold lands. I also want to thank two persons that have always been and will always be there: Giulia and Tomma. Thanks to all the great flatmates of Casa Montona.. There I will always feel at home (and that’s because of you!). Thanks to all my old good friends now spread all over (Billy, Pit, Cris, Met, Sasso, Javi, Tai and so on).. it’s always great when we see each other! Thanks to my team-mates in Stuttgart, Ilyes and Xavier.. it was such a good pleasure working with you! When people ask me how it was my period in Stuttgart I always say “well.. the city is not really my thing but.. I met so many great people there!”. You really managed to make me feel good in the end: Pilar, Stefan, Ruben, Laura, Marcus, Carlos, Kata.. thanks! But the greatest hug goes to Daniel.. you are really an amazing person! Thanks for what you did to make all of us feel at home there!

Now it’s time to thank a very special person with whom I had the luck to share the last one year and a half.. Anna! Thanks for the infinite patience you had with me, for bearing all my stress and for all the happiness you brought into my life. I am so happy for all the good moments we passed together and for those to come! I love you!

Finally I want to thank my beloved brother and sister Olly and Gaia.. I know it’s not that easy to have me like the big brother.. but somehow we do it! Thank to all my family.. to my granies and specially to Mum and Dad for the unconditioned love and support I receive from you every time! This work is dedicated to you!

Padova, January, 15th, 2018



Abstract

Buildings are responsible for over one third of the energy demand in Europe. Thus, reducing their energy consumption, increasing energy efficiency and integrating low carbon energy sources have become primary goals in the transition towards a sustainable society. District heating and cooling (DHC) systems play a key role to achieve these targets, as they allow any available source of heat to be exploited, including waste heat and renewable heat sources such as geothermal or solar heat. Nowadays, state-of-the-art DH networks have supply temperatures of 70°C in winter and 55°C in summer. Due to their top-down structure, today's networks are not well-suited for decentralized heat supply. The present thesis explores the potential of a new generation of DHC systems, that distribute heat at lower temperature (from 15°C to 45°C) and use booster heat pumps in the customers substations to raise the temperature level according to the needs of the building served. This concept brings several advantages over conventional networks, such as the abatement of thermal losses, the extension of the temperature range of recoverable heat sources and the potential decentralization of heat supply. In a preliminary analysis, the implementation of the system was investigated for a small town in the North-East of Italy with a large amount of available wastewater in a temperature range between 45 and 55°C. In this case-study, the DH system with booster heat pumps reduced the primary energy consumption of about 70% compared to a heat supply scenario based on individual gas boilers and of 30% compared to a traditional DH system with a central heat pump and an auxiliary gas boiler. Such improvement occurs also because the distributed heat pumps can be adapted to the supplied buildings: this is particularly relevant considering the heterogeneity of the building stock in the urban environment. The optimal design and management of this kind of networks is a new topic in the scientific literature. Therefore, the first part of the work tries to answer the following general question:

“What are the most critical aspects in the system design?”

The thesis analyses the effect of some critical design parameters on the cost of heat for the final user, using the payback time for the DH utility as a fixed constraint. It emerges that a higher supply temperature leads to two positive effects: the heat sales increase and the expenditure for electrical energy is reduced. The levelized cost of energy of the system drops by 17% when the network supply temperature goes from 40°C to 20°C, provided that the heat can be recovered at the same price. Moreover, the network temperature difference plays an important role in the design phase. Depending on the business model adopted by the DH utility to purchase the heat and on the specific energy consumption of the considered building stock, an optimal temperature difference may arise from the trade-off between low initial investment and low operational costs. The decentralized structure of these networks also introduces new challenges in the control strategies. Indeed, if the utility purchases and/or produces the electricity needed by the heat pumps, the control strategy should possibly take into account the price and/or the production cost of electricity. Secondly, the control system of the network manager must be able to react on increasing shares of decentralized heat supply from the prosumers. These issues can be summarized by the following research question:

“How can the network manager control its heat supply units in a smart way?”

This part of the thesis was developed within the H2020 Project FLEXYNETS. In order to minimize the operational cost for the network manager, an intelligent control method based on MILP optimization was developed and tested via computer simulations. The proposed control system proved capable of self-adapting to the current situation of heat demand, waste heat availability and electricity price, such as to increase the share of electricity self-consumption and the share of low-grade heat recovered from the remote prosumers. During two simulated winter months, the advanced control strategy was able to reduce operational costs by 11% compared to a conventional rule-based control. The receding horizon scheme makes the system potentially feasible for real-time applications. The novelty of this work consists not only in the aforementioned findings *per se*, but also in the methodological framework that led to those results. In fact, the developed models allowed to integrate the whole energy system (buildings, substations, district heating network and heat supply stations) into a unique simulation environment.

Keywords

district heating networks, booster heat pump, low temperature heat sources, prosumers, waste heat, energy modelling

Riassunto

Gli edifici sono responsabili di oltre un terzo della domanda di energia in Europa. Ridurre il consumo di energia, aumentare l'efficienza energetica ed integrare fonti di energia a basso impatto ambientale sono diventati obiettivi fondamentali nella transizione verso un futuro sostenibile. Le reti di teleriscaldamento e teleraffrescamento hanno un ruolo fondamentale nel raggiungimento di questi obiettivi, in quanto permettono di recuperare ed utilizzare il calore da qualsiasi fonte sia disponibile a livello locale: dal calore di scarto al calore di fonti rinnovabili come il geotermico e il solare. Oggi le reti di teleriscaldamento più efficienti hanno temperature di mandata pari a circa 70°C in inverno e 55°C d'estate. A causa della loro struttura centralizzata, le reti di oggi non sono predisposte per la generazione distribuita del calore. Questa tesi analizza il potenziale di una nuova generazione di reti, che distribuiscono il calore ad una temperatura più bassa (in generale tra 15°C e 45°C) e usano pompe di calore di rilancio nelle sottostazioni d'utenza per fornire calore alla temperatura desiderata da ogni singolo edificio. Questa nuova filosofia progettuale porta diversi benefici rispetto alle reti tradizionali, come l'abbattimento delle perdite di calore, la possibilità di integrare fonti a più bassa temperatura e la decentralizzazione del sistema. In una analisi preliminare, l'implementazione del sistema proposto è stata studiata per una cittadina italiana in cui è presente un'ingente quantità di acqua di risulta tra i 45°C e i 55°C. In questo caso studio, la rete di teleriscaldamento con le pompe di calore distribuite riduce il consumo di energia primaria e le emissioni di anidride carbonica di circa il 70% rispetto allo scenario costituito da caldaie autonome e del 30% rispetto ad una rete tradizionale con pompa di calore centralizzata e caldaia a gas di integrazione. Questo miglioramento si verifica anche perché ogni pompa di calore viene adattata all'edificio, il che assume notevole importanza in virtù dell'eterogeneità del parco edilizio normalmente presente nel contesto urbano. La progettazione e la gestione di questo tipo di reti

è un argomento nuovo nella letteratura scientifica. La prima parte della Tesi cerca perciò di rispondere ad una domanda di carattere generale:

“Quali sono gli aspetti più importanti nella progettazione del sistema?”

La tesi analizza gli effetti di alcuni parametri di progetto sul costo dell'energia all'utente finale, mantenendo fisso il tempo di rientro dell'utility. Ne è emerso che una elevata temperatura di mandata porta a due benefici: (a) aumentano le vendite di calore da parte dell'utility e (b) si riduce il consumo di energia elettrica delle pompe di calore. Come conseguenza, passando da 40°C a 20°C ato dell'energia si abbassa del 17% a parità di costo del calore che alimenta la rete. In più, anche la differenza di temperatura tra mandata e ritorno ha un ruolo importante nella fase di progetto della rete. Il compromesso che nasce per contenere da un lato l'investimento iniziale e dall'altro i costi operativi può portare ad una differenza di temperatura ottimale tra mandata e ritorno. La struttura decentralizzata di queste reti inoltre fa nascere la necessità di studiare nuove strategie di controllo. Infatti, se l'utility compra e/o produce l'energia elettrica di cui le pompe di calore necessitano, la strategia di controllo deve tenere in considerazione anche il prezzo e/o il costo di produzione dell'energia elettrica. Inoltre, il sistema di controllo del gestore della rete deve essere in grado di far fronte a quantità ingenti di calore fornito dai prosumers. Questi problemi possono essere riassunti nel seguente quesito:

“In che modo il gestore di rete può controllare i suoi impianti?”

Questa parte della tesi è stata sviluppata nell'ambito del progetto H2020 FLEXYNETS. Al fine di minimizzare il costo operativo per il gestore di rete è stato sviluppato e successivamente testato attraverso simulazioni un metodo di controllo intelligente basato su ottimizzazione MILP. Col metodo proposto il sistema è stato in grado di adattarsi alla situazione di domanda di calore, disponibilità di energia da parte dei prosumers e prezzo dell'elettricità in modo tale da aumentare la quota di autoconsumo e aumentare la quota di energia recuperata dai prosumers. Durante i due mesi di simulazione, la strategia di controllo è stata in grado di ridurre i costi operativi dell'11% rispetto ad un sistema di controllo convenzionale. Lo schema “receding horizon” rende il metodo potenzialmente fruibile in applicazioni real-time. Il contributo della tesi non è solamente relativo ai risultati in quanto tali, ma anche alla metodologia utilizzata per raggiungerli. Infatti i modelli sviluppati hanno permesso di studiare il sistema energetico nel suo insieme.

Contents

ACKNOWLEDGEMENTS	1
ABSTRACT	3
KEYWORDS	5
RIASSUNTO	6
LIST OF FIGURES	11
LIST OF TABLES	14
CHAPTER 1 INTRODUCTION	15
CHAPTER 2 LITERATURE REVIEW	21
2.1 Heat demand and supply in Europe	21
2.1.1 Current situation	21
2.1.2 Reference scenarios for heating and cooling projections to 2050	22
2.2 The role of district and cooling systems	24
2.2.1 Current situation	24
2.2.2 Expansion potential	26
2.3 Unexploited heat potential for DHC systems in Europe	28
2.3.1 CHP from fossil-fuelled thermal power plants	28
2.3.2 Municipal solid waste	29
2.3.3 Geothermal heat	31
2.3.4 Biomass	34
2.3.5 Industrial processes	37
2.3.6 Solar heat	40
2.3.7 Other low temperature heat sources for district heating	41

2.4	Integration of low temperature heat sources into district heating systems	42
2.4.1	Examples of practical barriers	42
2.4.2	New concepts for district heating and cooling systems	43
2.4.3	Design and operational aspects of DH systems with booster heat pumps	47
2.5	Discussion	48
CHAPTER 3 MODELS		50
3.1	Model of the buildings at district scale	50
3.1.1	Simplified dynamic models	50
3.1.2	Geospatial data	52
3.1.3	Structure of the model	53
3.1.4	Comparison with detailed simulation software	57
3.2	District heating network model	62
3.2.1	Network pre-processing	62
3.2.2	The hydraulic balance	62
3.2.3	The thermal balance	64
3.2.4	Comparison with measured data	66
3.3	Heat pump model	70
3.3.1	Description of the model	70
3.3.2	Comparison with measured data	72
3.4	Discussion	74
CHAPTER 4 CASE STUDIES		75
4.1	Case study 1: Abano Terme (Italy)	75
4.1.1	Background	75
4.1.2	Thermal water withdrawal: historical data	77
4.1.3	Thermal water withdrawal: on-field measurements	78
4.1.4	The building stock	82
4.2	Case study 2: Aarhus South-West (Denmark)	84
4.2.1	Background	84
4.2.2	The DH network and the heat demand	85
4.2.3	Description of the case-study	86
4.2.4	The low temperature heat sources	87
CHAPTER 5 PLANNING AND DESIGN ASPECTS		89
5.1	Preliminary analysis	89
5.1.1	Methods	89
5.1.2	Results	92
5.1.3	Potential for Abano Terme	95
5.2	Techno-economic analysis	97

5.2.1	Methods	97
5.2.2	Results	107
5.3	Conclusions	115
5.4	Discussion on the validity of the results	117
CHAPTER 6 SYSTEM CONTROL		119
6.1	Introduction	119
6.2	Method	120
6.2.1	Basic control	120
6.2.2	Advanced control	121
6.3	Models	123
6.3.1	The optimization problem	123
6.3.2	Detailed simulation model	125
6.4	Results and discussion	127
6.4.1	Optimal planning	127
6.4.2	TRNSYS Simulations	130
6.4.3	Comparison between basic and advanced control	132
6.5	Conclusions	133
CHAPTER 7 CONCLUSIONS		135
7.1	Original contributions	135
7.2	Future work	140
REFERENCES		143

List of figures

Figure 2.1 - Primary energy supply, final consumption and end use of energy in the EU27 in 2010.	22
Figure 2.2 - Final energy consumption by heat source in the EU28 in 2012	22
Figure 2.3 - RES2016 projection of (a) specific heat demand for space heating, (b) residential final energy demand by end-use	23
Figure 2.4 - Fuel input to DH and CHP units in the REF2016 scenario	24
Figure 2.5 - Share of people served by DH in the EU28 in 2013	25
Figure 2.6 - Energy share (a) and generation by heat source (b) in the EU28 from 1990 to 2012.....	25
Figure 2.7 - Share of cogeneration in electricity production in year 2012 for 25 countries	29
Figure 2.8 - MSW management in the EU28 in 2012: (a) treatment options and (b) recovery efficiency for heat and electricity (with respect to the sum of incinerated and landfilled MSW volume).....	30
Figure 2.9 - Incineration capacity in the EU28 area in 2012: (a) installed facilities and (b) installed capacity per-capita	31
Figure 2.10 - Distribution of geothermal resources and potential use in Europe	33
Figure 2.11 - Geothermal district heating systems production in Europe	33
Figure 2.12 - Growth of installed capacity of geothermal district heating systems in Europe between 2011 and 2015	33
Figure 2.13 - Predicted growth of number of geothermal district heating systems in Europe between 2015 and 2019.	34
Figure 2.14 - EU28 gross final energy consumption (ktoe) of bioenergy per market segment in 2014.....	35
Figure 2.15 - EU28 gross final energy consumption (ktoe) of bio-energy: projection to 2020.....	37
Figure 2.16 - Map of industrial waste heat	38
Figure 2.17 - Share of industrial waste heat by industry sector	39
Figure 2.18 - Solar DHC systems in the EU28	40
Figure 2.19 - Conceptual scheme on the evolution of District Heating and Cooling networks.	46
Figure 3.1 - Example of vector data (left) and DEM (right) of the same neighbourhood.	53
Figure 3.2 - Data flow of the model.....	54
Figure 3.3 - 5R1C model of the building according to ISO 13790.	55
Figure 3.4 - Reference node.....	56

Figure 3.5 - RMSE of lumped-capacitance models and peak load for the apartment with envelopes: (a) H1, (b) H2, (c) L1 and (d) L2.	60
Figure 3.6 - The relative error ϵ in the heating and cooling seasons.	61
Figure 3.7 - Schematics of the experimental site.	67
Figure 3.8 - Measured data at pipe outlet versus models with (a) $\Delta t = 300$ s and (b) $\Delta t = 30$ s.	69
Figure 3.9 - Error of the models and computational time with (a) $\Delta t = 300$ s and (b) $\Delta t = 30$ s.	70
Figure 3.10 - The heat pump prototype.	72
Figure 3.11 - Measured data versus model output: (a) COP, (b) Wk, el , (c) Q_{ev}	73
Figure 4.1 - Hydrothermal circuit of groundwater reaching the ETB.	76
Figure 4.2 - (a) Annual volumes of groundwater extracted in Abano Terme between 2006 and 2013; (b) estimated mean monthly profile.	78
Figure 4.3 - (a) Thermal water well; (b) hot water pool for mud maturation with mechanical displacement of the clay; (c) hot water pool for mud maturation; (d) drainage system discharge into open canals.	79
Figure 4.4 - Hourly average mass flow rate extracted from 16/12/2015 to 16/5/2016.	80
Figure 4.5 - Temperature of the water in the (a) covered and (b) uncovered thermal water pool.	80
Figure 4.6 - Temperature in the drainage system of Abano Terme.	81
Figure 4.7 - Neighbourhood in Abano Terme with buildings grouped by age class.	83
Figure 4.8 - Overview of Aarhus including settlement typologies. The case in the south-western part is highlighted with a red circle.	86
Figure 4.9 - (a) Aggregation of user nodes; (b) scheme of the resulting network (after aggregation).	86
Figure 4.10 - Layout of (a) central heat supply station and (b) waste heat substations.	87
Figure 4.11 - Waste heat profiles used in the case study.	88
Figure 5.1 - Supply temperature curves of (a) c-HPDH, (b) distributed heat pumps according to the building supplied.	90
Figure 5.2 - Topology of the district heating network and buildings.	91
Figure 5.3 - (a) Energy consumption of the neighbourhood by age class; (b) Specific heat consumption vs shape factor for old buildings ($< L. 373/76$).	93
Figure 5.4 - Heat load profile of the reference neighbourhood and outdoor air temperature.	93
Figure 5.5 - (a) Primary energy consumption and (b) carbon dioxide emissions of c-HPDH, d-HPDH and individual gas boilers.	94
Figure 5.6 - Four scenarios for the use of thermal wastewater in Abano Terme and comparison to the heat demand of the residential building stock.	97
Figure 5.7 - 3D-view of the reference building.	98
Figure 5.8 - Schematic view of the substation.	100
Figure 5.9 - (a) Limits of operative conditions of the selected compressors; (b) supply temperature curves for the reference buildings.	101
Figure 5.10 - Specific cost of pipelines from [117] updated to current prices.	103
Figure 5.11 - Cash flow in Business-as-Usual (BaU) and Investment-on-Utility (IoU) business models.	103
Figure 5.12 - SCOP for buildings (a) B70, (b) B90 and (c) NB.	109

Figure 5.13 - Components of heat price ph in the IoU case with supply network temperature of (a) 20°C and (b) 45°C; components of fuel costs for (c) 20°C and (d) 45°C.....	112
Figure 5.14 - Levelized cost of energy of the d-HPDH system and of gas boiler for multi-family buildings (a,d) B70, (b,e) B90; (c,f) NB with an incentive of 26 €/MWh.	114
Figure 6.1 - Temperature driven unit commitment of the basic control logic.....	121
Figure 6.2 - Schematic overview of the advanced control logic.	122
Figure 6.3 - Topology of the considered DH network.	126
Figure 6.4 - (a) Forecast and (b) optimization output for a typical winter day.	128
Figure 6.5 - (a) Forecast and (b) optimization output in a typical summer day.	128
Figure 6.6 - (a) Forecast and (b) optimization output in a typical day of spring/autumn.	129
Figure 6.7 - Example of supply network temperature with the advanced control (targets and actual values from simulation).	130
Figure 6.8 - Example of temperatures in the CS tank with the advanced control (targets and actual values from simulation).	131
Figure 6.9 - CHP electrical total power output, power sold to the market and price of electricity with the advanced control during two winter weeks.....	132
Figure 6.10 - Waste heat recovered, heat from the GB and target (set point) network supply temperature during two winter weeks.....	132

List of tables

Table 2.1 - Estimated bioenergy potential (PJ/y) in the EU27.....	36
Table 2.2 - Estimated industrial waste heat potential in the EU from Swedish recovery factors	37
Table 2.3 - Summary of outcome from recent studies on industrial waste heat potential in the EU.....	39
Table 3.1 - Summary of building properties.....	57
Table 3.2 - Peak load for space heating and cooling.....	58
Table 3.3 - Seasonal energy needs for space heating.....	58
Table 3.4 - Parameters of the pre-insulated pipes (valid for both cases).....	66
Table 3.5 - Boundary conditions.....	66
Table 3.6 - Resume of accuracy and computational time.	69
Table 3.7 - Summary of measured data on the heat pump prototype.....	73
Table 4.1 - Instruments used in the monitoring campaign.....	79
Table 4.2 - Summary of measured values during the monitoring campaign.....	82
Table 4.3 - Classification of the buildings per “age class”.	83
Table 5.1 - Summary of the considered buildings and specific consumption.....	92
Table 5.2 - Summary of energy balance and SCOP.....	93
Table 5.3 - Assumptions for the waste-water utilization scenarios.....	96
Table 5.4 - Synthetic description of the reference buildings.....	99
Table 5.5 - Operating costs under BaU and IoU condition.....	104
Table 5.6 - Assumptions used for the calculation of heat price.	104
Table 5.7 - Assumptions used for the calculation of the LCOE.....	106
Table 5.8 - Peak loads and specific energy needs of the considered buildings.....	107
Table 5.9 - Low-temperature heat price $plth$ [€/MWh] in the BaU case.....	110
Table 5.10 - Heat price ph [€/MWh] in the IoU case.....	111
Table 6.1 - Economic parameters used in the case-study (*see Appendix A).	122
Table 6.2 - Variables used in the optimization	125
Table 6.3 - Energy and cost balances of the simulated energy systems.....	133

Chapter 1 Introduction

Traditionally, energy sectors have been de-coupled from both operational and planning viewpoints, whereas tight interactions have always taken place and are increasing. MES (multi-energy systems) whereby electricity, heat, cooling, fuels and transport optimally interact with each other at various levels (for instance, within a district, city or region) represent an important opportunity to increase technical, economic and environmental performance relative to “classical” energy systems where sectors are treated separately [1]. Thus, local energy policies necessarily involve the planning and the design of efficient solutions at the community level [2]. Poly-generation is a promising conceptual framework, for both building and district scale applications, in particular where different types of energy demand are simultaneously present and when, at the district level, a sufficient spatial energy intensity justifies investments in smart grids, district heating and cooling networks [2]. This typically occurs in cities and in general in the urban context, where there is an increasing demand for energy services. Since almost half of the final energy use in Europe is related to heating services, the construction and expansion of district heating networks is one of the main possibilities for the large scale utilisation of renewables (such as geothermal and solar thermal energy) and waste heat sources [3]. Therefore, efficient district heating and cooling networks are one of the key-points of the European energy policy in the transition towards future energy systems [4]. This framework helps understand why recently a growing attention has been dedicated to the analysis of districts rather than to single buildings. The analysis of energy consumption at neighbourhood, district or city level paves the way to the evaluation of efficiency measures, to the integration of decentralized energy sources and to the optimal interconnection among systems that were traditionally considered separately (electricity, heating and cooling, industry and transport). Renewable electricity is growing rapidly in recent years and it is developing based

on a variety of resources such as wind, solar and biomass. As a result, electrifying additional parts of the energy system is viewed as an ideal opportunity to convert from fossil fuels to renewable energy [5]. A great opportunity in this direction is offered by heat pumps, that are able to convert low temperature, renewable heat sources (such as the air or the ground) and electrical power into thermal energy for heating buildings and for domestic hot water production (DHW).

In most European countries a large part of the existing building stock has poor thermal insulation due to a lack of regulation on energy performance of buildings in force at time of construction. The European Directive 31/2010 [6] addresses this problem by setting guidelines for energy savings in the residential sector. These guidelines have already been implemented by the national legislation of most member countries. This implementation will lead to a significant reduction in the energy demand of the residential building sector in the next decades. The predicted reduction jeopardizes the competitiveness of district heating and cooling networks, which profitability relies on the density of heating and cooling demand [7]. In Nordic countries, where these systems are widely used, researchers developed the concept of low temperature district heating (LTDH), or 4th generation district heating (4GDH) [8]. The basic idea behind this concept is to reduce both supply temperature and pipe diameters to abate distribution heat losses and to enable the heat supply from unconventional sources such as solar heat and industrial waste heat [9]. A number of demonstration projects carried out in different locations (mainly in Denmark in the period 2008-2013) has demonstrated the effectiveness and the competitiveness of low temperature district heating systems for both new low energy buildings and existing buildings in low heat density areas [9]. The fourth generation of DH systems, which is nowadays the state-of-the-art, uses supply temperatures of 70°C in winter and 55°C in summer. However, due to their top-down structure and to the relatively high temperatures, these systems are not well suited to allow a decentralized heat supply and the integration of low temperature heat sources at temperatures lower than 50°C.

The present thesis explores the potential of a new generation of DHC systems, that distribute heat at lower temperature (supply temperatures between 15°C and 45°C have been considered here) and use booster heat pumps in the customers substations to raise the temperature level according to the needs of the building served. This concept brings several advantages over conventional networks, such as the abatement of thermal losses, an increased number of recoverable heat sources and the potential decentralization of heat supply. Moreover, the system

is capable of adapting to the heterogeneity of the building stock that normally occurs in the urban context, as each heat pump can be tailored on the corresponding building. Therefore, the proposed system seems to be suitable for immediate use to efficiently supply heat to those district where old poorly-insulated and new low-energy buildings coexist. Moreover, the system is perfectly aligned with the strategy of the EU Commission for the decarbonisation of the heating and cooling sector, that aims at “improving linkages between electricity systems and district heating systems which will greatly increase the use of renewable energy” [10]. Contrary to conventional district heating systems where the main sources are fossil fuels and the marginal cost for heat production is rather high, the proposed DH concept relies on low-quality, low-cost heat sources. As a consequence, the main operational cost is related to the electrical energy consumed by the heat pump compressors. Who pays for this energy and who owns the heat pumps –either the customer or the utility- is an interesting question that can be answered case by case based on economic convenience. It is clear that the system lends itself to the development of new business models. This aspect is not the main focus of the present work but it is partially considered in the analysis described in the following.

As there is not a monitored pilot plant, most of the work relied on computer simulations. Models were developed ad-hoc for the present study and are available for future use. The simulations focused both on system design and operation. The first part of the work analyses the system from an energy, environmental and economical perspective, trying to answer the following general question:

“What are the most critical aspects in the system design?”

This question has been addressed using the Italian town of Abano Terme as a case study. Here, a large amount of wastewater is available in a temperature range that goes from 45 to 55°C depending on the season. Part of the work was dedicated to on-field measurements of mass flow rates and temperatures of the wastewater, thus providing a database for a future implementation of a pilot plant. A preliminary study was conducted to find out whether the proposed system brings an advantage in terms of primary energy savings and reduction of carbon dioxide emissions over two alternative heat supply solutions: a benchmark case with individual gas boilers and a conventional district heating network supplied by a centralized heat pump with auxiliary gas boiler.

As a follow up, a detailed dynamic simulation of the booster heat pumps in the substations of the district heating network have been performed using the commercial software TRNSYS [11]. The simulations included the heat supply for both space heating and domestic hot water (DHW) production, considering three representative building typologies. The yearly performance was summarized by the seasonal coefficient of performance (SCOP) of the heat pumps. Several simulations were run to assess the impact of the network design temperature difference on the SCOP of the heat pumps at different network temperature levels. In order to extend the conclusions of the work to different heat sources, the parametric study includes network supply temperatures from 15°C to 45°C. The design heat loads of the buildings were then used to size a district heating network using the same temperature difference previously set in the simulations. The investment costs for the network were evaluated accordingly. Then, the heat price for the DH customers was calculated according to two different business models adopted by the DH utility to sale the heat. Finally, the levelized cost of energy for the end user was evaluated for each case and compared to that of the individual gas boilers.

Since the network manager does not control directly the remote feed-in from the low temperature heat sources, also the operation of the system poses several issues. Therefore, this work tries to address a further research question:

“How can the network manager control its heat supply units in a smart way?”

In this second phase of the work, the attention was paid on the control of the system. This part of the thesis was carried out within the H2020 Project FLEXYNETS [12], where a different case study was adopted. Here, a district of the Danish city of Aarhus was considered as a reference district and the aim was to develop and test two strategies for the control of network manager plants, namely a gas boiler and an internal combustion engine (ICE) that produces heat and power (CHP plant) coupled with a thermal storage tank. The network supply temperature was modulated in a range between 20 and 30°C. Two remote waste heat substations, i.e. the cooling circuit of an industrial process and the condensing units of the refrigerators of a shopping mall, inject heat into the network. The available temperature of the mentioned waste heat sources was around 80°C and 50°C, respectively. The advanced control method used forecast of heat load, electricity price and waste heat availability to schedule the operation of the CHP, of the gas boiler and to set the network supply temperature with the goal of minimizing the cost of the overall heat generation mix. This performance indicator was used as

objective function in an optimization based on a Mixed-Integer Linear Programming (MILP) approach solved in a receding horizon scheme. A dynamic simulation of the system including the heat supply stations, the district heating network and the heat pumps allowed to quantify the improvement of the proposed control strategy compared to a conventional rule-based control based on local feedbacks from the system.

The Thesis is structured as follows. Chapter 2 provides a framework on the evolution and the last trends of district heating networks, as well as on the potential of low temperature heat in Europe. Chapter 3 describes the models used in Thesis and Chapter 4 describes the case studies. Chapter 5 presents the results concerning system design and Chapter 6 those about the control. Finally, some conclusions and prospects for future work are outlined in Chapter 7.

Chapter 2 Literature review

The present Chapter aims at giving an updated overview on the current status of district heating and cooling (DHC) systems and on the potential of low temperature heat in Europe. Before that, an introduction describes the current and predicted levels of demand for heating and cooling and the possible heat supply scenarios. The final section provides a framework to understand the latest developments in the integration of low temperature heat sources into district heating systems.

2.1 Heat demand and supply in Europe

The first Section describes the current situation, whereas the second one focuses on the trends predicted for the next decades.

2.1.1 Current situation

Fig. 2.1 shows the energy balance in the EU27 area in 2010. The heat demand of residential and commercial buildings amounted to 11.8 EJ, i.e. approximately 24% of the final energy consumption. This percentage reaches 40% when considering the industrial sector. In 2012, the European buildings consumed 546 MToe (22.9 EJ) for space heating and cooling. According to [10], 45% of this energy consumption supplied the residential sector, 37% the industry and 18% the services. Fig. 2 shows the energy mix supply to meet the energy demand for heating and cooling [10]. Natural gas has the largest share in the overall area, mainly due to the widespread use of autonomous gas boilers. Biomass also shows a large diffusion, especially in Nordic countries due to the high availability of this resource. A significant penetration of coal is still present in Eastern Europe and in the UK.

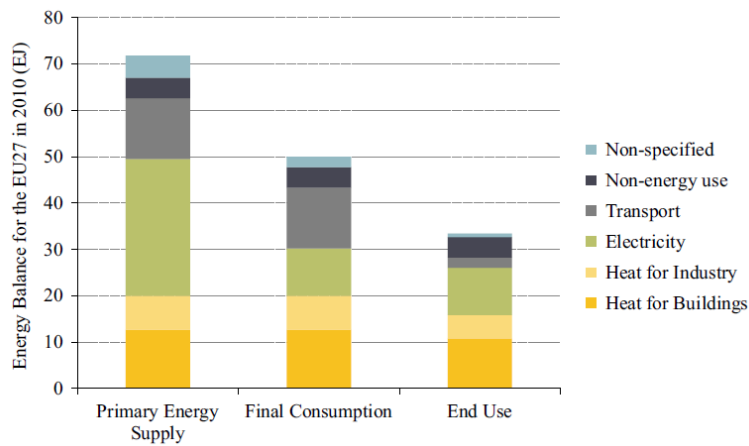


Figure 2.1 - Primary energy supply, final consumption and end use of energy in the EU27 in 2010 [13].

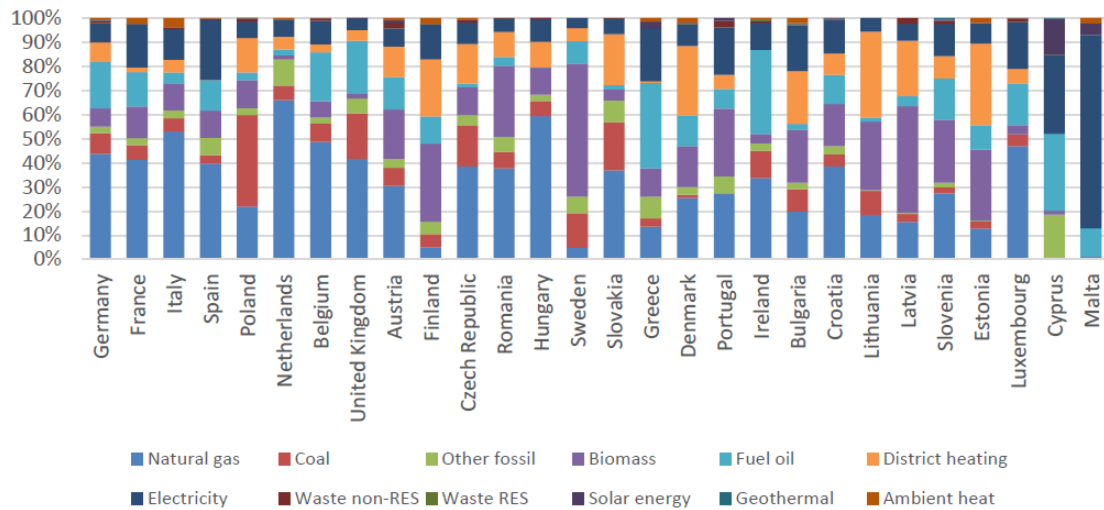


Figure 2.2 - Final energy consumption by heat source in the EU28 in 2012 [10].

Fuel oil and other fossil fuels are still present with minor but significant share in most countries. Solar energy is obviously present in Southern Europe to meet the need of DHW production. Geothermal heat still amounts to an insignificant share of the overall heat supply at EU level.

2.1.2 Reference scenarios for heating and cooling projections to 2050

The European Commission predictions for future energy, transport and emissions trends rely on the PRIMES model, which simulates a market equilibrium solution for energy supply and demand. The latter is complemented with three other models: PROMETHEUS for defining fossil fuel import prices, GAINS for the estimation of non-CO2 emissions and GEM-E3 for the macro-economic input values required by PRIMES. According to this modelling ap-

proach, the final energy demand cannot be determined independently but results from market equilibrium, i.e. from policies, investments and energy prices that at the same time determine the energy supply [14]. According to REF2016 scenario [15], steam and heat demand in EU28 rises slightly in 2020 and 2025 and then remains approximately stable throughout the projection period. The trend for the residential -see Fig. 2.3b- and commercial sector comes from the combination of two counteractive trends: the diminishing specific heat demand per building area -see Fig. 2.3a- due to efficiency-oriented policies that will boost investments in the residential and tertiary sector in the short-term and an increasing building area due to an average increase of the living area per person and to the increased amount of services. As it may be observed in Fig. 2.3b, this implies a reduced final energy demand for heating while electrification and increased thermal comfort requirements will drive the increase of energy demand for appliances and cooling systems.

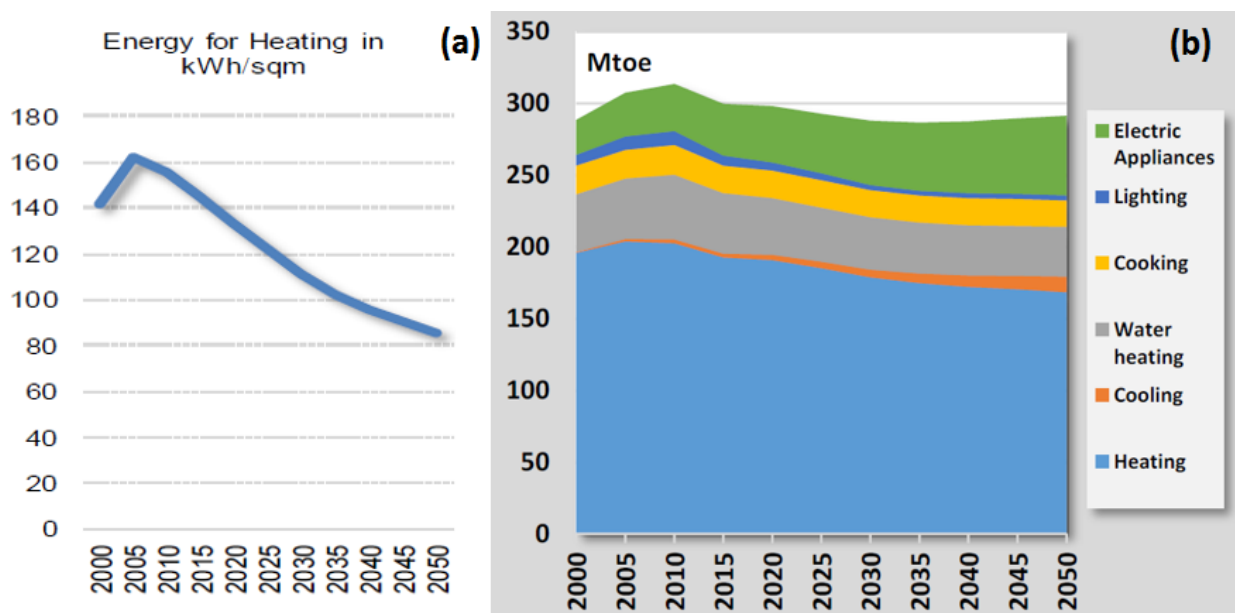


Figure 2.3 -RES2016 projection of (a) specific heat demand for space heating, (b) residential final energy demand by end-use [15].

District heating is projected to maintain its share in demand for heat. In the short and medium term there is a gradual shift from solids (coal and others) and gas district heating boilers to biomass/waste boilers. In the long term electricity boilers, heat pumps, geothermal and thermal solar penetrate the district heating market and gain in market share. In terms of district heating fuel input, the share of coal and oil decreases considerably, as well as the share of gas. Biomass and waste as well as other RES and electricity in fuel input to district heating boilers

increase, representing almost 42% of fuel input to district heating excluding heat from CHP in 2020 and 88% in 2050 (in comparison to 31% in 2010) [15].

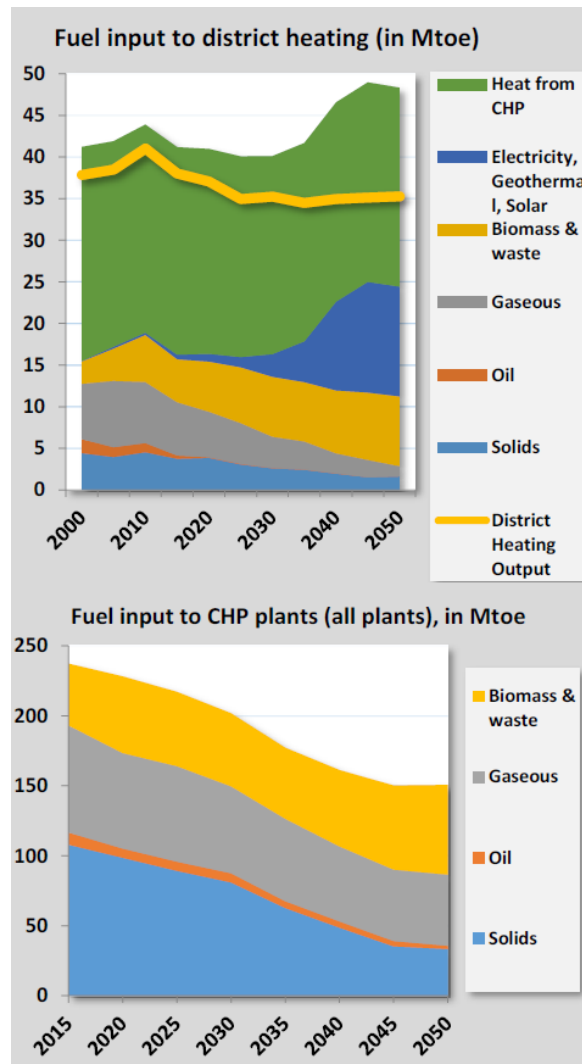


Figure 2.4 - Fuel input to DH and CHP units in the REF2016 scenario [15].

2.2 The role of district and cooling systems

2.2.1 Current situation

In the EU28SIN, district heating provides 9% of heating in the residential sector, 10% in the service sector and 8% of industry's heat needs [10]. There are more than 10,000 district heating (DH) systems in EU-28SIN, which supply around about 8 % of the Europe's total demand for space heating [10]. Today, approximately 70 million EU citizens are served by DH systems. Nonetheless, the distribution of people served by DH varies widely within the Member countries, as shown in Fig. 2.5. Indeed, they are diffused especially in Nordic countries, due

to the long winter seasons and to local and national policies oriented towards a long-term planning of the energy supply.

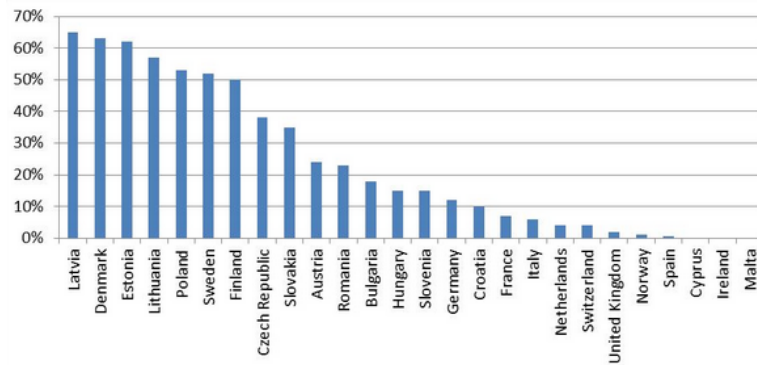


Figure 2.5 - Share of people served by DH in the EU28 in 2013 [10].

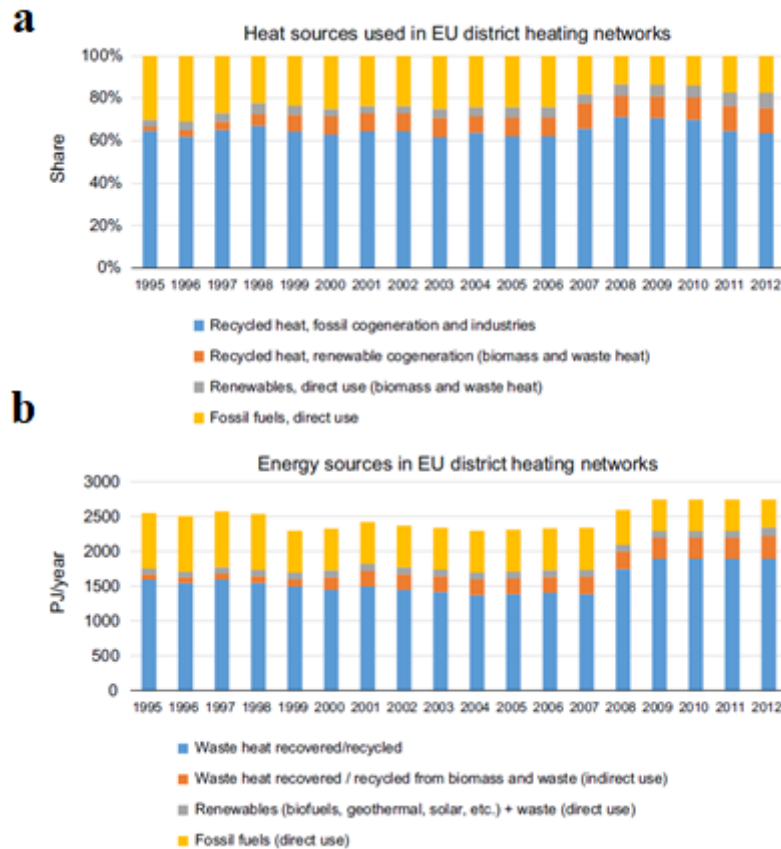


Figure 2.6 - Energy share (a) and generation by heat source (b) in the EU28 from 1990 to 2012 [16].

District heating systems are particularly interesting as they can be supplied by low-carbon energy sources such as waste heat (from thermal power plants, waste-to-energy plants and industrial processes) and renewable energy (geothermal and solar thermal energy). Nonetheless, according to [16] in 2012 the main fuel was gas (40%), followed by coal (29%) and bi-

omass (16%). Indeed, Figure 2.6 shows that fossil fuels hold approximately 80% of the heat supply, either through direct generation or through cogeneration plants. Biomass and MSW are responsible for the remaining share of the energy supply.

2.2.2 Expansion potential

The ECOHEATCOOL Project [17] showed that district heating has a great expansion potential within Europe (2003 was selected as reference year). Compared to 2.0 EJ/year district heat sales of 2003, the additional possible expansion was quantified to be as high as 6.8 EJ/year. Among the potential unexploited heat sources, geothermal heat was indicated as the most promising, followed by combined heat and power (CHP) plants and biomass. Further possibilities arise from higher utilization of industrial waste heat and urban waste incineration. According to this study, doubling the district heat sales would bring to a reduction of 2.14 EJ/year of primary energy consumption corresponding to a reduction of 5.5% of the overall primary energy consumption and of 9.3% of carbon dioxide emissions in Europe. The study complained about the scarce awareness and interest of the International Organizations regarding the environmental benefits of a district-heating-oriented energy policy. In 2011 the European Commission released the *Energy Roadmap 2050* [14], a document that drew seven alternative scenarios for the development of the European energy system. Aside two *current-trend scenarios*, five *decarbonisation scenarios* were outlined based on different assumptions and constraints concerning the policies supporting investments and driving the heat demand. Despite the mentioned effects that district heating and cooling systems could bring with regard to primary energy savings and GHG emission reductions, the latter were not considered to play a key-role in any of the considered decarbonisation scenarios. According to the Energy Technology Perspectives 2012 (*IEA, 2012*), heating and cooling remain neglected areas of energy policy and technology, but their decarbonisation is a fundamental element of a low-carbon economy. According to Connolly et al. [13], the reason for neglecting DHC systems was due to the inadequate tool used for the analysis of the continent-wide energy system. The scenarios of the Energy Roadmap document were built with the PRIMES model, which is a market-equilibrium model based on macro-economic assumptions. The authors claimed that due to the local nature of the energy sources that typically supply the DHC systems, the PRIMES model overlooked their expansion potentials (see section 2.2 for further details on PRIMES). Conversely, the EnergyPLAN tool uses a bottom-up approach, thus making it possible to gauge this untapped potential. They thus tuned the model on the *energy efficiency*

scenario (EU-EE), i.e. one of the five decarbonisation scenarios of the Energy Roadmap 2050 and then provided alternative scenarios, named Heat Roadmap Europe (*HRE-EE*) based on the assumptions of a significant expansion of DHC systems in the heating and cooling market, i.e. up to 30% of the heating market in 2030 and 50% in 2050 [13]. In the STRATEGO project this methodology was used to build individual scenarios at national level to support policies in the heating and cooling sector of five strategic countries (Czech Republic, Croatia, Italy, Romania, UK) differing by population, climate, income etc [18]. The results from this study indicate that a total investment of approximately €1.1 trillion in energy efficiency measures across all five of these countries, between 2010 and 2050, will save enough fuel to reduce the costs of their energy systems. After considering both the initial investment and the resulting savings, the total annual cost of the heating, cooling, and electricity sectors is reduced by an average of approximately 15% in each country. This study confirms one of the key findings of all the decarbonisation scenarios analyzed in the *Energy Roadmap 2050*, i.e. the transition from a system with high fuel and operational costs to an energy system based on higher capital expenditure and lower fuel costs. For the aforementioned *REF2016* [15], the PRIMES sub-models were also upgraded by splitting the output of CHP units and industrial boilers and the power sector, previously considered together. This allowed to consider the effects of investments in cogeneration plants and in DHC networks. Other renewed assumptions include a progressive reduction of heating degree days and an increase of the cooling degree days, reflecting the increasing trend of mean air temperatures registered from the 1980s. The study showed that the use of RES in final demand for heating and cooling is the main driver of RES-H&C increase in the short term going from 17% in 2015 to 25% in 2030, but its contribution stagnates in the long term. In the long-term, CHP and DH networks as well as heat pumps play a major role in the decarbonisation of the H&C sector. Energy efficiency, implying lower demand for heat in all sectors, is also an important driver in the medium and long term (for further details see Section 2.2). In the recently released document on the EU strategy in the heating and cooling sector [10], the EC analyzed several options “to help buildings and industry shift to efficient, decarbonised energy systems based on renewable energy sources and the use of waste heat”. Among them, DHC systems are regarded as the first point of the strategy. Further options include electrification of heating through heat pumps, demand response, thermal storage in the electricity system and other issues related to energy policy. In the Energy Technology and Perspective 2016 [19], it is reaffirmed that the possibility of connecting to district energy networks can provide urban households with a

more cost-effective and less carbon-intensive heating and cooling supply than would be available through individual heating systems.

2.3 Unexploited heat potential for DHC systems in Europe

In the following, the potential of the five main low-carbon heat sources is investigated: CHP, urban waste, geothermal, biomass and residual heat from industrial processes. Two additional Paragraphs are dedicated to solar heat and to other low temperature heat sources that can contribute to a sustainable energy supply.

2.3.1 CHP from fossil-fuelled thermal power plants

Fig. 2.7 shows the share of cogeneration (CHP) in the electricity production of 25 countries in 2012. It may be noticed that for most European countries the share is rather low, thus offering a big expansion potential. Among others, high investment costs for the infrastructure (pipeline, accumulators, boilers, substations etc) are a major barrier for the development of DHC systems. A Joint Research Program supported by the European Commission [20] addressed this problem for the conversion of thermal power plants to the CHP-DH mode in three representative cities of Southern, Central and Northern Europe –i.e., Barcelona, Cologne and Liverpool. It came out that in most cases the investment would be paid back in 4-10 years with a reduction of carbon dioxide emissions by 12-19% in the considered cities. Moreover, retrofitting a power plant for CHP was shown cheaper than constructing a new CHP plant for all cities. It would be cost efficient to replace the existing power plant with a new power plant in all cities both at 3.5 and 5.5% discount rates, while at 7.5% discount rate the conversion was not worthwhile. According to the authors, if all EU combustion power stations were converted to CHP-DH an additional 5320 PJ/year of low carbon heat are likely to be made available at an investment cost of 319 billion euros (60 M€/PJ). Nonetheless, the validity of these values is rather questionable, since the study does not consider problems such as distance between power stations and heat load and the availability of combustion power station heat (it only considers the total installed capacity).

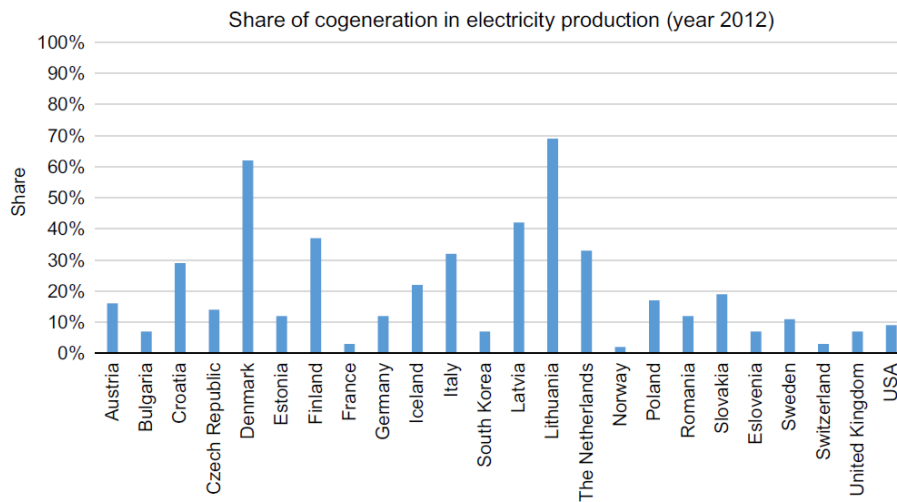


Figure 2.7 - Share of cogeneration in electricity production in year 2012 for 25 countries [20].

A similar result was obtained in a recent study by Colmenar-Santos et al [16], although the authors claimed that only half of the installed electric capacity from conventional thermal power plants is located at an appropriate distance to convert these plants into cogeneration plants for district heating. With an annualized investment in infrastructures of 315 billion euros, the fuel costs would be reduced by 95 billion euros per year and would save about 6400 PJ of primary energy. Persson [21] showed that if all Member States would have the same efficiency of Denmark (best Member State practice) in the excess heat recovery from thermal power plants, the EU27 would gain 8680 PJ/year, i.e. 5.4 times the amount of heat recovered in 2008. This is only a reference value, since it does not account for geographical and financial constraints. Connolly et al. [13] used the EnergyPLAN tool, a GIS-supported energy model, to estimate the expansion potential of different energy sources by 2030 and by 2050 within the Heat Roadmap Europe (HRE) framework. The model considers a current potential of 7070 PJ from fossil-fuelled thermal plants, that is almost 20% less than the reference target of the Best Member State Practice suggested by Persson. Although this considerable amount of heat is apparently available nowadays, it must be considered that large thermal plants could meet a significant loss of competitiveness in the near future due to the high penetration of renewable power sources. The HRE scenarios estimate an expansion potential of 2410 PJ/year by 2030 and of 1540 PJ/year by 2050.

2.3.2 Municipal solid waste

Due to the huge amount of waste production of modern societies due to high consumption of goods and services, waste management represents one of the biggest challenges in the EU.

According to the principles outlined in the Waste Framework Directive [22], the treatment options must be given the following priority order: re-use, recycling, composting, incineration (with and without energy recovery) and, as last choice, landfilling (deposit). Nonetheless, landfilling still constitutes the largest treatment option in waste management in the EU, although the latter showed a linear reduction from 1995 to 2012 and in particular from 40% to 34% from 2008 to 2013 [23]. Fig. 2.8 shows the share of the treatment options by country and the weighted average in the EU28 area. This picture reveals that the most virtuous countries (Sweden, Denmark, Germany, Netherlands, Austria and Belgium) share similar distributions of the mentioned management options: approximately 30-50% recycling, 10-20% composting and 30-50% incineration. Thus, incineration offers a large unexploited energy potential for all those countries that still make large use of landfilling, thus disregarding the indications of the mentioned European Directive.

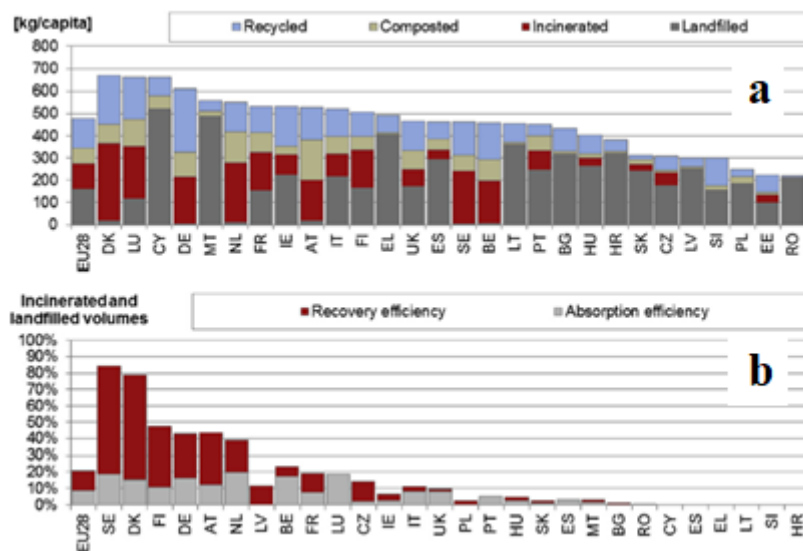


Figure 2.8 -MSW management in the EU28 in 2012: (a) treatment options and (b) recovery efficiency for heat and electricity (with respect to the sum of incinerated and landfilled MSW volume) [23].

Fig. 2.9 shows the geographical distribution of the waste-to-heat incineration facilities and of the installed incineration capacity per capita.

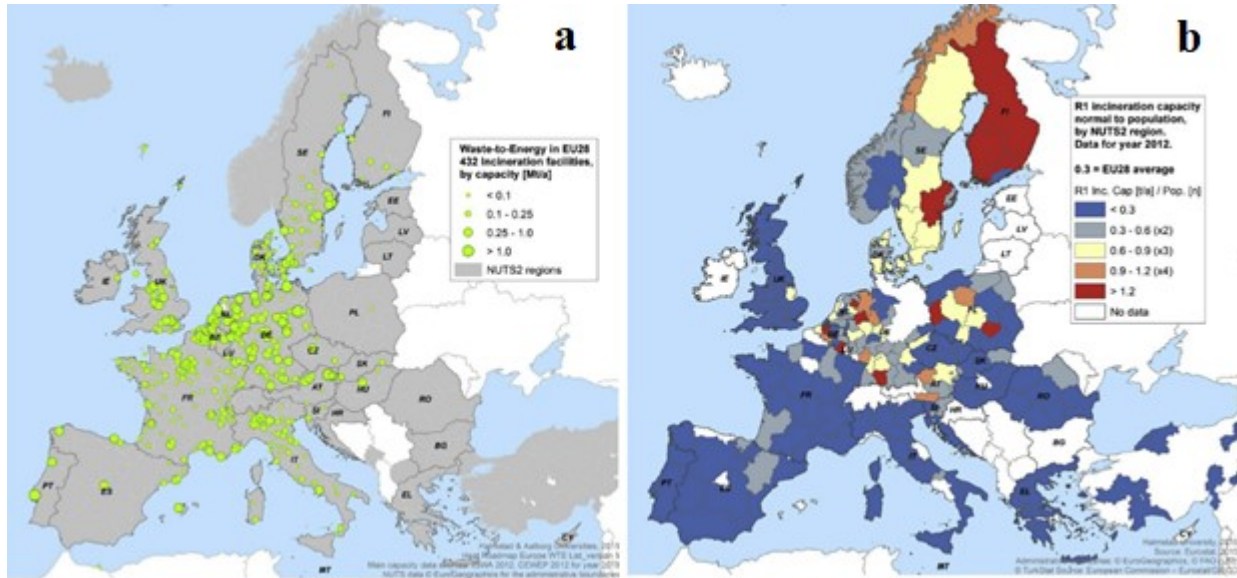


Figure 2.9 - Incineration capacity in the EU28 area in 2012: (a) installed facilities and (b) installed capacity per-capita [23].

Persson [21] showed that if all Member States recovered the same relative amount of heat per incinerated and landfilled volume of MSW of Sweden, that is the Member State with the best performance in terms of recovery efficiency (see Fig. 6b), the EU27 would gain 1100 PJ/year heat, i.e. 6.5 times the amount of heat recovered in 2008 (170 PJ). Since there has been no evidence so far of an imminent decoupling between human well-being and waste production in the EU, most energy scenarios for future European energy systems assumed a linear increase of the MSW production until 2030. Under this assumption, the Heat Roadmap Europe (HRE) scenarios estimate that waste-to-energy heat recovery could achieve the targets of 330 PJ/year by 2030 and 580 PJ/year by 2050.

2.3.3 Geothermal heat

Geothermal heat is a key-player towards a sustainable energy supply of Europe, since it is capable of producing both electricity (mainly with ORC and steam power plants depending on the available temperature) and thermal energy for buildings. Geothermal heat can be extracted either by deep wells or by shallow (near-surface) pipes buried into the ground. The systems may be direct (extract thermal groundwater and re-injecting it into the ground at sufficient distance) or indirect (a secondary fluid is heated up by the thermal gradient present in the ground). In this latter case, the supply temperature depends on the boreholes depth and by the eventual presence of thermal activity in the considered area. The qualitative map of geothermal activity shown in Figure 2.10 helps to have an immediate overview on the geothermal

potential in the different regions of Europe. A better resolution and detail can be found in the interactive map developed within the European project *GeoDH* [24]. High enthalpy thermal basins that are already commercially suitable for electricity production are limited to some restricted regions, such as Iceland, Central Italy and Turkey. When going to lower temperature the economical affordability of conversion systems for power production must be checked based on performance of the available technology. However, high and medium temperature thermal basins have a much larger diffusion, touching almost all Member countries. According to EGEC [25], around 25% of European citizens live in areas where geothermal district heating is technically feasible. This offers a huge untapped potential for the production of renewable thermal energy, since so far only 4.3 TWh (16 PJ) of geothermal heat is delivered through district heating systems [25], corresponding to less than 0.15% of the EU28 heat demand. In 2015 there were 257 geothermal district heating systems in Europe corresponding to a total installed capacity of 4.7 GW [26]. Among those, 177 DH systems are within the EU28 countries, totaling an overall installed capacity of only 1.55 GW. Figure 2.10 shows how the geothermal district heat is produced among the European countries (including Turkey and other non-Member States). Due to the resource availability and to the technological maturity of geothermal DH systems, the latter have seen an increase during recent years (Fig. 2.12) and even a more significant increase is predicted for the years to come (Fig. 2.13), with France and Germany as leading countries followed by Italy and Hungary. According to the HRE scenarios, the geothermal district heating holds a potential of 430 PJ/y, with targets for 2030 and 2050 of 190 and 370 PJ/y, respectively.

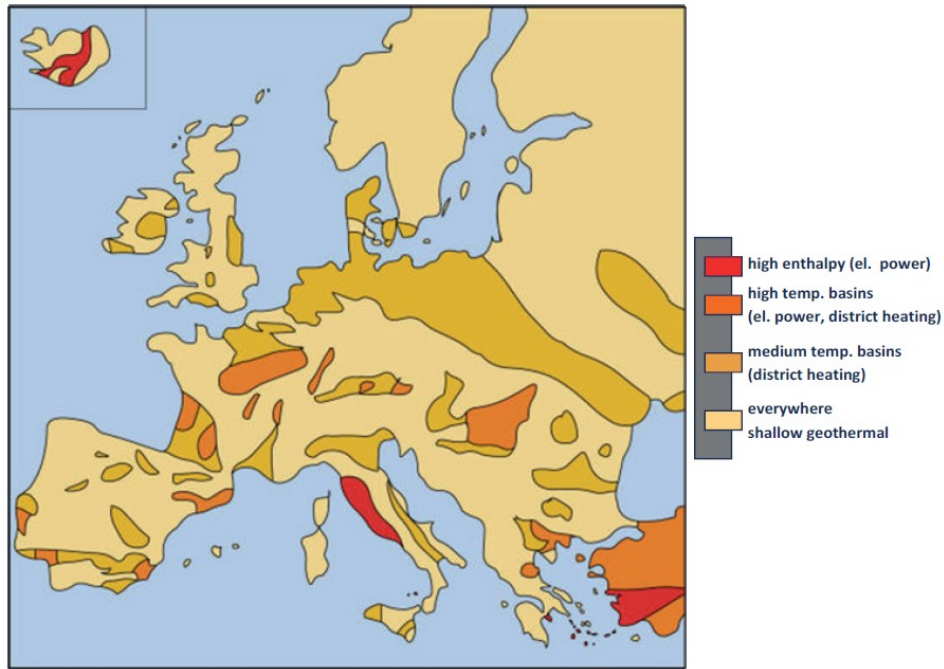


Figure 2.10 - Distribution of geothermal resources and potential use in Europe [25].

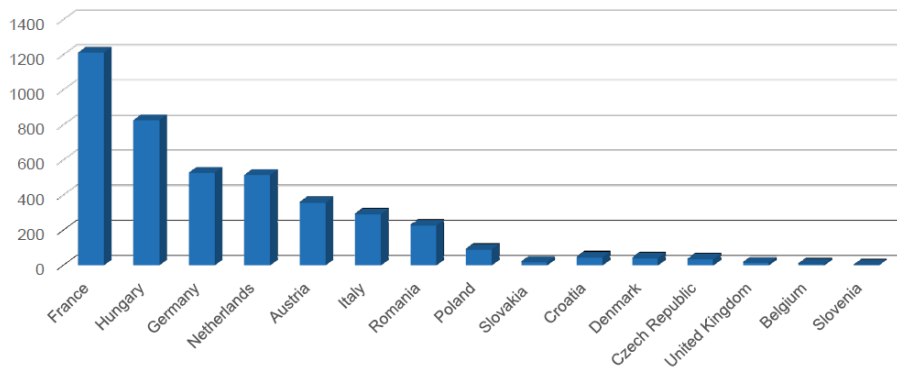


Figure 2.11 - Geothermal district heating systems production in Europe [26].

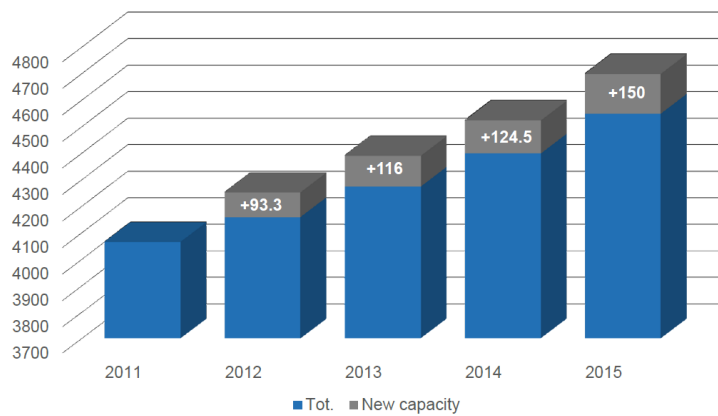


Figure 2.12 - Growth of installed capacity of geothermal district heating systems in Europe between 2011 and 2015 [26].

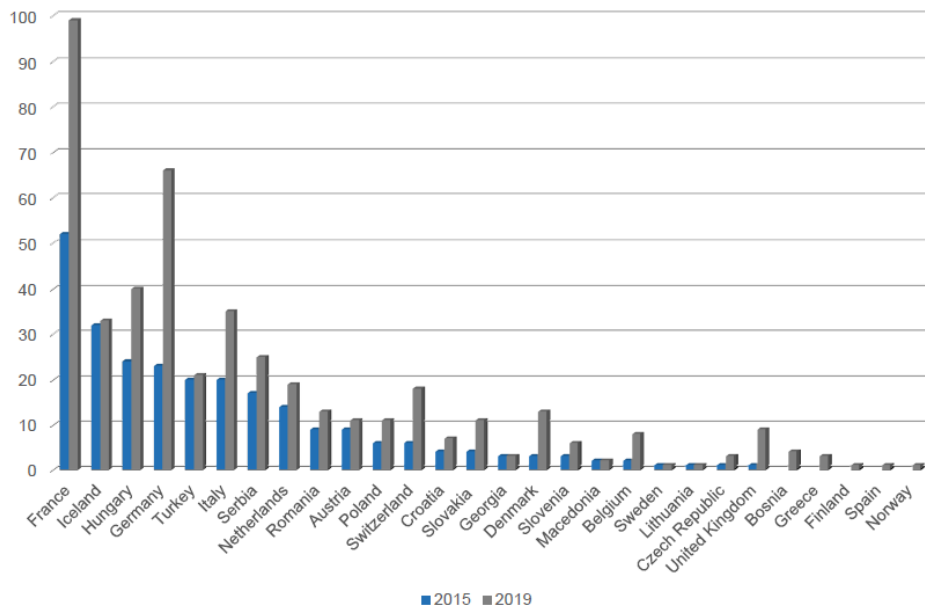


Figure 2.13 - Predicted growth of number of geothermal district heating systems in Europe between 2015 and 2019 [26].

2.3.4 Biomass

Biomass can be used for multiples purposes: electricity and heat production, biofuels production for transport and plastic production in the green chemistry. The first three biomass uses are referred to as “bioenergy uses”. The biomass sources can be classified into three groups:

- (a) *Waste*: biodegradable waste from road side verges, households and gardens, solid and wet waste from agriculture products and organic waste from industry and trade;
- (b) *Agriculture*: energy crops (ligno-cellulosic, sugar, starch, oil, maize), dry and wet manure and other agricultural primary residuals (grass, straw and stubble from cereals, sunflowers etc)
- (c) *Forestry*: woody biomass from forests or other wooded lands.

Fig. 2.13 outlines the share of the bioenergy market segments with regard to the final energy use and regardless of the biomass source. Electricity production and heat production do not have to be considered competitive uses, since more than 60% of the electricity from biomass-fired power plants comes from cogeneration plants [27]. This involves a gross final energy consumption of 510 PJ/y of the district heating sector in 2014, i.e. almost 16% of the total. Biomass constitutes one of the main energy sources in some countries such as Sweden, Latvia etc –see Fig. 2-, but it accounts for a rather small share of the overall energy supply to district heating systems at European level -see Fig. 2.6-. According to AEBIOM [27], the bioheat development differs significantly among the Member countries due to different markets. In

some countries -such as Italy- there has been a quick development of pellet heating in all sectors (residential, services and small industries). Other countries –such as Latvia- build new large-scale CHP plants for biomass, and district heating is moving from fossil fuels to biomass. Even big cities embrace biomass for district heating, like Paris and Copenhagen. Many countries have discovered biogenic waste as a good renewable energy source. Recycled wood and other waste products are used for energy when landfills close down. In industry we see use of biomass not only in the forest industry, which is the traditional large-scale use, but also in the food industry, laundries, asphalt production, cement plants and others.

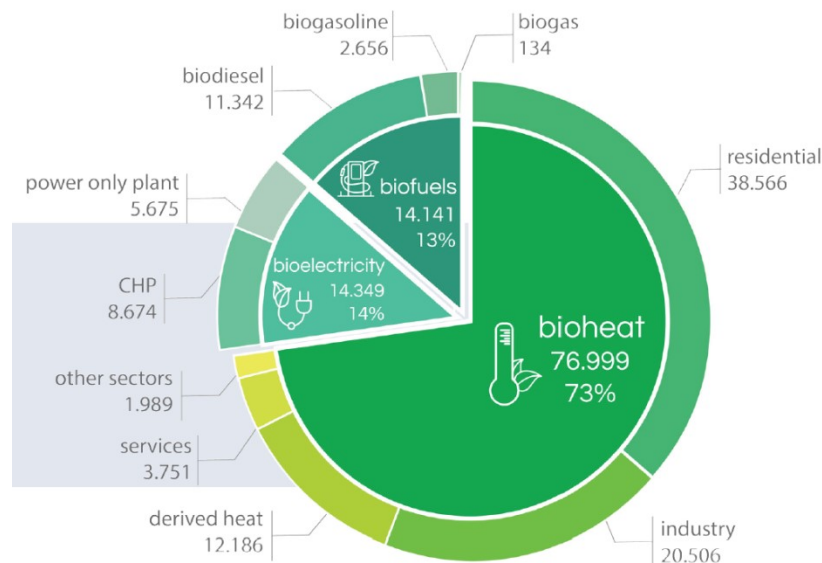


Figure 2.14 - EU28 gross final energy consumption (ktoe) of bioenergy per market segment in 2014 [27].

There is a new interest in renewable heating and cooling from EU level. But the effort sharing targets for the sectors outside ETS for 2030 are sadly low, and the incentives are too weak. Carbon pricing, a carbon tax on fossil heating fuels, would do wonders on all markets. According to the Directive on the promotion of energies from renewable sources (RES Directive) [28] only part of the available biomass for energy use (bioenergy potential) can be used in a sustainable way. In particular, two sustainability criteria should be used when implementing the RES Directive at national level:

- 1) Prohibition of biomass from land converted from primary forest, high carbon stock areas and highly bio-diverse areas;
- 2) Minimum greenhouse gas (GHG) emission savings according to a common calculation methodology.

The “Atlas of EU biomass potentials” outlined two scenarios for the evolution of biomass potential to 2020 and 2030 with regard to the adoption of less (reference scenario) or more strict (sustainable scenario) sustainability criteria as constraints to the biomass use [29]. The bioenergy potential in 2030 ranges from 14.78 EJ to 17.21 EJ, while the final energy use from biomass was 4.42 EJ in 2014, of which 3.22 EJ (73%) for heat production [29]. Out of the overall bio-heat consumption, only 510 PJ was district heat (15.8%). The projection to 2020 outlines a linear growth of the bioenergy undergoing an increase in absolute terms but a decrease from 73% to 64% of the bioenergy use due to the foreseen growth of the biofuel production share –see Fig. 2.14. This means that, if the district heating share out of the overall bio-heat segment remains unaltered at 15.8%, in 2020 biomass district heating will provide 132 PJ in the EU28.

Table 2.1 - Estimated bioenergy potential (PJ/y) in the EU27 [29].

Type	Subtype	2008 Ref. potential	2020 Ref. scenario	2020 Sust. scenario	2030 Ref. scenario	2030 Sust. scenario
Waste	Wastes	1758	1507	1507	1382	1382
Agriculture	Agricultural	3726	4438	4438	4438	4438
	Rotational crops	377	712	0	837	0
	Perennial crops	0	2428	2177	2052	1549
	Landscape care wood	377	628	461	502	461
	Roundwood production	2386	2345	2345	2345	2345
	Additional harvestable roundwood	1717	1591	1465	1633	1507
Forestry	Primary forestry residues	837	1717	795	1758	795
	Secondary forestry residues	586	628	628	712	712
	Tertiary forestry residues	1340	1884	1884	1591	1591
Total		13147	17961	15701	17208	14779

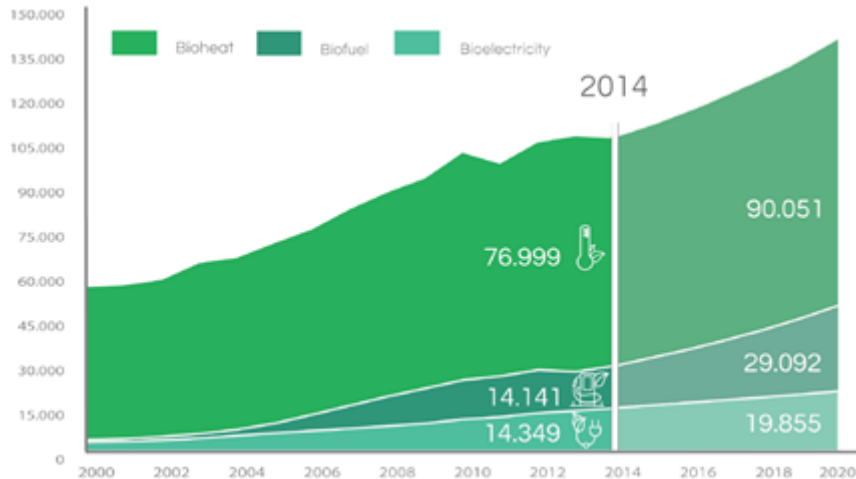


Figure 2.15 - EU28 gross final energy consumption (ktoe) of bio-energy: projection to 2020 [27].

Thus, the scenarios outlined in the Heat Roadmap Europe [13] seem quite optimistic, as they indicate 325 PJ by 2030 and 810 PJ by 2050. Nevertheless, these values make sense due to the assumption of a growing share of the district heating and cooling market.

2.3.5 Industrial processes

The ECOHEATCOOL WP4 showed that if all Member States had the same efficiency of Sweden (best Member State practice) in the recovery from industrial excess heat, the EU27 would gain 1106 PJ/year [17]. This study individuates six energy-intensive industrial sectors and applied them the Swedish heat recovery factor, as shown in Table 1. Indeed, in Sweden around 10% of DH energy is recaptured from industrial processes [21].

Table 2.2 - Estimated industrial waste heat potential in the EU from Swedish recovery factors [17].

Sector	Total energy supply 2003	Swedish heat recovery factor	Total industrial surplus heat potential (PJ/y)
Petroleum refineries	33202	0.6%	196
Food and tobacco	1443	3.6%	53
Pulp and paper	1616	2.4%	38
Chemical	2573	12.2%	315
Non-metallic minerals	1890	2.9%	55
Basic metals	2602	17.3%	449
Total EU			1106

Connolly et al [13] used emission data from the E-PRTR dataset to individuate the heat recovery potential of industrial sites. They estimated a potential of 2708 PJ/year for the EU27 area. So far, this is the most complete work on industrial excess heat potential since it pro-

vides the waste heat potential for all the European Member States. As a drawback, this reference seems to be too optimistic compared to other estimates. Due to high technical and operational constraints, only part of this heat can be actually recovered: 204 PJ/year in the 2030 scenario and 385 PJ/year in the 2050 one. Currently, only PJ/year of industrial excess heat are recovered. These two studies were included in the review of Miró et al. [30]. Here, we take advantage of this review to draw a complete picture on the available data concerning with industrial excess heat in Europe.

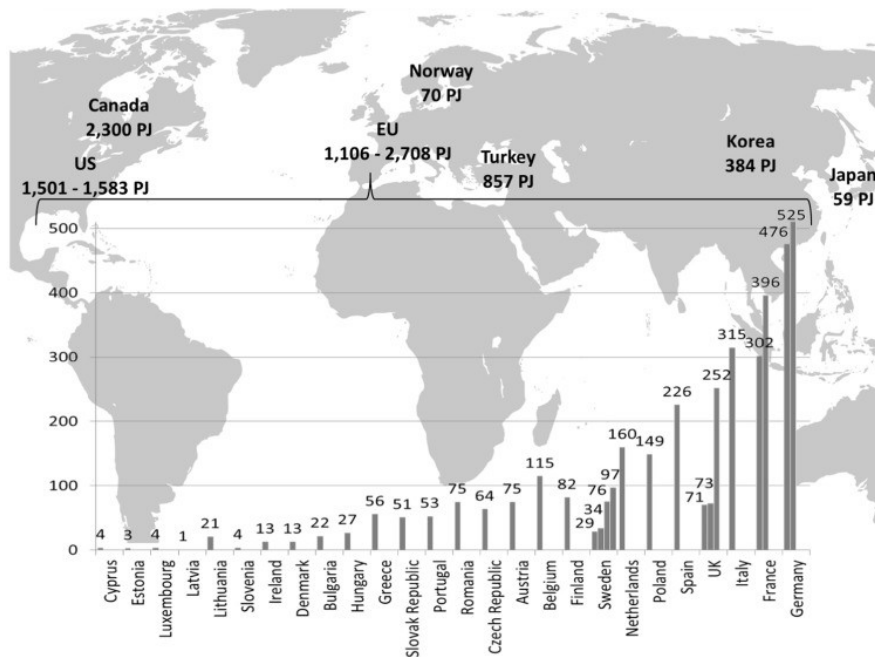


Figure 2.16 - Map of industrial waste heat [30].

Among all the industrial sectors, previous works have identified the some sectors which are usually the main waste heat producers: metal industry (iron and steel production), chemical and petrochemical industry, food and beverage sector, paper, pulp and printing, non-metal minerals (including cement, glass, ceramic and lime). Figure 2.16 shows the share of heat wasted by these energy-intensive industry sectors among industrial countries. The EU average is slightly higher than 60%.

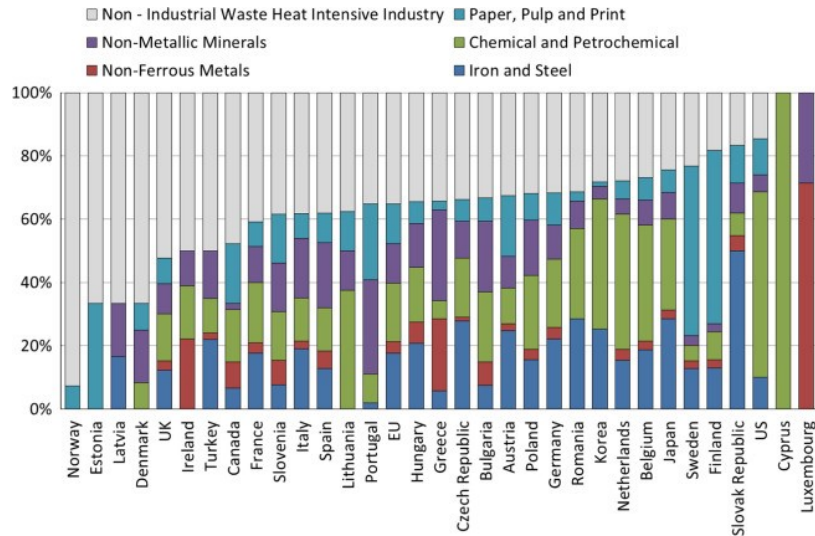


Figure 2.17 - Share of industrial waste heat by industry sector [30].

To our scope, it would be useful to know what is the available temperature of this waste heat. Although there is still a lack of information at EU level, there are some interesting surveys at regional/national level.

Table 2.3 - Summary of outcome from recent studies on industrial waste heat potential in the EU.

Country/ region	Author, year	Technique	Temperature range	Estimated potential (PJ/y)
France	Berthou & Bory, 2012 [31]	Survey/ Investigation	40-250°C	360
Norway	ENOVA, 2009 [32]	Survey to 72 companies + 4 incineration plants	>140°C	70
Sweden	Chronholm et al, 2009 [33]	Top-down estimation	-	22.3 – 28.4
	Broberg et al, 2012 [34]	Survey to 85 companies (42 answered)	25 – 160°C 160 - 350°C	75.6 7.2
Germany	Pehnt & Bödeker, 2010 [35]	Estimation with heat recovery factors	60 – 140°C >140°C	158.4 316.8
EU	Werner et al, 2006 [17]	Estimation with heat recovery factors	-	1106
	Connolly et al, 2014 [13]	Local emission data and heat recovery factors	-	2708

Technical barriers to the deployment of the industrial waste heat include: distance from heat sinks, short winter seasons, continuity of operation of production plants, financial constraints. In particular, companies consider the investment to connect to existing DH grids only when the latter is profitable and at the same time has a low pay-back time. Discount rates play an important role in making the investment feasible. It must also be considered that when heat is

available above a certain temperature, the electricity production becomes really competitive due to advancement in the ORC technology. In this case waste heat can still be delivered by a CHP plant but at a lower temperature, i.e. according to the normal boiling point of the considered working fluid.

2.3.6 Solar heat

Today -end of 2015- there are 252 operating solar thermal plants with more than 350 kW_{th} of installed thermal capacity that provide heat and cold in Europe, reaching a total installed capacity of 750 MW_{th}. The market is growing with a +30% upturn especially in Denmark, that is the leading country with regard to the number of installations, followed by Sweden, Germany and Austria –see Fig. 2.17. This market is developing in other countries such as France and Italy. According to a study of 2012, the potential of solar heat in Europe amounts to 200-580 TWh/y (720-2100 PJ/y) in 2030. Assuming that district heating will keep the same market share in 2030 and that 10% of the solar heat potential will be supplied to DH grids, the potential for solar district heat ranges from 72 to 210 PJ/y [36].

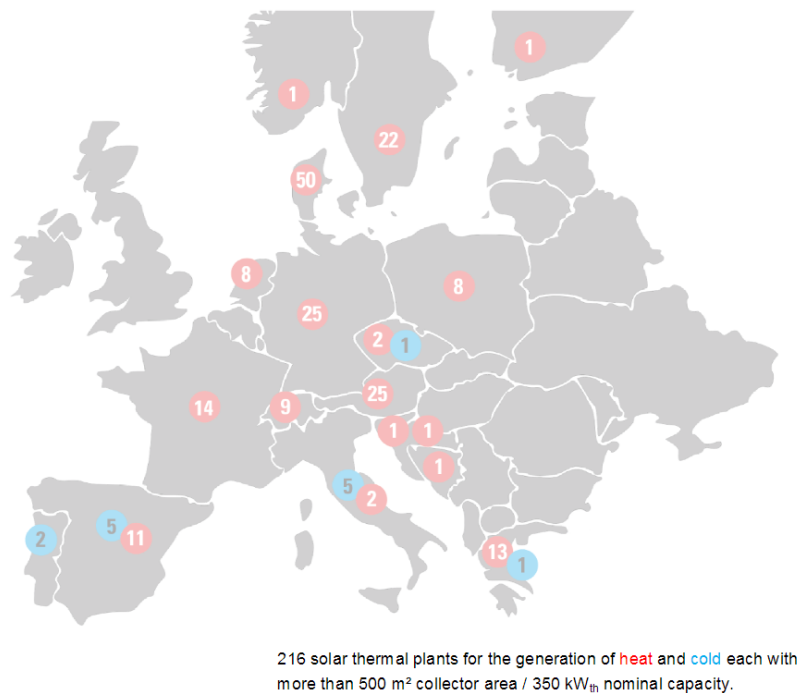


Figure 2.18 - Solar DHC systems in the EU28 [37].

Typical solar fractions of solar assisted block heating systems range from 10-20 % for installations with diurnal storages and from 40-70% for installations with seasonal storages [37].

2.3.7 Other low temperature heat sources for district heating

Besides the mentioned heat sources, there is an additional potential from heat sources that lie in a temperature range between 10°C and 50°C. These sources can't supply heat directly in 4th Generation DH networks due to the temperature gap between source and sink. One possible solution consists in the use of large scale heat pumps. The latter was indicated in the scenarios of the Heat Roadmap Europe as one of the main contributors to the decarbonisation of the European heat market on a long term. In fact, the deployment of heat pumps can be useful both to integrate further renewable energy sources in district heating networks as well as absorb excess electricity production peaks during periods of low energy demand and high availability of renewable non-programmable energy (wind turbines or PV). A recent study investigated the potential of seven low temperature heat sources in Denmark: low temperature industrial excess heat (at <100°C), supermarkets, waste water, drinking and usage water, ground water, rivers, lakes and sea water [38]. In this Country, wind turbines are slowly pushing CHP plants out of operation, thus reducing the energy efficiency of the DH (district heating) supply. The mentioned study considered the proximity to existing DH networks as a constraint, and showed that these sources can significantly contribute to the heat demand of the Danish DH systems, but alone are not enough to cover it entirely. In particular, 99% of the DH systems could benefit from at least one of the mentioned sources. Ground water showed the highest potential in terms of both geographical availability and potential heat volume. Sea water and rivers also showed a high potential heat volume. Supermarkets can be found in every city or town, but have a rather low (but not negligible) potential heat volume. The excess heat from industrial processes also showed significant potential [38]. However, neither the temporal resolution of the heat sources nor the practical, environmental or technical barriers relevant in each specific case were considered. Thus, further research in this direction is needed to assess the actual potential of these energy sources. In order to have a more rigorous framework, low temperature heat sources are grouped here into four categories:

- (a) Low temperature industrial waste heat (at <100°C);
- (b) Natural low temperature heat storages: sea, rivers, lakes, ground (shallow geothermal), groundwater;
- (c) Urban infrastructures: tunnels, sewage and drinking water conducts;
- (d) Condensers of cooling and refrigeration units: supermarkets, shopping malls, data centers, indoor ice rinks.

The next Section discusses some concepts proposed for the integration of these sources within DHC systems.

2.4 Integration of low temperature heat sources into district heating systems

Traditional DH networks distribute energy from a centralized generation plant to a number of remote customers. The opportunity to reduce the heat losses and to enhance the efficiency of supply plants (typically CHP) has driven many DH utilities to lower the network operating temperatures [39]. The opportunity to integrate alternative energy sources such as waste heat and renewable heat sources has contributed to this trend. Nowadays, *state-of-the-art* DH systems have supply temperatures in the range between 70 (winter) and 55°C (summer) in order to guarantee thermal comfort and a safe production of domestic hot water (DHW). Therefore, heat pumps would be needed to exploit the heat sources mentioned in the previous Section, which are typically at temperatures lower than 50°C. This Section presents some practical barriers that may arise in the integration of low temperature heat sources into DH grids and then summarizes the main concepts that have been proposed so far to overcome operating problems.

2.4.1 Examples of practical barriers

The number of data centers (DC) worldwide is rapidly growing. It is estimated that DCs already accounted for 1.1-1.5% of the world's total electricity consumption in 2010. The electricity consumed in a DC is almost completely converted to heat. Therefore, DCs require vast amounts of cooling energy. However, most of the heat is not utilized, and is an interesting heat source for those buildings that must be heated in the surroundings. The temperature of captured waste heat depends on the location where it is captured and on cooling technology. In air-cooled data centers, waste heat can generally be captured between 25°C and 35°C. In liquid cooling solutions, waste heat can be captured closer to processors, where operating temperatures are higher and thus the captured waste heat is of a higher temperature, e.g. 50-60°C [40]. Therefore, if the supply water temperatures are below 50°C, waste heat from data centers could be directly fed to the DH network without the heat pump, especially from DCs with modern cooling technologies, which allow high waste heat recovery temperatures [40]. Also in case of supermarkets, the layout of the refrigeration system plays a key role in the effectiveness of the heat recovery [41]. The most diffused solution is called *Multiplex system*, where the refrigerant is expanded directly in the evaporators below the fridges and is then

compressed through a rack of parallel compressors that send it to the condensing units installed outdoors; the liquid is then sent back to the evaporators [41]. The main disadvantage of this solution is the huge amount of refrigerant that must be used, thus causing significant leakages. Another possible lay-out is the so called *Water Loop Self-Contained system* (WLSC). In this case, each fridge has its own refrigeration cycle and a water loop is used to remove the heat. A dry cooler, together with an additional chiller needed for freezers during the warm season, is used to dissipate the heat to the environment [41]. This system reduces the amount of refrigerant needed to 5-10% of the amount needed by the *Multiplex system*. The performance is better due to the possibility of having the correct evaporating temperature in each fridge. The amount of heat that can be recovered also depends on the considered layout. In Multiplex systems, only the de-superheating part can be recovered. An increase of the condensing pressure would lead to a significant reduction of the EER and is therefore not considered. On the other hand, the WLSC systems facilitate the heat recovery from the hydronic circuit by using water to water heat pumps. Therefore, standards concerning the charge of refrigerant in the system and new developments in compressor technology will play a significant role in determining the best alternative for supermarket refrigeration and, in turn, the heat recovery potential.

2.4.2 New concepts for district heating and cooling systems

The examples of data centers and supermarkets show that some practical constraints may reduce or enhance the possibility to recover heat from these sources. In any case, lowering the network temperatures to adequate levels is one of the key points to enable the heat recovery. So far, three generations of district heating networks have succeeded, leading to nowadays *fourth generation district heating* (4GDH) [8]. In the latter, the heat losses are reduced by using twin-pipe geometry (two media pipes in one casing), thicker insulation, and reduced supply/return temperatures: about 70/40°C in winter and 55/25°C in summer. In low energy districts, the supply temperature of 55°C can be maintained for the whole year, thus reducing the heat losses to approximately one quarter of the level they would have with networks working at 80/40°C [42]. According to Brand and Svendsen [42], a supply temperature of 55°C is enough to provide thermal comfort for 98% of the heating season for Danish houses built in the 1970s, thus extending the solution of 4GDH to existing buildings. Moreover, 4GDH networks must be designed with the goal of reducing the pipe diameters to the lowest possible level, thus enabling the use of twin pipes. Oversizing, that was a typical feature of

traditional networks, must be avoided. This leads to lower investment costs but also to higher pressure drops, which turn into higher operating costs for water circulation. Moreover, large-scale heat pumps are expected to play a key role in 4GDH systems, as they are able to absorb the electricity production of renewable, non-programmable power sources during peak hours and store it for later use in large thermal energy storages [8]. On the other hand, heat pumps can be supplied by low temperature heat sources as those described above. This is an example of the “polygeneration” concept described in Chapter 1. While large-scale heat pumps remain in the framework of centralized heat supply, an emerging field of research and development concerns the integration of “prosumers” into new or existing DH networks. Prosumers are already well established in the electricity sector, but they represent a rather new concept in the world of thermal networks. A prosumer must be intended as a customer of the DH utility that has also the possibility to inject excess heat into the network, when the latter is available. In this thesis, the term prosumer will indicate all those heat suppliers that are able to supply heat to the network and that are not controlled by the network manager (used here as synonym of DH utility). Recently, some studies have investigated the potential integration of prosumers in district heating grids. For example, Brange et al. [43] investigated the potential of the bidirectional exchange of heat in Hyllie, an area under construction in Malmö (Sweden). The study considered four scenarios, depending on whether the heat produced could be distributed outside Hyllie or not and also depending on the chosen system. The first system used decentralized heat pumps to raise the temperature of the excess heat (30°C) up to the network level (65°C) and the other one had a network supply temperature of 30°C and electric heating for DHW production. The study showed that due to the high number of prosumers in the considered area (supermarkets, ice rink and buildings with space cooling demand), the potential of excess heat was fairly big, i.e. approximately from 30% to 60% of the heat demand on a yearly basis according to the considered scenario. However, since most of the heat was available during summer months, the environmental benefit of the proposed solution relied on the primary energy factor of the consumed electricity. Zvingilaite et al. [44] studied the feasibility of a district heating network with 40°C supply temperature and booster heat pumps for DHW preparation and compared its thermodynamic and economic performance with those obtained by distributed electric water heaters. They called this concept ultra low temperature district heating system (ULTDH). The study showed that the booster heat pump system has the highest annualised investment cost but yields the lowest operation expenditure due to the high COP (5.3) of the water-to-water units. Similarly to the second system presented above [43],

many studies or pilot plants proposed to couple thermal networks that distribute heat at low temperature with booster heat pumps at the customer substations. This concept goes beyond the guidelines of 4GDH, and is therefore also regarded as the 5th Generation of District Heating Systems (5GDH) [12]. The idea behind the new generation is to distribute heat at very low temperature, ideally approaching ground temperature to have no heat losses at all and to potentially recover all kind of local heat sources, including excess heat from prosumers as discussed above. The use of heat pumps becomes necessary for DHW production and also for space heating, if the supply network temperature is 30°C or below. In fact, temperatures in the range of 35-45°C are sufficient to supply heat to new and refurbished buildings with radiant floor systems. From another viewpoint, decentralized heat pumps offer the possibility to design the supply temperature of small heating grids based on the available heat source and at the same time to adapt the supply temperature to each building, as compared to a centralized solution with a single supply temperature fixed by the most demanding consumer. This advantage is particularly interesting when the building stock is heterogeneous, and both new and old buildings must be supplied by the same network. Figure 2.18 summarizes the evolution of network temperatures in the different “generations” of district heating systems. It is worth noting that 5GDH refers in general to a system where heat is distributed at very low temperature -see Fig. 19- and some local back-up systems (typically heat pumps or electric heating) are used, but there is not a univocal and accepted definition. Moreover, while 4GDH systems are already well established, the credibility of fifth generation DHC relies on a few pilot projects. One of them can be found in Kassel (Germany), where a ground-coupled heat pump supplies a new housing stock via district heating network with a supply temperature of 40°C. During the heating season, the network provides heat to the space heating systems and to the lower part of the DHW tanks, that are also supplied by solar collectors and electrical heating as backup; during the remaining periods, the solar collectors recharge the ground [45]. The concept of cold networks with decentralized heat pumps was already successfully applied to both new and existing building areas as in the case of Brig (Switzerland), where the heat source is an artificial canal of the river Rhône [46] or in Wüstenrot (Germany), where the central heat source is a shallow geothermal field and the electricity demand of the heat pumps is lower than the electricity produced by the PV modules on the roofs of the houses on a yearly basis, thus achieving the status of an “EnergiePlus” district [47]. In Ospitaletto (Italy), a DH grid with variable supply temperature -between 13 and 25°C- is supplied by groundwater and by the low temperature waste heat of a local steel company [48]. In these cases, the heat

pumps are supplied by cold water at around 10-16°C, depending on the period of the year. Since at this temperature heat cannot be converted into work due to its low exergy content, these networks are sometimes called “cold-“ or “anergy networks”. However, when the supply temperature of the district heating system is so low, a possible advantage is to provide buildings with heating and cooling at the same time. This is interesting when there is a significant amount of heat that is rejected during the heating season, as it typically occurs for the heat sources mentioned in Section 2.3.7, but also during middle seasons when different buildings could simultaneously need either space heating or space cooling.

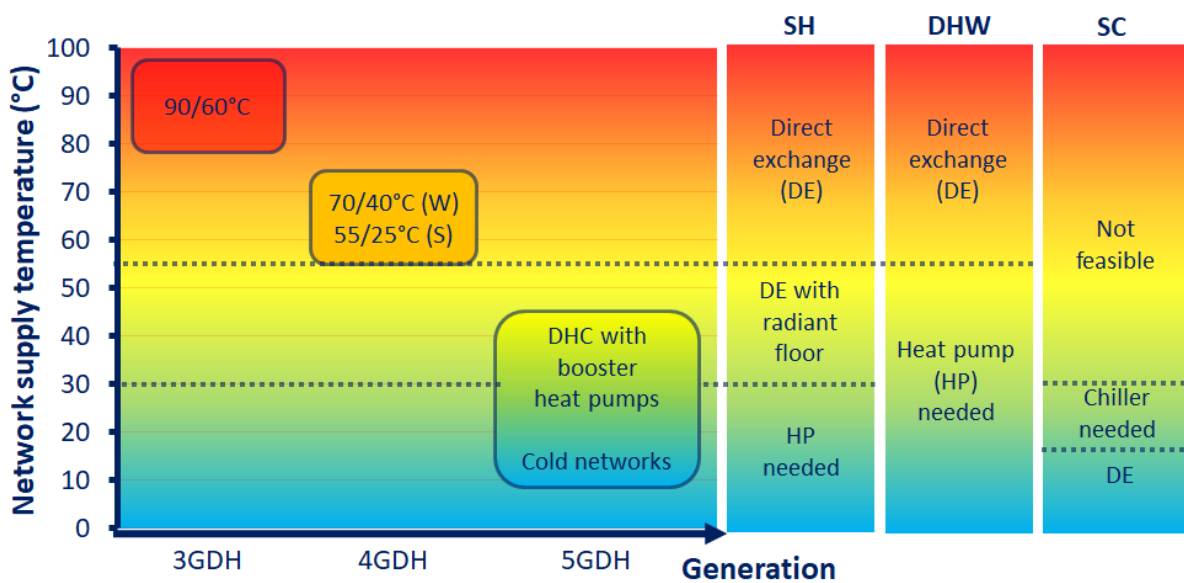


Figure 2.19 - Conceptual scheme on the evolution of District Heating and Cooling networks.

An example of integration of prosumers in existing DHC systems on a large scale can be found in Stockholm, where the local district heating utility launched ‘Open District Heating’. After a two year pilot study, the program was officially launched at the end of 2014. In open district heating, excess heat from data centres, supermarkets and other buildings with large cooling demands is utilised in the district heating or cooling network and sold to the DH companies at market price. The supply temperature from these prosumers is often raised with some kind of heat pump solution [28]. With regard to possible alternatives to water networks, Henchoz et al. [49] studied the possibility to replace water with refrigerants such as CO₂ and R1234yf. Due to their high latent heat of vaporization at ambient temperature, refrigerant-based networks could enable a significant reduction of piping dimensions and in turn the overall investment cost (considering both pipe cost and groundworks). The study considered 4

K as temperature difference between supply and return line in the cold water network. A comparison based on energy consumption revealed that the R1234yf brings a marginal improvement over the CO₂ based solution. Nonetheless, the saturation pressures of CO₂ and R1234yf at these temperatures are 47 bar and 61 bar, respectively, which could make these networks difficult to accept by public institutions.

2.4.3 Design and operational aspects of DH systems with booster heat pumps

In Denmark, heat pumps are gaining increasing interest as they are capable of utilizing the excess electricity produced by non-programmable renewables such as wind turbines. Due to the capillary presence of district heating networks across the country, the optimal integration of heat pumps with those systems is a crucial aspect for a sustainable energy supply scenario. Østergaard and Andersen [50] compared two solutions for the integration of heat pumps in DH systems: central heat pumps supplying heat to the network and central heat pumps combined with micro booster heat pumps. Sea water was considered as the heat source for the central heat pumps, with a temperature varying roughly between 10°C (winter) and 20°C (summer). The plant is equipped with a DH storage of 1000 m³ with water temperature varying between 80 and 40°C in the first solution and between 60°C and 20°C in the ULTDH solution, corresponding to 20 hours of average heat production. The analysis shows that the use of booster heat pumps is beneficial when a central heat pump is present, as it allows to improve its COP, to decrease grid losses and to avoid gas consumption. The DH system with booster heat pumps was found to be better than individual solutions (either HPs or gas boilers) and to a heat pump based DH system without booster heat pumps as far as operative costs and primary energy consumption are concerned. Ommen et al. compared the performance of LTDH and ULTDH systems for the heat supply of newly built multi-family houses [51]. The authors defined the coefficient of system performance (COSP) as the ratio between the heat supplied by both central and booster heat pumps minus the heat losses of the grid and the electrical energy consumed by the heat pumps compressors and by the pumps. The results showed that LTDH systems have higher COSP with respect to ULTDH when the network is supplied by an extraction CHP plant, whereas the ULTDH is preferable when the network is fed by a central heat pump supplied by water at 20/10°C at the evaporator. The presence of booster heat pumps gives the opportunity to optimize both supply and return temperatures in the design phase. In the case with central heat pump, the best COSP was found at 44/24°C [51], i.e. with a design temperature difference of 20 K. The analysis considered a reference

case where the fraction of heat demand for DHW production is equal to 50%. In the reference case, the ULTDH system outperforms the LTDH system by 12% in terms of COSP. A parametric analysis revealed that such improvement is reduced by increasing the share of DHW demand: it reaches 7% with a DHW fraction of 75% and 23% with a DHW fraction of 25%.

As pointed out by Lund et al. [8], the intelligent control for optimal operation is a one of the key challenges for the improvement of DH systems. The optimal operation of heat suppliers in DH systems and smart grids is not a new topic in the scientific literature. For instance, Fink et al. [52] proposed two control methods based on MILP (named global MILP and time-scale MILP) to flatten the power consumption profile of a group of heat pumps supplied by a bio-gas-fired CHP that also supplies heat to a district heating network. Both methods showed promising performance in flattening the power demand of the heat pumps compared to a standard PI on-off control. Verrilli et al. [53] proposed an optimal control strategy for a power plant consisting of a CHP, a thermal energy storage and three gas boilers. The methodology is based on a MILP problem solved in a receding horizon scheme. The proposed approach was tested using the data obtained from a DH system in both simulations and experiments in a DH plant in Finland, showing the potential benefits of the approach. Giraud et al. proposed an advanced control method based on MILP to determine the optimal planning for the on/off status and power of the heat generators as well as for the supply temperature and differential pressure at the production plant level [54]. The proposed method uses the heat storage capacity of the water in the DHS pipes and pursues the best compromise between heat losses and pumping costs. This advanced control strategy achieved -8% production costs with respect to a conventional control method in a 5-months-simulation of a representative DH network.

2.5 Discussion

The work of Ommen et al. [51] highlighted the possibility to optimize the network temperatures (both supply and return) when the network is supplied by a cogeneration unit or by a central heat pump. Increasing network temperatures improves the COP of the booster heat pumps and reduces that of the central heat pump. Therefore, optimal supply and return temperatures arise from the optimization of the system as a whole. In case the heat source feeds the thermal network directly through heat exchangers, the optimal temperatures shift upwards as far as primary energy or exergy is concerned. In fact, higher temperatures on the network side involve higher COPs of the booster heat pumps and, in turn, lower electrical consump-

tion. Since electrical energy has a high exergy content, the reduced electrical consumption overwhelms the benefit coming from the reduction of network heat losses. In other words, as Ommen and Andersen mentioned at the end of their paper, for the users the economically optimal return temperature is higher than that for the system if heat is cheaper than electricity –as it normally occurs. This is true if only running costs are considered. However, since part of the heat price covers the initial cost for the infrastructure, a lower return temperature does not necessarily involve a higher heat price for the end users. Moreover, many studies dedicated to LTDH systems and heat pumps by-passed an accurate simulation of the heat pump behavior by using simple performance curves. The literature review uncovered a lack in the methodology, as there are no studies based on an integrated simulation environment. Indeed, in presence of distributed heat pumps a variation in the physical variables of the network (temperature, pressures..) affects the substation's behavior. This is particularly important in the operational optimization of the network, where the control of supply network temperature impacts the power consumption of the heat pumps. The latter can be operated either by the DH utility or by the users, depending on the business model adopted to purchase the heat. In case the utility purchases and/or produces the electricity needed by the heat pumps, the control strategy must take into account the price and/or the production cost of electricity. Secondly, the presence of heat supply from a third party –the prosumers- implies that the network is no more configured as a “top-down” structure, but as a distributed system with multiple heat supply points that are not necessarily controlled by the network manager. Therefore, an interesting research issue is to investigate how the central heat supply plants reacts on increasing shares of decentralized heat supply without affecting the profitability.

Chapter 3 Models

3.1 **Model of the buildings at district scale**

Appropriate dynamic models are necessary both during early design stages of buildings and neighborhoods as well as when retrofitting solutions for existing ones are being evaluated. There are several approaches for the dynamic simulation of buildings at district level. Here, an overview on these approaches is given and then the chosen method is described. Finally, the validation of the model is presented.

3.1.1 **Simplified dynamic models**

The heat dynamics of a building can be modelled following two different approaches. The first consists in explicitly modelling the physical phenomena occurring within the building, i.e. all physical processes that significantly affect the energy balance of the thermal zone(s) considered. Models following this approach are termed white-box models. The second approach relies on statistical methods that are applied to available data (heat consumption and temperatures) without any explicit reference to equations governing their energy balance and are thus called black-box models [55]. In most cases, such as during the design of the building, data are not available and white-box models must be used. Since buildings are complex energy systems that are affected by multiple, overlapping physical processes such as transient heat conduction, parallel heat exchange by convection and radiation, radiative and convective heat generation by internal heat sources etc., energy needs for space heating/cooling can be calculated in a more or less detailed manner depending on the objective of the analysis. Steady-state, quasi-steady-state or dynamic methods can be used for this purpose [56]. Quasi-steady-state methods calculate the heat balance of the building zone over sufficiently long periods of time (typically one month or a whole season) and then take dynamic effects into

account using empirically determined gain/loss utilization factors [57]. Conversely, dynamic methods use short time steps (typically one hour long) to calculate heat balance taking into consideration thermal transmission, heat flow by ventilation, thermal storage, and internal and solar heat gains in the building zone [56]. The most frequently used softwares for building simulation (e.g. TRNSYS [11], Energy Plus [58], or ESP-r [59]) rely on models that require a detailed description of the building in terms of both its geometry and physical properties. Given the high number of input parameters and the detailed information that are requested, they are unsuitable for inexpert users. The underlying models find an explicit solution to the heat conduction equation by finite difference [60] or by analytical methods, namely the transfer function method [61] (an improvement with respect to the frequency response factor method [62]) and the admittance matrix methods [63]. A synthetic description of these methods has been provided by Underwood and Yik [64]. As these methods require a high computational effort and cannot readily be interfaced with optimization solvers, they are unsuitable for the simulations of neighborhoods or city districts. Simplified dynamic models of buildings have been receiving growing attention. The system domain of these models is discretized into a set of nodes connected by thermal resistances and capacitances (i.e. the parameters of the model); their main advantage is that once their parameters have been identified, the system can be solved analytically, thus avoiding problems of convergence and stability that typically arise with numerical schemes. Since each thermal capacitance of the equivalent circuit corresponds to a state variable of the model, the number of thermal capacitances leads to the order of the model. Reducing the model order curtails, in turn, the number of parameters to be identified, thus achieving the objective of describing the building dynamics with a simple model. The parameters of the equivalent thermal network can be identified analytically, by model order reduction (for a review of the techniques see [65]) or by tuning the model to the data set of temperature and energy consumption available. In the latter case, these models, which can be considered a hybrid between black-and white-box models, are often referred to in the literature as grey-box models [66]. It is clear that calculating parameters analytically can deviate the results of building simulation from real world conditions as the model receives no feedback from the conditioned space. On the other hand, parameter estimation from measured datasets is influenced by the case study being considered and thus lacks generality. For a comprehensive review on simplified thermal models, see [67]. Rouvel and Zimmermann [68] separated the building elements into those under symmetric and asymmetric loads, which are typically internal partitions and external walls, respectively. These groups of building ele-

ments were then aggregated (by parallel connection of the corresponding resistance-capacitance circuits), thus making it possible to find an analytical solution for all the building elements having the same boundary conditions. The result of this procedure is a lumped-capacitance model with two similar time constants: one for adiabatic walls and another for non-adiabatic ones. The model is now available in a software named GEBSIMU [69]. The International ISO 13790 Standard [56] fully prescribes a quasi-steady-state calculation method (monthly method) and a simple dynamic method (simple hourly method) based on a first-order lumped-capacitance model with five thermal resistances and one thermal capacitance. Despite the fact that the latter produces hourly results, it has been validated, in accordance with the ISO 15265 Standard, only at the aggregated monthly heat demand level [70].

The ISO 13791 [71] and ISO 13792 [72] Standards, which have recently been released, outline the procedure to validate simplified models to calculate the internal air temperature of a single room under transient hourly conditions. The models are suitable for warm periods, but they have been limited, until now, to situations characterized by free floating temperatures without any cooling system. Rouvel and Zimmermann's 2C model [68] was implemented in the German Guideline VDI 6007-1 [73].

3.1.2 Geospatial data

All the information concerning the geometry of the buildings (dimension, orientation) and their position in space is known as geospatial data and can be assessed through Geographic Information Softwares (GIS). The geospatial data (or GIS data) represents real objects, such as roads, land-use, elevation, trees, waterways, etc. with digital data. There are two methods to store GIS data: vector and raster. Vector data represents objects by considering those features as geometrical shapes. Different geographical features are expressed by different types of geometry: points, polylines, and polygons. Each of these geometries is linked to a row in a database that describes their attributes, such as length, area etc. For example, a database that describes lakes may contain a lake's depth, water quality, pollution level. Buildings can be described by polylines representing the external walls and/or polygons representing the floor area. The height of the building –or the number of inhabited floors- can be stored in the database as an attribute. Thus, vector data is well suited to describe the built environment. On the other hand, vector data does not work well with spatial phenomena that vary continuously over the space such as elevation, soil erosion, and precipitation. A better option for representing continuous phenomena is the raster data model. A wide variety of data used in GIS is en-

coded in a raster format; they include digital elevation model (DEM), satellite images, digital orthophotos, scanned maps, and graphic files. The raster data model uses a regular grid to cover the space. Raster data type consists of rows and columns of cells, with each cell storing a single value. For instance, cell value of the DEM is the elevation. The latter can be acquired through airborne LiDar (an acronym of Light Imaging, Detection, And Ranging), a surveying method that measures distance to a target by illuminating that target with a pulsed laser light, and measuring the reflected pulses with a sensor [74]. Differences in laser return times and wavelengths can then be used to make digital 3D-representations of the target. LiDar-based raster models can give a better description of the geometrical features of the urban environment, provided that the resolution of the raster is high enough. The third dimension (altitude of the ground and height of the object) is often missing in vector-based databases. On the other hand, it is not common to find 3D geospatial models in open source repositories. Figure 3.1 shows the representation of the same district with a vector-based data and with a DEM acquired via LiDaR technique.

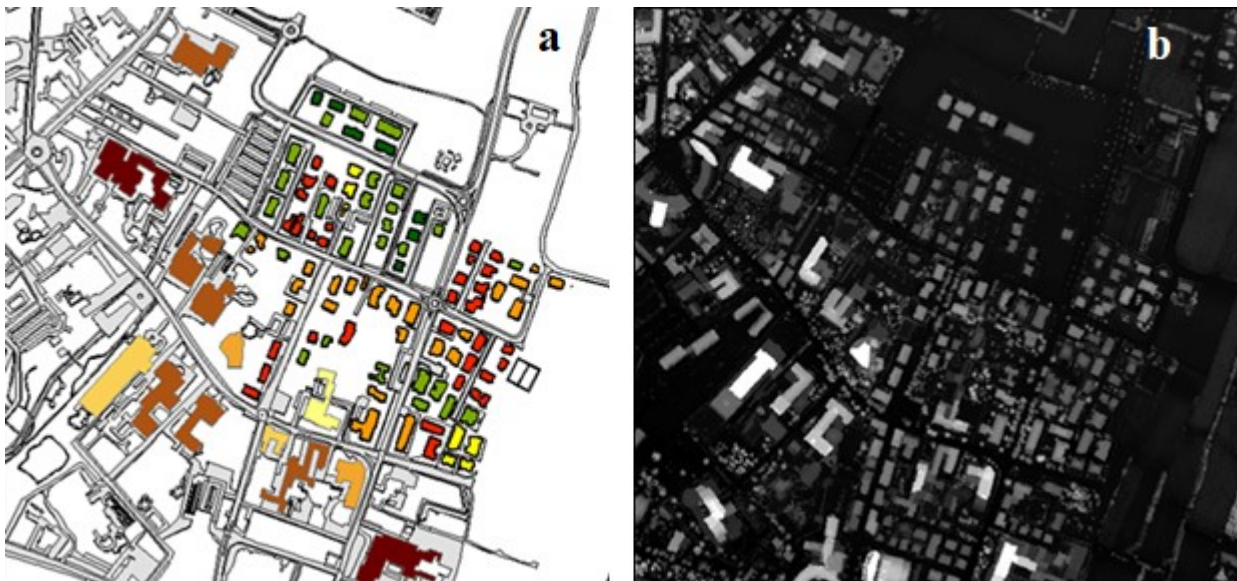


Figure 3.1 - Example of vector data (left) and DEM (right) of the same neighbourhood.

3.1.3 Structure of the model

The implementation of the model follows the structure proposed by Lauster et al [75]. The data flow is illustrated in Fig. 3.2. First of all, ArcGIS -a commercial GIS software- is used to access the data about building geometry. The buildings are described through a shapefile, which is a popular geospatial vector data format developed by ESRI. Here, we call the resulting model a quasi-3D model as information about the height are added as attributes to the

shapefile from external files. The age of construction is a further attribute that is linked to the shapefile. In Fig. 3.1, each building was given a color based on the age of construction: red buildings are the oldest, green ones are the newest. The reference envelopes are sometimes called archetypes. The *archetype method*, as it is sometimes called, is present in literature among the top-down engineering-based building stock models [76]. A building archetype describes the main building components that make up the envelope: pavement, external walls, ceiling, roof, windows and other glazed elements, and internal partitions. These components are described through their stratigraphy, i.e. an ordered list of layers with their corresponding thickness, thermal conductivity, density and specific heat capacity. The archetypes are chosen according to the prescriptions of national legislation in force at time of construction. Thus, each building of the district is given a reference envelope (archetype) according to its age. A MATLAB script reads the geometrical input file and the archetype file and parameterizes all the buildings according to the chosen simplified model. In other words, all the geometrical and physical information on the buildings is reduced to a set of thermal resistances and capacitances. Indeed, lumped-capacitance models assume that the distributed thermal mass of the dwelling is lumped into a discrete number of thermal capacitances, as discussed above.

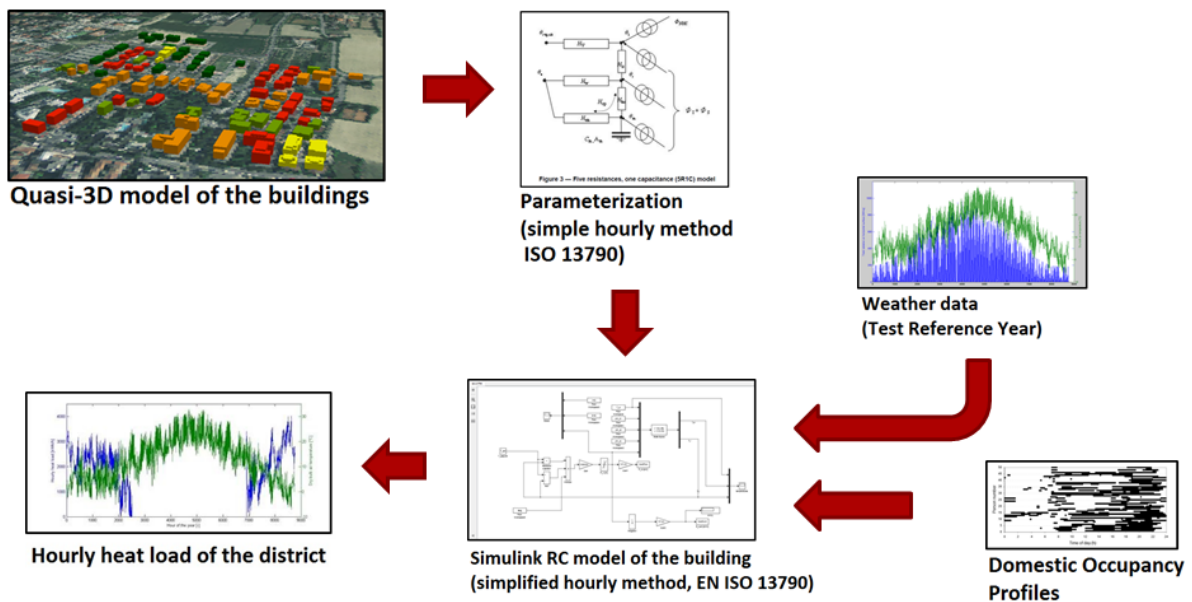


Figure 3.2 - Data flow of the model.

Therefore they are often referred to as xRyC models, where x is the number of thermal resistances and y the number of thermal capacitances of the equivalent electrical circuit. These models rely on the following assumptions: linearity of the heat transfer mechanism, represen-

tation of multilayer wall characteristics by lumped parameters and single zone approximation [77]. The parameterization was done according to the prescriptions of the ISO 13790, that reduces all the physical phenomena occurring within the building to a 5R1C model, as discussed in Section 3.1.1. The other inputs are weather data (external air temperature and solar radiation) taken from the Test Reference Year of the chosen location and building occupancy profiles. Yet the model is not capable of reproducing patterns of presence of occupants in buildings, that would be very important to account for simultaneity of internal heat gains, domestic hot water demand and other variables that depend on users behaviour rather than on physical quantities. Finally, the one year simulation is performed for all the buildings, each of them being modelled as a single thermal zone. All the buildings are considered as singular entities and there are no interactions -such as shading effects- between them. This simplification allows to parallelize the calculation, thus reducing the computation time of the overall simulation. The equations are formulated in state-space form as suggested by Michalak [78]. Figure 3.3 shows the 5R1C lumped capacitance model proposed by ISO 13790 [56]. The lumped-capacitance model was solved by a linear system composed of n heat balance equations, where n is the number of nodes of the corresponding thermal network.

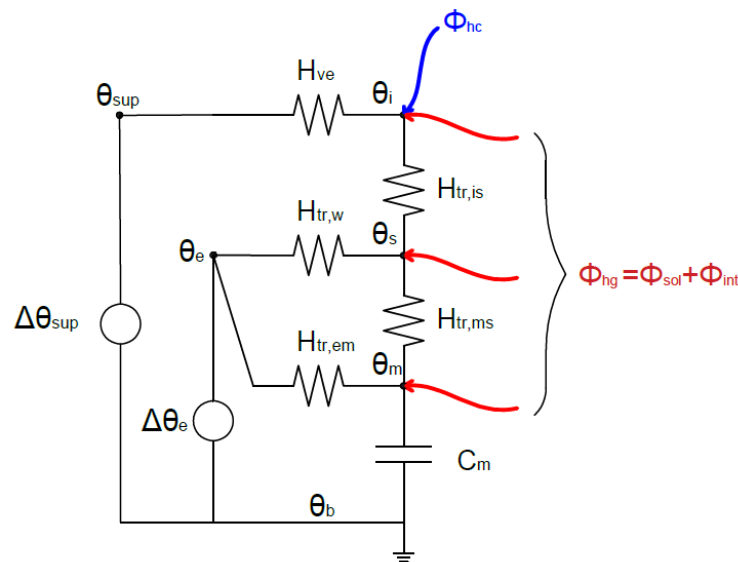


Figure 3.3 - 5R1C model of the building according to ISO 13790.

Figure 3.4 shows, by way of example, a temperature node of an equivalent circuit.

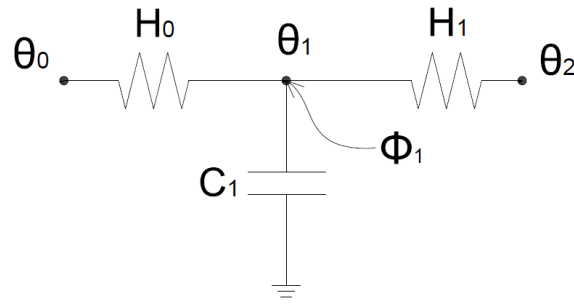


Figure 3.4 - Reference node.

The following heat balance holds true for the reference node.

$$H_0 (\theta_{0,t} - \theta_{1,t}) + H_1 (\theta_{2,t} - \theta_{1,t}) + \phi_{1,t} = C_1 \frac{\theta_{1,t} - \theta_{1,t-\Delta t}}{\Delta t} \quad (3.1)$$

As is usual in building simulations, the system has one degree of freedom unless one variable is fixed by the user. This leads to two possible model uses:

- (a) *Calculation of the heat load.* The indoor air temperature θ_i is set by the user and the output of the model is the heat load ϕ_{hc} , i.e. the energy needed by the building to maintain the specified set-point temperature θ_{set} ;
- (b) *Calculation of the indoor air temperature.* The heat load ϕ_{hc} is set by the user, and the output of the model is the indoor air temperature θ_i .

The models considered do not include the balance of water vapour in the indoor ambient which means that the calculation of the latent heat load (to be delivered to or extracted from conditioned spaces) is not included. The water vapour balance can, however, be included simply as a post-processing calculation after the thermal simulation. The parameters of the model are the thermal transmission coefficients of the glazed and opaque building components ($H_{tr,w}$ and $H_{tr,op}$ respectively), the ventilation coefficient H_{ve} , the coupling conductance $H_{tr,is}$ and the thermal capacitance C_m . The final variable was calculated in accordance with the ISO 13786 International Standard [47] The thermal transmittance of opaque building components $H_{tr,op}$ is divided into $H_{tr,em}$ and $H_{tr,ms}$ as shown in Figure 4. The nodes represent the temperatures of the outdoor air θ_e , the supply air θ_{su} , the indoor air θ_{air} , the internal wall surface θ_s and the thermal mass θ_m . Heat gains (ϕ_{int} and ϕ_{sol}) are distributed to nodes θ_{air} , θ_s and θ_m in accordance with the coefficients indicated in the standard. The solar heat gain ϕ_{sol} includes here not only the solar radiation entering through external windows but also the short-wave radiation absorbed by the external walls and the long-wave radiation

emitted by the external surfaces to the outdoor environment. In the 1C model, all these terms sum up to give an additional heat gain, as shown in Equations (3.2) and (3.3). The first term is the short-wave radiation absorbed by opaque building components, where F_{so} is the shading reduction factor for the external obstacles, I_{sol} the solar irradiance, α_s the absorption coefficient, R_{se} the surface heat resistance, A_{op} and the projected area of the opaque building component. All these variables refer to the external surface of the exterior walls and must be considered separately for each orientation (the subscript of the orientation is omitted for the sake of simplicity). The second term is the extra heat flow due to the thermal radiation to the sky, where F_r is the form factor between the building element and the sky (0.5 for vertical walls), α_{conv} is the heat transfer coefficient, and $\Delta\theta_{er}$ is the difference between the external air temperature and the apparent sky temperature.

$$\phi_{sol} = F_{so} (\alpha_s R_{se} U_{op} A_{op}) I_{sol} - F_r \phi_r \quad (3.2)$$

$$\phi_r = R_{se} U_{op} A_{op} \alpha_{conv} \Delta\theta_{er} \quad (3.3)$$

Using models from well-known Standards makes the results reproducible and allows to generalize results pertaining to different climate conditions and building structures.

3.1.4 Comparison with detailed simulation software

An apartment was simulated with the one-capacitance (1C) model described in the ISO 13790 [5] and with the two-capacitances (2C) model described in VDI 6007-1 [73].

Table 3.1 - Summary of building properties.

Building components		U [W/m ² K]	m_f [kg/m ²]
External walls	EW_H1	1.06	410
	EW_H2	0.26	410
	EW_L1	1.04	50
	EW_L2	0.28	70
Internal partitions/ boundary walls	IW_H	2.53	150
	BO_H	0.95	310
	IW_L	1.59	30
	BO_L	0.95	50
Ceilings/ floors	CE_H	0.73	590
	FL_H	0.73	590
	CE_L	0.33	290
	FL_L	0.33	290
Windows	SP	5.68	-
	DP	2.83	-

Four diverse building structures under four different climate conditions (Palermo, Venice, Vienna and Helsinki) were considered. The properties of the considered building structures are summarized in Table 3.1. The results of the simplified models were then compared with those obtained from the well-established TRNSYS [11] software (used as benchmark), in order to quantify the improvement of the 7R2C model over the 5R1C one in both heating and cooling seasons in terms of seasonal energy needs, peak loads, and transient thermal behaviour. The 7R2C model was validated according to Standard VDI 6020. Peak loads and energy needs. Table 3.2 shows that lumped-capacitance models tend to slightly underestimate the peak load for the space heating of uninsulated building structures (down to -5.5% with the 1C model and to -2.2% with the 2C model) and to overestimate it for well insulated buildings (up to +8.1% with the 1C model and to +4.0% with the 2C model). On the other hand, the peak load for space cooling is systematically underestimated (from -6.3% to -14.5%) by the 1C model, as it can be observed in Table 3.2.

Table 3.2 - Peak load for space heating and cooling.

Env.	Clim.	Peak load for space heating [W]			Peak load for space cooling [W]		
		TRNSYS	5R1C	7R2C	TRNSYS	5R1C	7R2C
H1	PA	1564	1556	1529	2720	2435	2679
	VE	3321	3201	3264	2678	2510	2656
	WI	4882	4823	4865	3810	3516	3825
	HE	6037	5881	5934	2582	2436	2647
H2	PA	717	775	746	2346	2086	2318
	VE	1745	1780	1789	2307	2119	2298
	WI	2629	2695	2718	3390	3053	3438
	HE	3277	3341	3342	2571	2337	2618
L1	PA	1761	1677	1763	3164	2705	3205
	VE	3560	3363	3536	3184	2774	3238
	WI	5355	5106	5305	4602	3966	4696
	HE	6223	5988	6130	3290	2859	3425
L2	PA	803	856	826	2637	2273	2566
	VE	1831	1884	1868	2572	2295	2517
	WI	2796	2872	2892	3895	3373	3863
	HE	3378	3435	3436	3003	2625	2990

The 2C model seems instead to be quite accurate, with an error that ranges from -2.7 to +4.1% and a mean error of +0.3%. Table 3.3 seems to extend the patterns found for the peak load to the energy needs calculation. In fact, the energy needs for space heating is slightly underestimated by the RC models for buildings with low thermal insulation (approx. -4% for both

models), while it is overestimated for highly insulated building envelopes (+5% for the 1C model and +3% for the 2C model). The trends in the space cooling mode remained almost entirely unaltered, although in this case the error in the lumped-capacitance models was not as significant as that in the peak load calculation: the mean error of the simulations with the 1C model is approx. -2.2% and drops to -0.3% with the 2C model. This fact suggests that although they do not accurately follow the fluctuations of the heat load, simplified models are better able to estimate the energy needs of the building over the entire heating/cooling season.

Table 3.3 - Seasonal energy needs for space heating and cooling.

Env.	Clim.	Peak load for space heating [W]			Peak load for space cooling [W]		
		TRNSYS	5R1C	7R2C	TRNSYS	5R1C	7R2C
H1	PA	1293	1261	1209	3353	3231	3310
	VE	7377	7084	7070	2170	2104	2162
	WI	9304	8902	8936	2282	2280	2283
	HE	13557	12988	13069	809	843	836
H2	PA	137	182	159	3402	3302	3357
	VE	3055	3228	3158	2589	2512	2562
	WI	3890	4110	4036	3071	2973	3014
	HE	6528	6770	6686	1811	1719	1761
L1	PA	1336	1267	1252	3313	3232	3317
	VE	7300	7044	7047	2228	2149	2254
	WI	9203	8849	8902	2409	2358	2449
	HE	13291	12859	12912	952	917	997
L2	PA	179	204	192	3337	3241	3291
	VE	3129	3278	3215	2578	2496	2550
	WI	3989	4174	4118	3017	2931	2971
	HE	6531	6789	6697	1794	1702	1750

Transient behaviour. The accuracy in the transient response of the lumped-capacitance models is measured here as the mean distance (RMSE) between their heating/cooling load profiles and those obtained by TRNSYS simulations. Figure 3.5 shows the RMSE of the simplified models and the peak load in the corresponding season for the apartment facing east-west. The peak load, which was extracted from the heat load profile produced by TRNSYS, serves as a valid reference for both simplified models. The RMSE of the simplified models increased from Palermo to Vienna but showed a smaller increase with reference to the snow-dominated climate of Helsinki. Figure 3.5a, for example, shows that while the

peak load in Vienna is more than three times the peak load in Palermo (from 1564 W to 4882 W) and the $RMSE_{1C}$ is more than twice the $RMSE$ (from 81 W to 184 W), this proportion is no longer valid when we turn our attention from Vienna to Helsinki (+23% of peak load and only +5% of the $RMSE_{1C}$). This trend could be linked to the different patterns of temperature differences between the indoors and outdoors, which represents the main driving force for space heating load in winter months. Indeed, temperatures are less prone to register significant diurnal fluctuations in the Nordic climate of Helsinki than in the other locations considered in this study. This trend seems to be valid for both simplified models regardless of the building envelope.

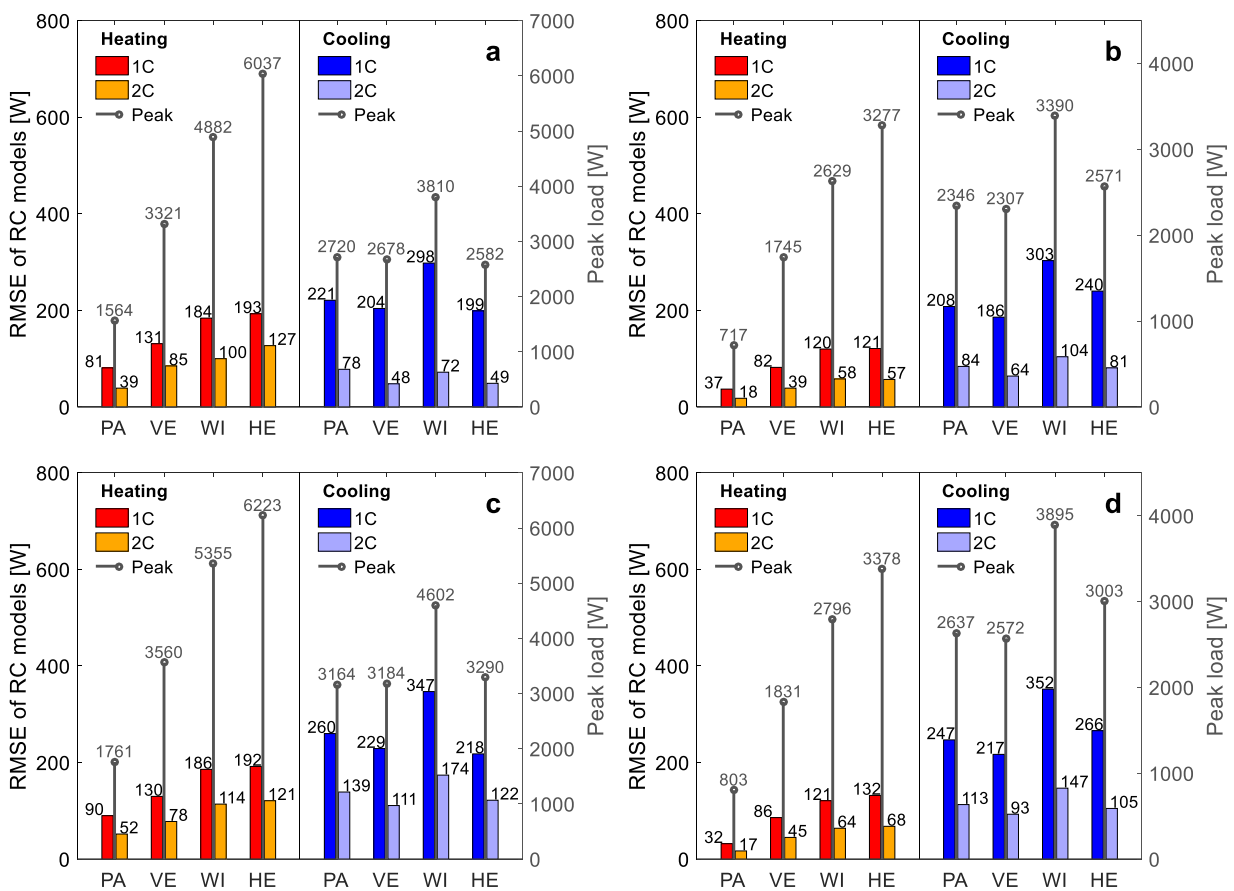


Figure 3.5 - RMSE of lumped-capacitance models and peak load for the apartment with envelopes: (a) H1, (b) H2, (c) L1 and (d) L2.

During the warm season, instead, the cooling load is a result of the overlapping effects of outdoor air temperature and solar radiation. Figure 3.5 shows that the accuracy of the 7R2C model is greater than that of the 5R1C one in all the cases considered and that such improvement is particularly relevant in the cooling season. Indeed, the RMSE from 1C to 2C drops from -35% to -53% in heating mode and from -44% to -76% in cooling mode. The

trivial reason for this improvement is linked to the presence of the second thermal capacitance that makes it possible to distinguish between adiabatic and asymmetrically loaded building components. Moreover, the presence of two internal surface temperature nodes (θ_{IW} and θ_{AW} in Figure 3.3) may lead to further improvement with respect to the 1C model due to both a more coherent distribution of heat gains throughout the wall surfaces and the introduction of the radiative heat exchange between the inside surface of external walls and the surfaces of internal building components. The relative errors ε of both simplified models are presented graphically in Figure 3.6 for the 32 simulations of the apartment (with both orientations). Here, it is evident that the type of building structure does not significantly affect the accuracy of the simplified models in the heating mode, as the effect of climate conditions prevails. In fact, the blue indicators that represent the climate of Helsinki are always lower than the red ones that represent the climate of Palermo, while the green and the orange indicators are always somewhere in between. This holds true both for the 1C and 2C models, although the error of the former presents a higher dispersion. The improvement of the 2C model over the 1C one is evident for both seasons.

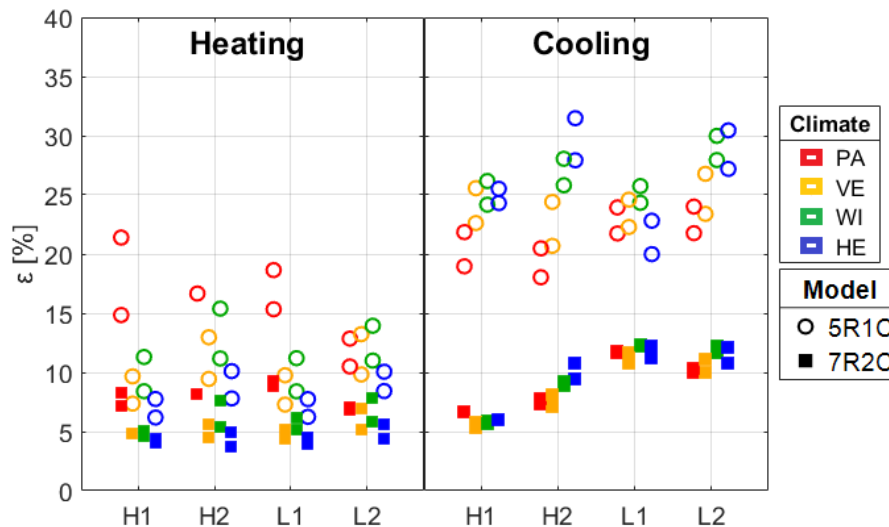


Figure 3.6 - The relative error ε in the heating and cooling seasons.

Figure 3.6 shows that while the error ε_{1C} of the 1C model shoots to very high values (20-30%) when the transition is made from the heating to cooling mode, the error ε_{2C} of the 2C model does not undergo such a sharp increase and always remains below the threshold of 12.5%. Contrary to what takes place in the heating mode, the type of building envelope does seem to affect the accuracy of the models during the warm season. Indeed, lightweight building structures present a higher error than heavyweight ones. This is particularly evident

when the error of the 2C model is compared, since ε_{2C} increases from 6-7% to 12% when there is low thermal insulation (i.e. from H1 to L1) and from 7-11% to 10-12% when it is high (i.e., from H2 to L2). This may be due to the difficulty that lumped capacitance models have in following the reaction of lightweight structures to rapid fluctuations of air temperature or heat gains.

3.2 District heating network model

The models have the same structure consisting of four consecutive blocks: network pre-processing, hydraulic balance, thermal balance and results post-processing. Since velocities do not depend on temperatures -as it happens in problems of natural convection-, the flow and pressure distributions can be calculated before setting the thermal balance. The model follows the same approach proposed by Guelpa et al [79].

3.2.1 Network pre-processing

The model uses graph theory to easily manage the complex topology typically introduced by networked systems. The DH system is described by a set of b oriented branches and n nodes that correspond to the pipes of the network and to their junctions, respectively. The *topological incidence matrix* A has a row for every node and a column for every branch. Each element $a_{i,j}$ is equal to +1 if i is the upwind (inlet) node for branch j , -1 if is the outlet node and 0 otherwise.

3.2.2 The hydraulic balance

Due to the incompressible nature of the heat carrier in modern DH systems –pressurized water-, two equations are sufficient to describe the flow and pressure distribution: the *continuity equation* and the *momentum equation*. The continuity equation (3.4) applies the law of conservation of mass to the i -th node of the network:

$$G_{i,in} - G_{i,out} = G_{i,ext} \quad (3.4)$$

G_{ext} is the $(n \times 1)$ vector of mass flow rates exiting/entering the system from/in the nodes. The momentum equation (3.5) applies the Navier-Stokes equations to the j -th pipe of the network including the effect of viscosity:

$$\Delta p_j = \frac{1}{2} \rho \left(f_j \frac{L_j}{D_j} + \beta_j \right) v_j^2 - \Delta p_{pump,j} \quad (3.5)$$

Velocities are linked to mass flow rates through Eq. (3.6)

$$G_j = \rho S_j v_j \quad (3.6)$$

By substituting Eq. (3.6) in Eq. (3.5), the following equation holds true:

$$\Delta p_j = r_j G_j^2 - \Delta p_{pump,j} \quad (3.7)$$

Where all the constant terms that refer to the j -th pipe are grouped into the constant r :

$$r_j = \frac{1}{2 \rho S_j^2} \left(f_j \frac{L_j}{D_j} + \beta_j \right) \quad (3.8)$$

Thus, all mass flow rates and pressures can be found by solving two systems of equations that can be written in matrix form as:

$$\mathbf{A} \dot{\mathbf{G}} + \dot{\mathbf{G}}_{ext} = \mathbf{0} \quad (3.9)$$

$$\mathbf{A}^T \mathbf{P} = \mathbf{r} \dot{\mathbf{G}}^2 - \mathbf{t} \quad (3.10)$$

Where G and P are the $(b*1)$ vector of mass flow rates and the $(n*1)$ vector of pressures, respectively. The heads provided by the pumps $\Delta p_{pump,j}$ are stored in the $(b*1)$ vector t . Thus, the overall system has $(n+b)$ equations and the same amount of unknown variables. These systems are coupled because the G appears in both equations. Moreover, the overall system is nonlinear because the pressure drops depend on the square of the flow rates. In order to solve the overall system represented by Eq. (3.9) and (3.10), the model uses the semi-implicit method for pressure linked equations, also known as SIMPLE method [80]. In this method, the pressure field is determined by first calculating an intermediate velocity field based on an estimated pressure field; and then obtaining appropriate correction so as to satisfy the continuity equation. The momentum equation is linearized by expressing the first term as product of a hydraulic resistance R (expressed in Eq. (3.8)) and of the mass flow rate G . Therefore Eq. (3.7) can be rewritten as:

$$\Delta p_j = R_j G_j - \Delta p_{pump,j} \quad (3.11)$$

In matrix notation:

$$\mathbf{A}^T \mathbf{P} = \mathbf{R}(\dot{\mathbf{G}}) \dot{\mathbf{G}} - \mathbf{t} \quad (3.12)$$

A guess-value vector for mass flow rates is used to calculate the ($b*b$) diagonal matrix of hydraulic conductances, Y , where $Y_{j,j} = 1/R_j$. Then, a guess-value vector for pressures P^* is assumed and used in Eq. 13 to calculate a new vector of mass flow rates G^* . Equation 3.13 is obtained by left-multiplying both members of Eq. 12 by Y :

$$G^* = Y A^T P^* + Y t \quad (3.13)$$

With this new vector G^* , the new conductance matrix Y^* can be calculated. Then, assuming that $Y=Y^*$ and using Eq. (3.9), both pressures and flows can be corrected simultaneously:

$$A Y^* A^T \Delta P^{corr} = -A G^* - G_{ext} \quad (3.14)$$

$$\Delta G^{corr} = Y^* A^T \Delta P^{corr} \quad (3.15)$$

The pressure correction can be obtained by solving the linear system represented by Eq. (3.14). Then, the resulting vector can be used to calculate the mass flow correction, as shown in Eq. (3.15). Finally, under-relaxation factors can be used to calculate the new vectors of G and P that can be used as inputs for the next iteration. The loop ends when the norm of the residuals of both G and P are lower than 0.01 kg/s and 50 Pa, respectively. Since the momentum equation provides pressure differences, the pressure in one node must be fixed as boundary condition. After convergence, the guess vectors for pressure and mass flow are updated using those of the previous time-step in order to reduce the computation time.

3.2.3 The thermal balance

Once the flow rates are determined for all pipes, the thermal block calculates the propagation of the temperature front(s) in the network and the heat loss to the surrounding ground. The thermal balance of the network results from the application of the conservation of energy to the n nodes of the network. The control volume of the i -th node corresponds to half of the volume of all pipes connected to it. Thus, we have n equations in n variables (the temperature in each node).

$$\frac{\partial(\rho c_p T_i)}{\partial t} \Delta V_i + \sum_j c_p G_j T_j = \sum_j \lambda_j \left(\frac{dT}{dx} \right)_j S_j + \phi_{V,i} - \phi_{L,i} \quad (3.16)$$

The second term of the equation represents the summation (with the correct sign) of the mass flows entering and leaving the i -th node through the pipelines connected to it, each of them at the temperature T_j . The mass flow rates G were already found by the hydraulic balance. On

the right member of the equation, we have a term corresponding to the thermal conduction along the pipes (neglected in our model), the internal generation of heat inside the control volume and the heat loss from the control volume to the ground, as in Eq. (17).

$$\phi_{L,i} = \sum_j \frac{1}{2} L_j \Omega_j U_j (T_i - T_\infty) \quad (3.17)$$

Thus, Eq. (3.16) becomes:

$$\rho V_i c_p \frac{\partial T_i}{\partial t} + \sum_j c_p G_j T_j = \sum_j \frac{1}{2} L_j \Omega_j U (T_i - T_\infty) \quad (3.18)$$

In Eq. (3.18) it can be seen that together with temperature T_i there are many temperatures T_j , that correspond to all the pipes connected to that node. Thus, the system can't be solved correctly unless a correspondence is set between temperatures of the branches (i.e. temperatures at the borders of the control volume of the nodes) and temperatures of the nodes. This correlation follows the first-order upwind (FOU) scheme. Given the flow velocity distribution, the temperature associated with each stream is equal to that of the upstream node. This discretization method gives a smoothed solution –see [81]– but assures ease of convergence to the thermal problem. The problem can be rewritten as follows:

$$m_i c_p \frac{\partial T_i}{\partial t} + k(T_i) = q \quad (3.19)$$

Where m_i is the mass of water enclosed in the i -th node –as defined above–, and k expresses the temperature of the branches in function of the temperature of the nodes. The known term q includes all those terms of the equation that do not depend on T_i . In matrix form, Eq. (3.19) becomes:

$$\mathbf{M} \frac{\partial \mathbf{T}}{\partial t} = \mathbf{q} - \mathbf{K} \mathbf{T} \quad (3.20)$$

Where \mathbf{M} is the mass matrix, and \mathbf{K} is the so called stiffness matrix. The mass matrix is a $(n \times n)$ diagonal matrix with the thermal capacity of the water volume enclosed in each node on the corresponding i -th entry of the diagonal. The stiffness matrix is the matrix form of function k . Thus, its elements $K(i,j)$ are not zero if the branch j is connected to node i or if i is the upwind node for branch j , according to the *upwind scheme*. The temperature at the inlet node

is fixed (*Dirichelet condition*). The first-order ordinary differential equation (ODE) (3.20) is solved by the well-known Runge-Kutta algorithm implemented in the ODE solver *ode15s* of Matlab [82]. The ODE solvers implemented in Matlab do not give the possibility to decide the time step used in the calculation. Therefore, the latter can only be checked after the solution has been calculated. Previous researchers have shown that numerical solutions based on finite difference schemes suffer from artificial diffusion [81]. Reducing the size of the spatial grid allows to increase the accuracy. However, the CPU time is approximately proportional to the square of the total number of grid points because when the grid size is reduced, the time step size has to be reduced, too.

3.2.4 Comparison with measured data

In the first part of the work, the models were used to reproduce the propagation of a temperature front in a 470 m long pre-insulated pipe, as logged during an experiment that was carried out by Ciuprinskas and Narbutis [83] on the district heating system of Vilnius (Lithuania) during May 1997. This dataset was already used by other researchers for comparing and validating thermal networks models ([84], [85]). A schematic view of the experimental site is depicted in Figure 3.7 [83]. The inlet temperature and the mass flow rate of both supply (case 1) and return (case 2) pipes are set as a boundary conditions and the resulting outlet temperatures are compared with the measured values. Due to the very low water velocity in the considered period (about 0.036 m/s), it takes hours for the temperature front to reach the pipe outlet.

Table 3.4 - Parameters of the pre-insulated pipes (valid for both cases).

Variable	Value
Pipe length, L (m)	470
Internal diameter of the pipe, d_i (mm)	312.7
External diameter of the pipe, d_e (mm)	323.9
Diameter of casing, D (mm)	450.0
Thermal conductivity of insulation, λ (W/(m K))	0.033
Thermal conductivity of the ground, λ_g (W/(m K))	2.0
Depth, z (m)	1.0
Temperature of the undisturbed ground, T_g (°C)	8.0

Table 3.5 - Boundary conditions.

Case	1	2
Initial temperature at inlet node, $T_{st,in}$ (°C)	67.7	64.1
Initial temperature at outlet node, $T_{st,out}$ (°C)	66.3	62.6
Mass flow rate (constant),	2.646	2.646

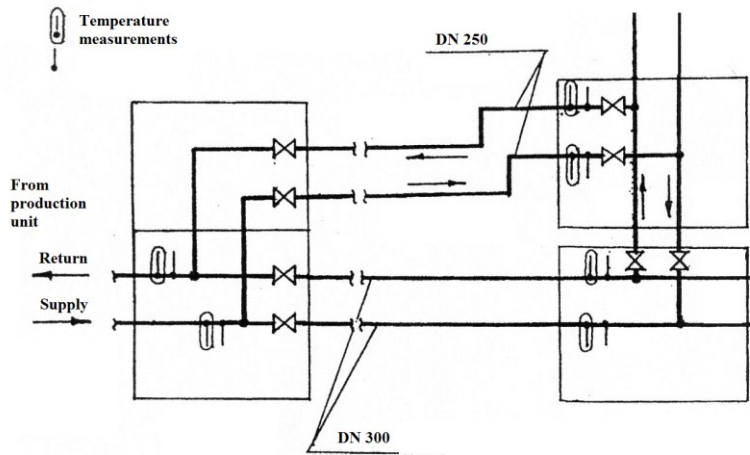


Figure 3.7 - Schematics of the experimental site (taken from [83]).

This unusual condition affects the accuracy of the models as discussed in [84]. The parameters and the boundary conditions used in the simulations are reported in Tables 3.4 and 3.5, respectively. The time-step of simulation is 5 minutes and the sample-time of the dataset is 10 minutes. Values at times between two consecutive loggings were interpolated linearly. In order to simulate the propagation of the temperature front in a single pipe, the pipe was discretized into sub-pipes in the pre-processing phase. The Courant number -Eq. (3.21)- is the ratio between the velocity of the flow and the velocity at which the system is “observed”. The latter is the ratio between the length of the pipe elements and the time step of the solver and thereby depends on how the system is discretized in time and space.

$$Co = \frac{v \Delta t}{\Delta x} \quad (3.21)$$

where v is the flow velocity, Δt is the simulation time step and Δx is the discretization interval of the pipe branches, i.e. the spatial resolution of the grid. The *Courant–Friedrichs–Lewy (CFL) condition* is a necessary condition for the convergence of partial differential equations solved by explicit finite difference schemes; this condition for one dimensional models reduces to $Co < 1$. This means that the velocity of the observer must be greater or equal than the velocity of the flow. If this condition is not met, finite difference schemes based on explicit integration are unstable. The solution is unstable when the errors made at one time step of the calculation are magnified as the computations are continued. The model presented here uses an implicit method, that is not sensitive to stability issues. However, although the CFL condition must not be necessarily met, the accuracy of the numerical solution depends on the resolution of the grid. An accurate discretization of the system help reducing numerical diffusion

at the expense of a higher computation time, as discussed above. The temperature wave obtained with the model and with the measurements have been adimensionalized with Eq. (22), as suggested in [84]

$$T_{d1} = \frac{(T_{tr} - T_{st})_{out}}{(T_{tr,max} - T_{st})_{in}} \quad (3.22)$$

where T_{tr} is the temperature during the transient period, T_{st} during steady state. Since the measurements were likely affected by thermal stratification due to very low velocities [85] according to the criteria given in [86], the peak temperature of the wave at pipe outlet was not considered as a reliable indicator. The accuracy was assessed by measuring the time of wave start and the wave width. The time of wave start was considered as the time when the adimensionalized wave reaches 0.05, and the wave width was measured at $T_{d1} = 0.20$. Ten simulations were carried out: five with $\Delta t = 30$ s and five with $\Delta t = 300$ s. In every simulation the pipe was modelled using different number of nodes. The Courant number was varied from 0.04 to 2. Figure 3.8 shows the temperature values at the outlet of the supply pipe with the two considered time steps. It can be seen that by increasing the number of nodes from 3 to 21 there is a significant improvement both in terms of phase and of wave amplitude. Due to the aforementioned effect of thermal stratification, it is difficult to understand whether the case with 46 nodes brings a further improvement. According to the criteria given in [86], the cross-sectional temperature difference could reach 50% of the wave amplitude under the considered conditions. The modelled temperature front arrives at pipe outlet long before the real front if the pipe is not discretized with a sufficient number of nodes. The discrepancy from measured values is also evident in terms of wave width –see Table 3.6. However, the computational time increases with the number of nodes, as shown in Table 3.6 and Figure 3.9. In Table 6 the computational time is also split between the hydraulic calculation (the SIMPLE loop) and the thermal calculation (that includes both the calculation of the stiffness matrix K and the numerical solution of the ODE equation).

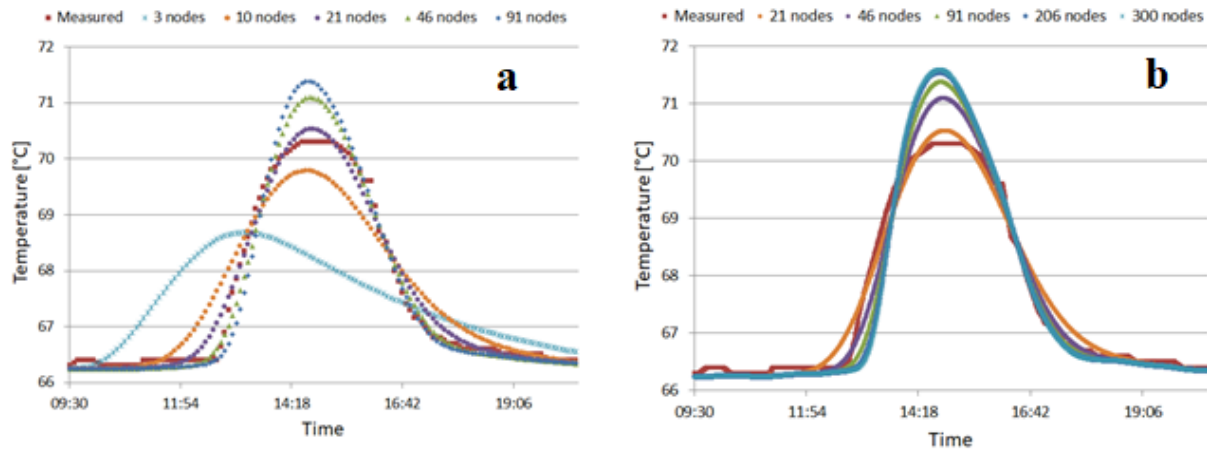


Figure 3.8 - Measured data at pipe outlet versus models with (a) $\Delta t = 300$ s and (b) $\Delta t = 30$ s.

For a given Courant number, the CPU time increases linearly with the number of time steps. The CPU time is spent mostly in the thermal balance when the number of nodes is low. When the latter grows, the hydraulic calculations become predominant and most of the time is spent to reach the convergence of the SIMPLE algorithm. Figure 3.9 also shows that it is counter-productive to refine the mesh above a certain Courant number, because it leads to unnecessarily high CPU time without improving the accuracy of the results. The solution seems to get even worst for Courant number higher than 1 (with $\Delta t = 300$ s) or higher than 0.1 (with $\Delta t = 30$ s).

Table 3.6 - Resume of accuracy and computational time.

Time step, Δt (s)	Number of nodes	Courant number, Co	Error start (min)	Error width (min)	CPU time (s) – hydro	CPU time (s) - therm	CPU time (s) – total
300	3	0.04	-135	100	0.39	2.47	3.18
	10	0.20	-55	60	0.71	3.00	4.04
	21	0.45	-25	25	1.55	3.31	5.18
	46	1.01	-5	0	2.97	3.98	7.26
	91	2.02	10	-10	9.34	5.61	15.3
30	21	0.04	-25	23.5	11.1	16.2	29.9
	46	0.10	-4	0.5	24.7	22.9	50.0
	91	0.20	9	-11	85.3	42.2	130
	206	0.46	18	-19.5	448	112	564
	300	0.67	21	-21.5	1255	251	1509

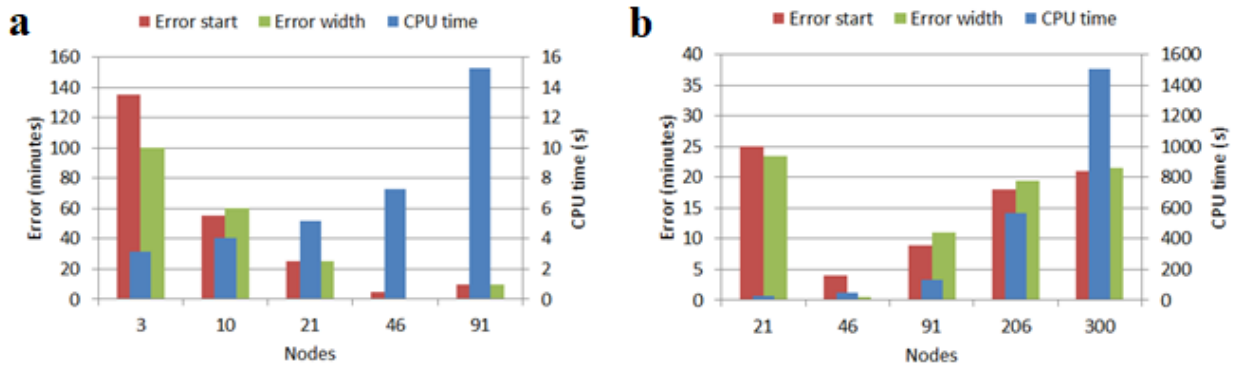


Figure 3.9 - Error of the models and computational time with (a) $\Delta t = 300$ s and (b) $\Delta t = 30$ s.

The simulations were run on a computer equipped with an Intel Core i7-4510U with 2.0 GHz (with Turbo Boost up to 3.1 GHz) and a 8 GB DDR memory.

3.3 Heat pump model

A TRNSYS Type was developed ad-hoc for this study to allow a full integration of the heat pump model in the TRNSYS environment, thereby making it possible to run several simulations in a short time. The model of a water to water heat pump was written in FORTRAN and a DLL was then compiled with Microsoft Visual Studio 10.

3.3.1 Description of the model

The heat pump model works either in SH-mode (space heating mode) or in DHW-mode, as it happens in the operation of heat pumps with a conventional regulation. The model calculates the heat flow rate at the evaporator and the electrical consumption of the compressor according to the parameters of the performance curves provided by the manufacturer, that are read by the heat pump Type from an external file. The curves are polynomial functions of the evaporating and condensing temperature, as shown in Equations (3.23-24).

$$W_{el,k} = a_0 + a_1 T_{ev} + a_2 \cdot T_{cd} + a_3 T_{ev}^2 + a_4 T_{ev} T_{cd} + a_5 T_{cd}^2 + a_6 T_{ev}^3 + a_7 T_{ev}^2 T_{cd} + a_8 T_{ev} T_{cd}^2 + a_9 T_{cd}^3 \quad (3.23)$$

$$Q_{ev} = b_0 + b_1 T_{ev} + b_2 T_{cd} + b_3 T_{ev}^2 + b_4 T_{ev} T_{cd} + b_5 T_{cd}^2 + b_6 T_{ev}^3 + b_7 T_{ev}^2 T_{cd} + b_8 T_{ev} T_{cd}^2 + b_9 T_{cd}^3 \quad (3.24)$$

The heat flow rate at the evaporator and the mechanical power of the compressor are then summed up to give the thermal capacity of the heat pump Q_{cd} , i.e. the heat flow rate available at the condenser. A global efficiency of $\eta_{el} = 0.95$ was assumed for the motor that drives the

compressor. The remaining 5% of electrical power is considered as a loss in the conversion from electrical to mechanical energy and is therefore not available at the condenser, as in Eq. (3.25). The coefficient of performance of the heat pump is defined as the ratio between the heat flow delivered from the condenser to the building and the electrical work of the compressor -see Eq. (3.26).

$$Q_{cd} = Q_{ev} + \eta_{el} W_{el,k} \quad (3.25)$$

$$COP = \frac{Q_{cd}}{W_{el,k}} \quad (3.26)$$

The pressure drop in the condenser and in the evaporator are not considered. Therefore, the phase change is considered as an isothermal process. The evaporating temperature of the refrigerant T_{ev} depends on the inlet temperature and on the mass flow rate of the water in the evaporator –see Equations (3.27) and (3.28).

$$T_{w,ev_out} = T_{w,ev_in} - \frac{Q_{ev}}{\dot{m}_{w,ev} c_{p,w}} \quad (3.27)$$

$$T_{ev} = T_{w,ev_in} - \frac{T_{w,ev_in} - T_{w,ev_out}}{\varepsilon_{ev}} \quad (3.28)$$

The condensing temperature depends on the set point temperature of the water at the condenser outlet $T_{su,set}$ and on the approach point $\Delta T_{cd,ap}$. In this case, the water at the condenser inlet $T_{cd,in}$ is the return temperature from the building, which is a dependent variable. Thus, the Equations (3.29-31) hold true for the condenser in SH-mode.

$$T_{w,cd_out} = T_{su,set} \quad (3.29)$$

$$T_{cd} = T_{w,cd_out} + \Delta T_{cd,ap} \quad (3.30)$$

$$T_{w,cd_in} = T_{w,cd_out} - \frac{Q_{cd,bui}}{\dot{m}_{w,cd} c_{p,w}} \quad (3.31)$$

Otherwise, if the machine is producing heat for the DHW tank, the condensing temperature depends on the return temperature from the DHW storage tank, T_{w,hs_ret} . In this case the outlet temperature and heat flow rate at the condenser are outputs of the model. Thus, the behaviour of the condenser in DHW mode is governed by Equations (3.32-34).

$$T_{w,cd_in} = T_{w,hs_ret} \quad (3.32)$$

$$T_{w,cd,out} = T_{w,cd,in} + \frac{Q_{cd}}{\dot{m}_{w,cd} c_{p,w}} \quad (3.33)$$

$$T_{cd} = T_{w,cd,in} + \frac{T_{w,cd,out} - T_{w,cd,in}}{\varepsilon_{cd}} \quad (3.34)$$

Since the variable heat load influences the temperature drop in the condenser and in turn the condensation temperature, at each time step the thermal capacity and the power consumption of the compressor are iteratively calculated until the condensing and evaporating temperatures converge to stable values. The two heat exchanger are modelled assuming a constant effectiveness ε – common assumption for heat pumps, see for instance [87]. This assumption relies on the fact that in usual working conditions, the heat transfer of the refrigerant in both heat exchangers is mostly isothermal and only a negligible part of the heat exchange surface is occupied by superheated gas. A maximum condensing and evaporating temperature is set according to the feasible operation domain of the selected compressor. Dynamic effects are not considered in the current version of the model. One may argue that the flow of calculation in SH-mode does not follow the physical flow as it does in DHW-mode. This choice was deliberately taken to utilize the heat load profile of the building as input for the heat pump model.

3.3.2 Comparison with measured data

The model was validated using data from a water to water heat pump specifically designed for high temperature applications in the lab of a local heat pump manufacturer. All the details of the considered machine are specified in [88]. Figure 3.10 shows a picture of the prototype.

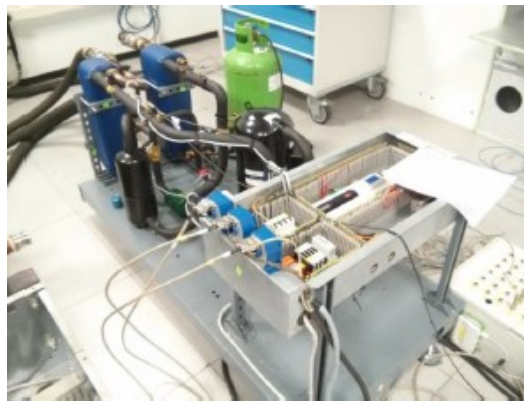


Figure 3.10 - The heat pump prototype.

The heat pump is equipped with a scroll compressor and the working fluid is R134a. The performance of the machine was tested in seven working conditions, obtained by changing the temperature of the water at the condenser inlet $T_{w,cd,in}$ and the mass flow rate of water in the

condenser $\dot{m}_{w,cd}$. The mass flow rate and the inlet temperature of the water in the evaporator were kept almost constant. Table 3.7 summarizes the working conditions and performance logged during the experiments. It is worth noting that all the tests were run under full load condition.

Table 3.7 - Summary of measured data on the heat pump prototype.

Test	1	2	3	4	5	6	7
$T_{cd,in}$ [°C]	54.9	60.9	67.1	50.1	44.9	44.7	44.7
$T_{cd,out}$ [°C]	65.1	70.6	76.3	60.6	55.6	60.7	65.7
$\dot{V}_{w,cd}$ [l/h]	2400	2390	2415	2420	2315	1540	1140
$T_{ev,in}$ [°C]	38.3	38.1	38	38.2	37.9	38.1	38.1
$T_{ev,out}$ [°C]	28	28.6	29.6	27.4	26.7	27.2	27.8
$\dot{V}_{w,ev}$ [l/h]	2056	2041	2035	2027	2024	2020	2020
T_{cd} [°C]	64.1	69.6	75.1	59.6	55.3	59.1	63.3
T_{ev} [°C]	26.6	27.2	28.3	25.8	25.3	25.8	26.3
$T_{k,out}$ [°C]	73.6	77.8	83.2	70.5	65.6	68.6	71.8
Q_{cd} [kW]	28.0	26.6	25.5	29.1	28.5	28.4	27.5
Q_{ev} [kW]	24.5	22.4	19.7	25.3	26.2	25.4	24.0
$W_{k,el}$ [kW]	5.84	6.56	7.34	5.22	4.78	5.15	5.65
COP [-]	4.80	4.06	3.48	5.57	5.96	5.51	4.86

It was assumed to have an approach point of $\Delta T_{cd,ap} = 1$ K at the condenser and an evaporator with an effectiveness $\varepsilon_{ev} = 0.7$. Figure 3.11 shows the comparison between measured data and model output (in SH-mode) for the heat flow at the evaporator, the electrical power consumed by the compressor and the COP of the heat pump.

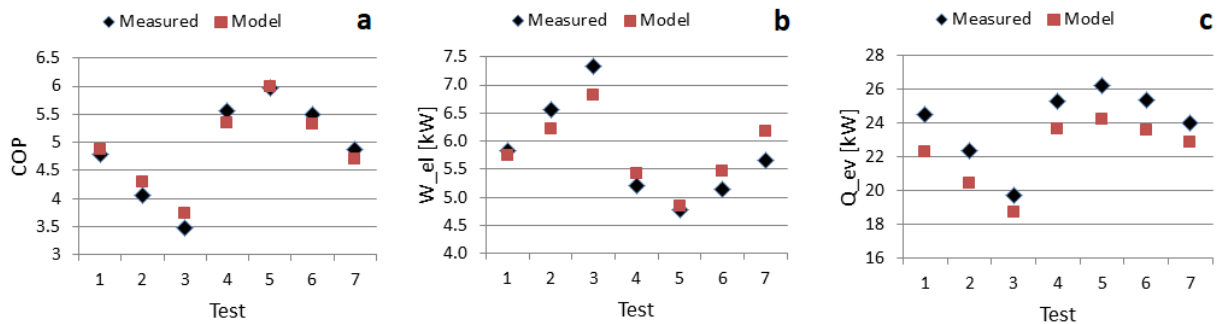


Figure 3.11 - Measured data versus model output: (a) COP, (b) $W_{k,el}$, (c) Q_{ev} .

Figure 3.11 shows that the model is able to follow the trend of all the considered variables. The COP is slightly overestimated by the model in tests 1, 2 and 3, i.e. those with the highest temperatures in the condenser. In tests 6 and 7, i.e. those with a significant reduction of water mass flow rate in the condenser, the model overestimates the electrical consumption of the

compressor. In all the considered cases, the model underestimates the heat flow at the evaporator. The RMSE, i.e. the deviation of the model from the data over the sample of 7 measurements, is 0.18 for the COP, 0.34 kW for the power consumption of the compressor $W_{k,el}$ and 1.73 kW for the heat supplied to the evaporator.

3.4 Discussion

The modular structure, the level of physical simplification and the user-friendliness of the interface makes it possible to merge the models into an energy-system-wide simulation environment including the buildings, the substations, the thermal network and the heat supply units. Although the construction of such a tool goes beyond the scope of the thesis, the models have been combined in different ways: the preliminary analysis described in Chapter 5 uses both the 5R1C lumped-capacitance model to calculate the heat load of the neighbourhood with hourly time step and the district heating network model in the “steady-state” version. In the parametric study that follows the heat pump model is used in TRNSYS Simulation Studio together with heat load profiles previously obtained by other TRNSYS simulations. In Chapter 6 the loads are instead obtained from a dataset of another DH network. The thermal network model utilized is *spHeat*, that was already implemented in a TRNSYS type. The combination of the thermal network model and of the heat pump model allowed to consider the impact of supply network temperature on the electricity consumption of the heat pumps.

Chapter 4 Case studies

Two case studies are considered in this work. The first is an area in the North of Italy with a huge unexploited thermal energy potential. Section 4.1 quantifies the potential of the heat source with an analysis on historical data and on-field measurements. A qualitative description of the building stock is included, that will be later used as an input for quantifying the heat demand of a representative neighborhood in Chapter 5. Section 4.2 briefly describes a representative district heating network and the low temperature heat sources that will be utilized as a case study in Chapter 6.

4.1 Case study 1: Abano Terme (Italy)

The Section presents the particular situation of Abano Terme, a Municipality situated in a well-known geothermal area in the North-East of Italy. In the first three parts, attention is paid on the low temperature heat source. In the fourth part, the building stock of a real neighbourhood close to the city centre is described.

4.1.1 Background

Abano Terme is the main Municipality of the Euganean Thermal Basin (ETB), situated 10 km south-west of Padova. The ETB is an attractive site for the expansion of geothermal resource utilization due to presence of groundwater at temperatures going from 60 to 87°C at depths of 300-500 m [89]. The thermalism originates in the Pre-Alps about 100 km north-west of the hotspot, where rainwater infiltrates and reaches depths of 3000–4000 m, is warmed up by the normal geothermal gradient, and circulates towards the South East, flowing through a complex of hills, namely Lessini, Berici and Euganean Hills. The structural shape of the latter leads to a rapid ascent of the fluids and to temperature homogenization, which is linked to the presence of convective motions. Aside fractures and faults in the structure of the Euganean

Thermal Basin (ETB), other factors facilitate upwards movement, such as the side of the system being sealed with low permeability sediments and the hydraulic load being generated by cold groundwater. The first researchers to propose the meteoric origin of the groundwater in the ETB were Piccoli et al. [90], that reached this conclusion on the basis of a detailed geological knowledge of the region, hydrogeological and geophysical studies, and above all, data on oxygen-18 isotopes and saltwater contents. Figure 4.1 shows the path of the groundwater towards the ETB. The hypothesis was confirmed by later studies, such as [91], and is today widely accepted in the scientific community.

The thermal properties of the water in the Euganean area were known to the ancient Romans, but they were only marketed on a large scale at the beginning of the 20th century. During the 1960s, artesian wells stopped the natural outflow of thermal water and pumps were used to extract thermal water from the sandy aquifers in the alluvial cover [92]. Due to its economic and environmental importance, in 1966 the Italian Department of Industry decided to impose a united management of the local geothermal resources. Only after that date piezometric levels over the entire region together with the total production of hot waters began to be systematically monitored and recorded. The volume of water pumped in the two urban centres of Abano Terme and Montegrotto Terme in the period 1978-1992 -satisfying the demands from more than 2 million daily visitors per year- was about 20 million m³/year with a maximum of over 25 million in 1985 [93]. The exploitation was mainly concentrated in such area of about 20 km², the entire basin being about 30 km² wide. The average piezometric level trend showed in the same period not only a progressive reduction but also clear seasonal cycles as a consequence of the corresponding demand and touristic flow [94].

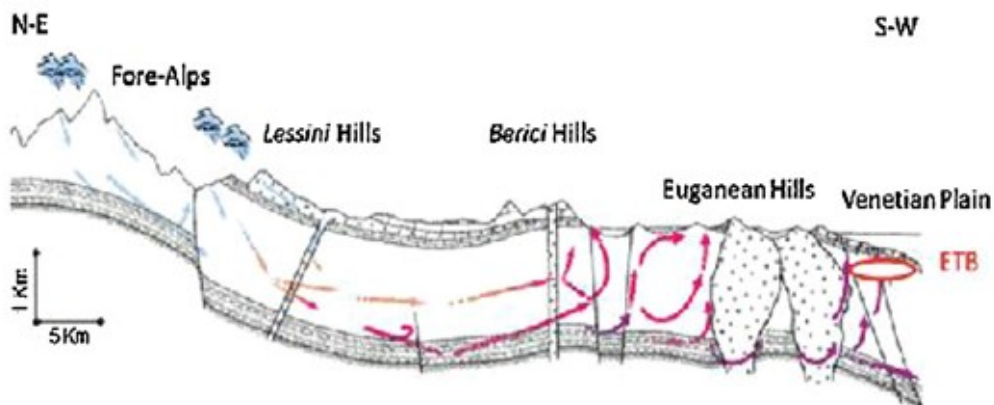


Figure 4.1 - Hydrothermal circuit of groundwater reaching the ETB [90].

It was evident how quick the system could reply to substantial variations of the volume of water withdrawn. This would suggest that aquifers are in general rapidly and continuously supplied with the previously described deep circulation system. Therefore, their exploitation is possible, but only partially and under controlled conditions [93]. Indeed, it was estimated that, if all the wells were shut down, there would be a sudden recovery of the piezometric head up to above the ground level [93]. The high withdrawal of groundwater during the boom of thermal tourism overtook the recharge rate, thus causing subsidence [93]. Subsidence rates exceeded 20 mm/year in the recent past, with an average of 15 mm/year between 1970 and 1986 and progressively decreasing towards 3-4 mm/year between 1992 and 1996 [95]. The land-subsidence phenomenon, which normally takes long time to fully develop, in the ETB was speeded up by the presence of hot groundwater: lower water viscosity and specific weight at high temperature imply higher permeability and thus higher rate of consolidation [93]. The comparison between measurements and models suggests that the phenomenon is now being exhausted [93]. The deepening of the wells contributed to this trend, as water could be drawn directly from the fractured rock [92] and not from aquifers. Nowadays, about 134 mining claims have been issued in the area and more than 400 groundwater wells have been drilled, of which about 250 are currently under exploitation [89].

This overview was necessary to stress the dynamic nature of the hydrothermal system, that rapidly responds to variations of water withdrawal. At the same time, the touristic business born around the therapeutic properties of the groundwater has brought economic wealth in the area. In light of these reasons, the management of the hydrothermal area has been demanded to a regional regulation Authority (named G.U.B.I.O.C.E.) and the priority on thermal water utilization was given to health-related activities by a Regional Law [96], thus limiting the possibilities of exploitation of its thermal energy content for other purposes such as space heating.

4.1.2 Thermal water withdrawal: historical data

In order to estimate the thermal energy potential of the area, a qualitative monthly profile of the groundwater extracted was estimated and compared to the estimated heat demand of the residential building stock of Abano Terme. Figure 4.2a shows the total amount of water extracted in Abano Terme in the period 2006-2013 (from G.U.B.I.O.C.E.). Figure 4.2b shows an estimated monthly profile of thermal water withdrawal in the Municipality of Abano Terme. The annual amount was evaluated as the average over the period 2006-2013, i.e. 7.8 million

m³/year. The profile was instead obtained from a monitoring of the volumes withdrawn by five hotels of the area in the period 2007-2009. The extraction temperature varies between 60°C and 87°C depending on the position of the well. The use of thermal water for space heating, swimming pool warming and mud maturation cools down the water and then the latter is released either in open canals or in a drainage system where it is mixed with grey water.

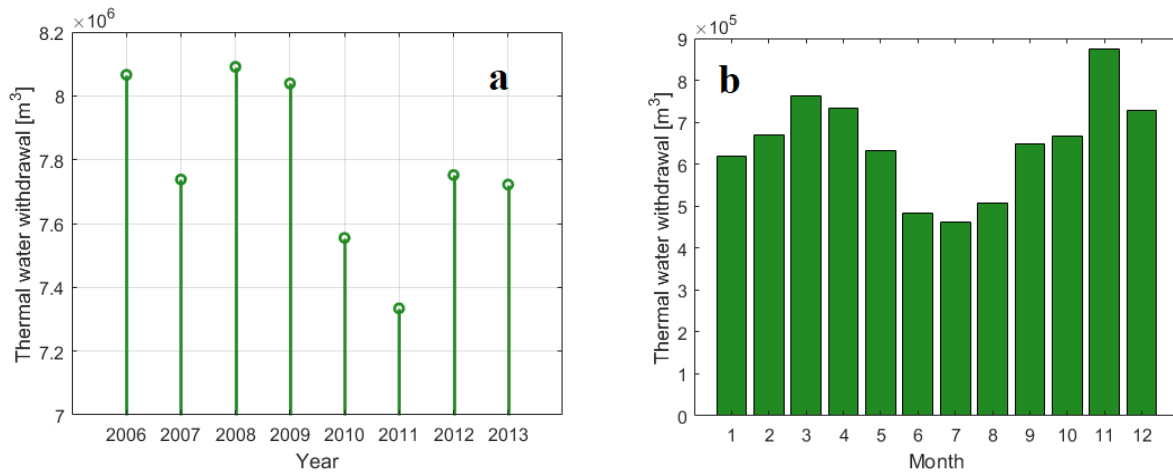


Figure 4.2 - (a) Annual volumes of groundwater extracted in Abano Terme between 2006 and 2013; (b) estimated mean monthly profile.

The water withdrawal is not constant throughout the year. The amount of water pumped from the wells is high during the touristic season (spring and autumn) and lower during summer and winter. In fact, the water is used not only to warm up the hotels and the swimming pools, but also to produce therapeutic mud through a mud maturation process. The thermal mud is a natural product derived from the long mixing of clay and thermal water. During its maturation, organic substances are provided by the microalgae contained in the groundwater, thus providing therapeutic properties to the resulting mud [97].

4.1.3 Thermal water withdrawal: on-field measurements

The discharge temperature and the mass flow rate of extracted water were monitored during the heating season 2015/16 in two hotels of the ETB, one in Abano Terme and the other in Montegrotto Terme. The equipment used in the monitoring campaign has been summarized in Table 4.1. In Abano Terme, the mass flow rate extracted from the well (see Figure 4.3a) within the concession “Molino” and successively used by hotel “Ariston Molino Buja” was monitored from 16/12/2015 to 16/5/2017. During the winter period, the discharge temperature of the water was monitored in the drainage system in proximity of the discharge from the hotels (see Figure 4.3d).

Table 4.1 - Instruments used in the monitoring campaign.

Commercial name	Description	I/O	Accuracy
AP501, Automation Progetti	Electromagnetic Flowmeter (calibrated)	4-20 mA	$\pm 0.15\%$
P1AS3000	Waterproof Pt100 temperature sensor	Pt100	$\pm 0.15 \text{ K @ } 0^\circ\text{C}$ $\pm 0.45 \text{ K @ } 150^\circ\text{C}$
Microtemp, Madgetech	Waterproof data logger with embedded IC temperature sensor, AISI 316	Digital	$\pm 0.5 \text{ K}$
LogBox, Novus	IP65 IR communication with PC via software (LogChart)	4-20 mA, 0-12 V, Pt100 (other inputs not used)	$\pm 0.2\%$ of full scale for Pt100, voltage and current

During spring, it was possible to monitor the temperature of two hot water pools where the thermal water is collected before being released into the drainage system. One of the pools is uncovered, thus being prone to further cooling in case of rain, and one is instead covered (Figure 4.3c).



Figure 4.3 - (a) Thermal water well; (b) hot water pool for mud maturation with mechanical displacement of the clay; (c) hot water pool for mud maturation; (d) drainage system discharge into open canals.

The mass flow rate of the extracted groundwater extracted was logged with 1 minute time step. Figure 4.4 shows the average hourly values over the whole monitored period. The velocity of the pump is regulated through an inverter by the hotel technicians following the touristic seasonality: from Christmas holidays to the beginning of March it is still at 50% of the nominal value. Intra-day variations in the order of 1 l/s are evident and probably depend on head variations due to simultaneous withdrawal from other wells.

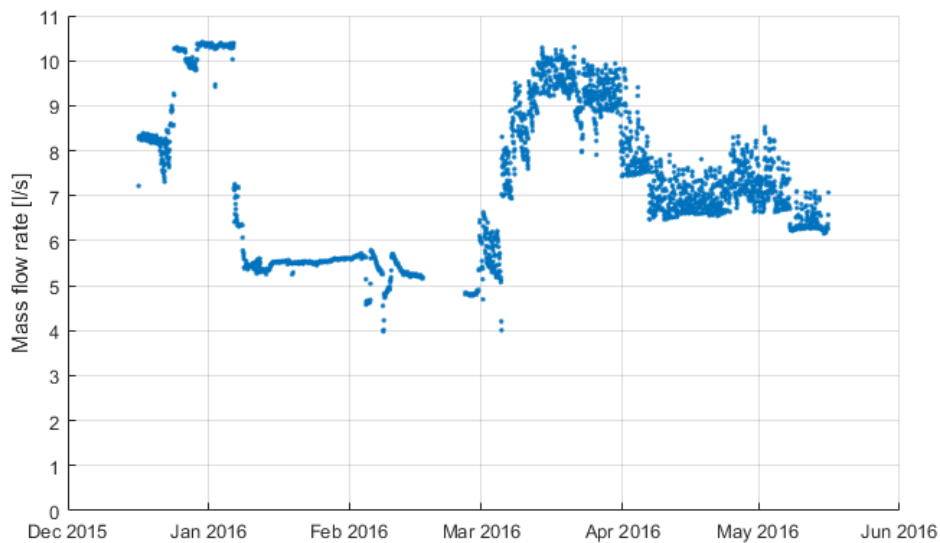


Figure 4.4 - Hourly average mass flow rate extracted from 16/12/2015 to 16/5/2016.

The temperature of the thermal water before the discharge was monitored from 7/3/2016 to 12/4/2016 (see Fig. 4.5a) in the hot water pool shown in Figure 4.3c and from 12/4/2016 to 5/5/2016 (see Fig. 4.5b) in an open-air hot water pool uncovered from rain.

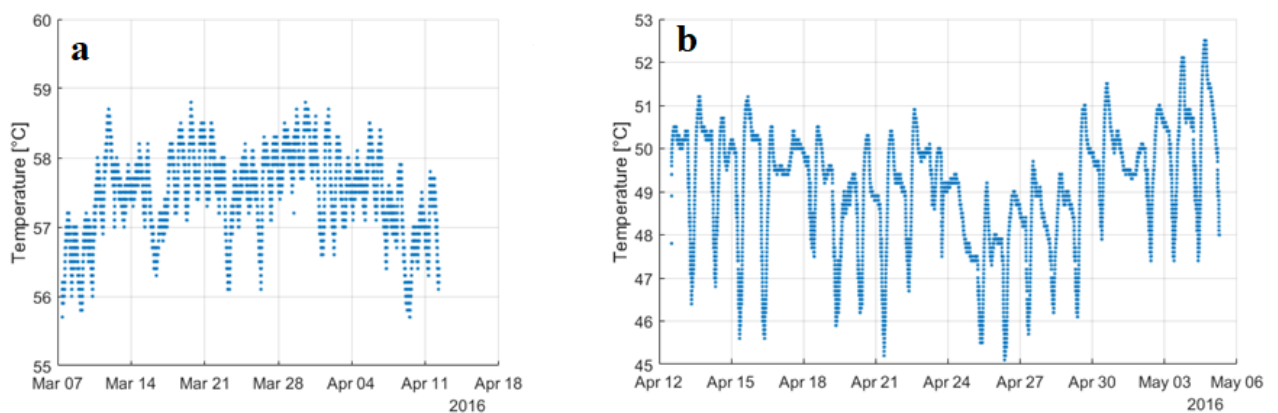


Figure 4.5 - Temperature of the water in the (a) covered and (b) uncovered thermal water pool.

During the winter period (from 23/12/2015 to 25/1/2016), it was only possible to monitor the temperature of the water in a canal in proximity to the discharge of the drainage system supplied by the wastewater of all the hotels of the area. However, this temperature must be considered as a “lower limit” to the available temperature since the thermal water is mixed with grey water and meteoric water during rainy days. These measurements are reported in Figure 4.6. A part from four drops in temperature that likely depend on mixing with rain or water from other sources, the temperature coming from the drainage system almost never goes below 40°C. During the remaining periods, the average temperature is around 43.2°C. Due to absence of thermal insulation, it is possible to consider 45°C as a reliable lower limit to the temperature of the waste water available during the heating season. Measurements from the pipelines of the circuit for space heating and swimming pool warming are missing to have a complete overview. However, from the measurements of the hot water pools for mud maturation commented above, it emerges that most of the heat loss occurs due to heat exchange with the air, leading to evident temperature drops in the night. Therefore, it is conceivable to suppose that by containing the process in prefabricated buildings or greenhouses, discharge temperatures of at least 55°C could be easily achieved.



Figure 4.6 - Temperature in the drainage system of Abano Terme.

Similar conclusions can be done by observing the measurements in Montegrotto Terme, where the temperature of the thermal water in uncovered water pools is at even higher temperatures. All the measurements –including those in Montegrotto Terme are summarized in Table 4.2.

Table 4.2 - Summary of measured values during the monitoring campaign.

Municipality	Variable	Position	Period	Average	Standard deviation
Abano Terme	Mass flow rate (l/s)	Well	16/12/15-16/5/16 (23/12/15 - 7/1/16)	6.83 (9.91)	2.01 (0.94)
		Well	23/12/15 - 7/1/16	83.3	0.3
	Temperature (°C)	Covered pool	7/3/16 – 12/4/16	57.5	0.6
		Uncovered pool	12/4/16-5/5/16	49.2	1.3
Montegrotto Terme	Temperature (°C)	Drainage system	23/12/15 – 25/1/16	42.6 (43.2)	2.6 (1.0)
		Uncovered pool	26/2/16 – 18/3/16	52.6	3.8
		Uncovered pool	12/4/16 – 23/4/16	61.7	3.8
		Open canal	23/12/15 – 25/1/16	36.3	2.2

4.1.4 The building stock

In Italy, the first Law was issued in 1976 (L. 373/76) [98]. Before that date, there was no constraint on the energy efficiency of buildings. Starting from 1976, a penalty was foreseen in the event of non-compliance with a minimum degree of thermal insulation and efficiency of the HVAC system. Later on, this Law was updated by considering a dispersion coefficient, function of the climatic zone and of the shape factor of the building. However, the most important regulatory step towards energy efficient buildings was done in 1991, with Law n. 10 [99]. This Law imposes to draw up a document with the energy balance of the building during the winter season and sets new thresholds for the energy performance of buildings. The last important step on the energy performance of buildings was done in 2005 with D.Lgs. 192/05, that sets severe requisites in terms of thermal insulation and energy efficiency [100]. Moreover, it prescribes criteria for the improvement of the energy performance of existing buildings and for the integration of renewable energy sources (RES), thus implementing Directive 2002/91/CE [101].

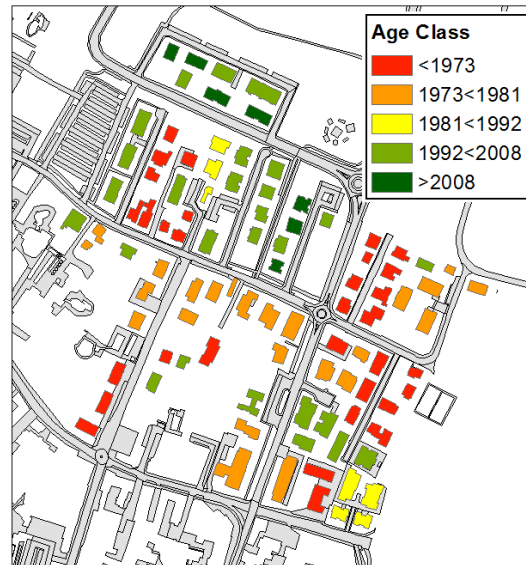


Figure 4.7 - Neighbourhood in Abano Terme with buildings grouped by age class.

In order to analyze the composition of the building stock, an area of approximately 0.25 km² close to the city center of Abano Terme has been analyzed. In particular, vector based topographic maps available on “Carta Tecnica Regionale”, an online open-source GIS tool of the Veneto Region [102] and aerial photos available in the cadastral archive of the Municipality of Abano Terme of different ages have been compared to determine the age of construction of 98 buildings. As explained in Chapter 3.1, the model for calculating the heat demand of the buildings uses a limited number of archetypes that define the envelopes of the considered buildings. The division into age classes must therefore be coherent with the regulation in force at time of construction. According to the available aerial photos, the buildings of the aforementioned neighborhood could be grouped into five age classes. Table 4.3 shows the five periods and the reference regulation. The time windows of construction year and regulation are not exactly overlapping. However, the chosen periods allow to have a representative description of the building stock. The different colors in Figure 4.8 allow to visualize the age distribution of the buildings in the neighborhood.

Table 4.3 - Classification of the buildings per “age class”.

Age of construction	Buildings [-]	Gross heated volume [m ³]	Reference regulation
<1973	32	54910	-
1973<1981	23	61865	-
1981<1992	8	15165	L. 373/76
1992<2008	27	57470	L. 10/91
>2008	8	15260	DPR 59/09
TOTAL	98	204670	-

4.2 Case study 2: Aarhus South-West (Denmark)

The second case study differs from the first one because the low temperature heat source is considered as an additional heat source that integrates a conventional heat supply system. While case study 1 will be used to study the planning and design of a small network supplied entirely by low temperature heat sources –Chapter 5-, this case study will be used to study a control problem where uncontrolled, distributed substations supply heat to the network from low temperature heat sources –Chapter 6. The low temperature heat distribution and use of distributed heat pumps is a common feature for both case studies.

4.2.1 Background

This case study comes from a European project, named FLEXYNETS, aimed at developing a new generation of intelligent district heating and cooling networks. The FLEXYNETS concept is a generalization of the district heating network with booster heat pumps. The energy transportation losses are reduced by working at “neutral” (15-20°C) temperature levels and reversible heat pumps are used to exchange heat with the DHC network on the demand side, providing the necessary cooling and heating for the buildings. In this way, the same network can provide contemporary heating and cooling. Moreover, the heat normally rejected by buildings (for example through a common split unit), can be fed into the network by the heat pumps (which are working in “cooling mode”) and recycled by other heat pumps that are producing domestic hot water. In the same way, these networks allow to recover and recycle the waste heat available along the network path, even at very low temperatures, contrary to traditional District Heating Networks, that can harvest thermal energy only at high temperature (usually higher than 100°C). In the FLEXYNETS concept, it is possible to reuse the waste heat e.g. from supermarkets’ chillers, data centres and several industrial processes. Moreover, working at low temperature reduces the heat losses to the ground, thus increasing the network efficiency. This system does not substitute nor is opposed to traditional district heating networks. In urban contexts not exploiting district heating yet, this new generation networks can represent the main heating and cooling system. In cities already making use of district heating, low temperature DHC networks can use thermal energy from the return pipes (in addition to waste heat), which otherwise is considered as waste heat by the network utility. This allows them temporarily to sell additional energy with the same infrastructure and makes the network more efficient, reducing the return temperature to the station.

The project includes several work packages aimed at investigating different aspects of the system, such as its planning, design, control, trading of heat etc. The case study presented here is thoroughly described in work package 3, “Integration of energy sources and sinks in DHC networks” [12].

4.2.2 The DH network and the heat demand

In the town of Aarhus, more than 90% of the municipal residents are connected to the DH network. Customers range from large housing companies to single-family houses. In addition, DH is delivered to several neighbouring municipalities. Most of the heat is purchased by the local transmission company which purchases heat from heat producers. The existing DH utility in Aarhus is utilizing some excess heat from the harbour area to the east in the city. Even though some excess heat is utilised, this is still only a fraction of the total heat production (less than 100 GWh in 2016) in the existing network.

In the context of FLEXYNETS WP3, the building stock of the whole city was divided into ten building typologies, each having a specific heat demand [12]. This analysis relied on the Danish Heat Atlas, a GIS-based database with extensive information about more than 2.5 million buildings in Denmark [103]. A representative area in the south-western part of the city was selected, as shown in Figure 4.9. The case study used in this thesis corresponds to approximately one third of this area. In order to aggregate the demands from the Aarhus SW area to maximum 50 nodes, an affiliation function in the software program Termis [104] is used. Termis is a hydraulic modeling tool that simulates the behavior of flow directions, pressure, and thermal conditions in a DHC network [104]. The network from the GIS tool and the demand points from the Heat Atlas are loaded in Termis as shape files. To affiliate the demand, the nodes are placed on different locations in the network chosen strategically for the affiliation of demand to be dependent on typology type. Figure 4.10 shows how buildings were aggregated into a limited number of nodes (a) and the resulting network (b). The latter was then designed according to the FLEXYNETS concept, as described in [12]. The yearly heat demand is approximately 20.7 GWh with a peak load of approximately 6.0 MW.

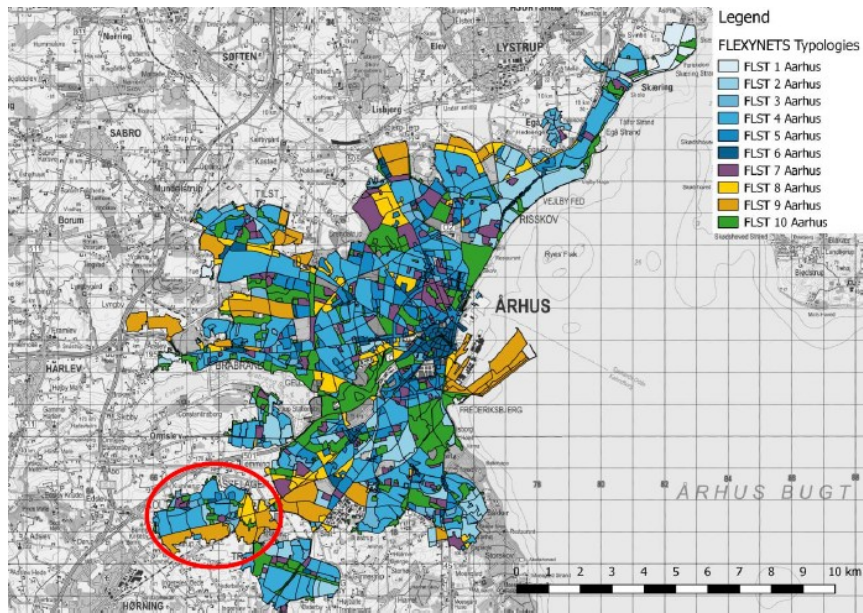


Figure 4.8 - Overview of Aarhus including settlement typologies. The case in the south-western part is highlighted with a red circle (taken from [12]).

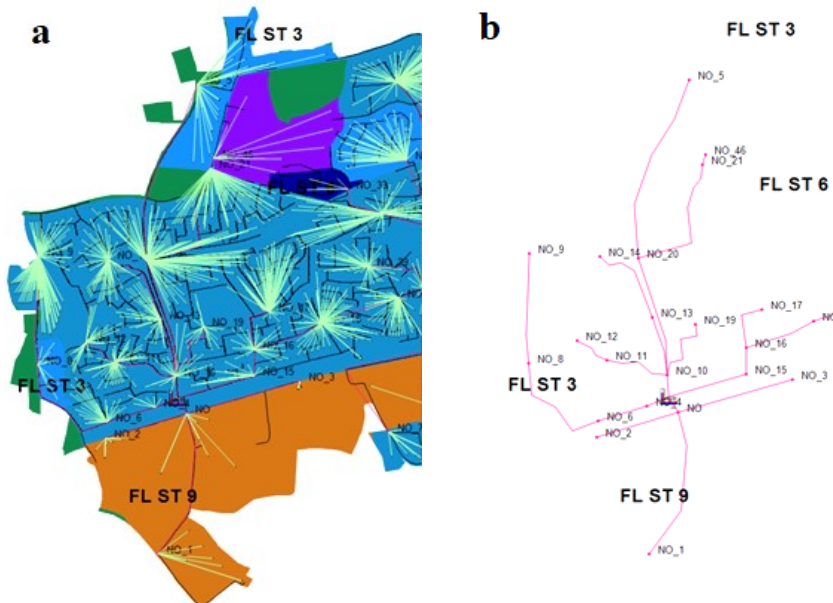


Figure 4.9 - (a) Aggregation of user nodes; (b) scheme of the resulting network (after aggregation).

4.2.3 Description of the case-study

As already mentioned above, in this case study the low temperature heat source integrates a conventional fossil fuelled heat supply station. Indeed, the highest share of the heat supply comes from a central station owned by the DH utility, called here also network manager. The latter is responsible for balancing the energy flows and owns the central supply station of the district heating grid that consists of a 2.2 MW gas-fired reciprocating engine that produces

combined heat and power (CHP) and a 2.3 MW auxiliary gas boiler (GB) assumed here to have a constant efficiency of 80%. A 330 m³ central storage tank is used as a thermal buffer between the CHP unit and the network. These plants are not part of the real system; they were chosen as they are typical heat supply units, thus representative of several DH systems.

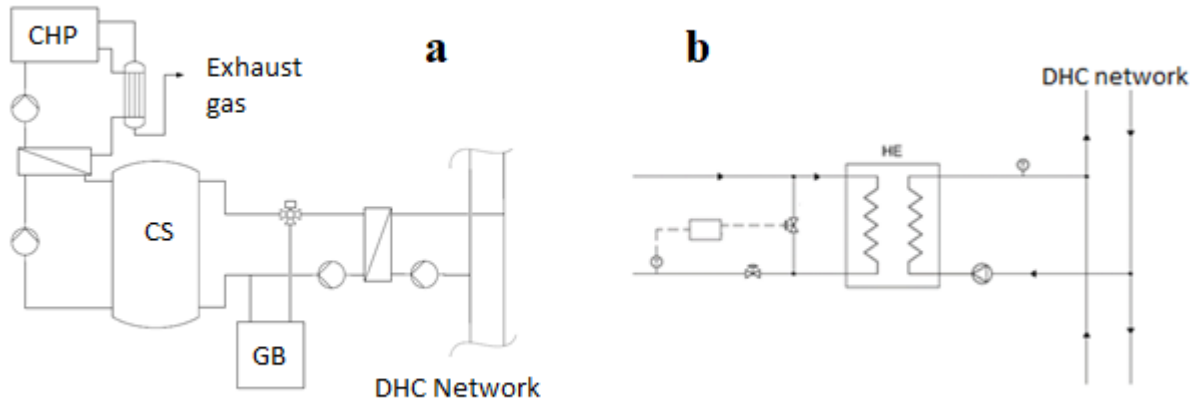


Figure 4.10 - Layout of (a) central heat supply station and (b) waste heat substations.

The layout of the central heat supply station is shown in Figure 4.11a and the scheme of the waste heat substations is shown in Figure 4.11b. Furthermore, two additional substations supply waste heat to the network. The district heating network transports heat at low temperature (supply temperature between 20°C and 30°C) to decentralized heat pumps. The NM is also responsible for the supply of the electricity needed by the heat pumps, both in technical and financial perspective. The water-to-water heat pumps use R407c as refrigerant and provide water to the buildings at 55-65°C.

4.2.4 The low temperature heat sources

Two low temperature heat sources have been considered: condensing units of a shopping mall (SMCU) and low temperature waste heat from an industrial process (IWH). The first heat source has only two levels (base or maximum) depending on the hour of the day and the heat carrier is water at 40-50°C. The second source is water at 80-90°C and the load is intermittent. There is no heat available when the process is not running, and there is a variable heat flow rate when the industrial process runs. The first profile was estimated by [105] while the industrial waste heat profile is based on measured data of flue gases in a foundry [106]. In both cases, the normalized profile was used and then scaled up to the desired level, shown in Figure 4.12.

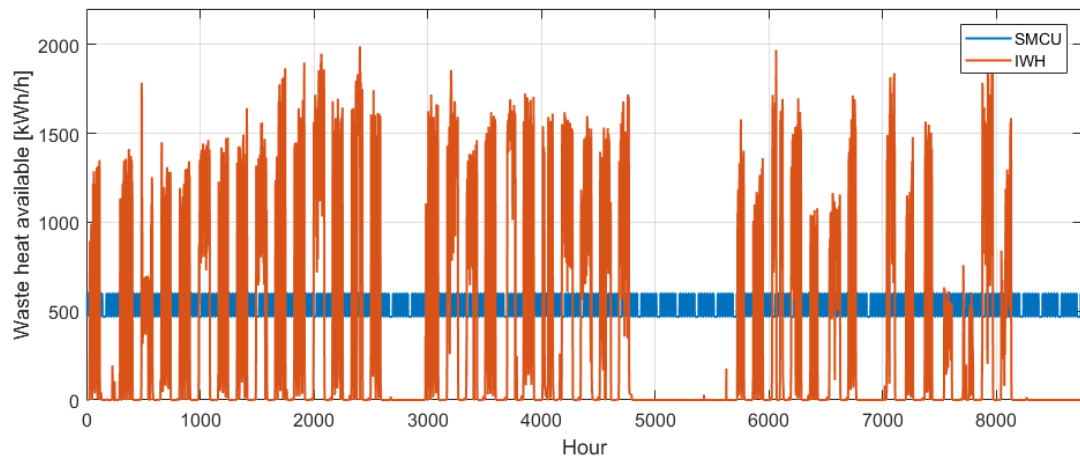


Figure 4.11 - Waste heat profiles used in the case study.

Chapter 5 Planning and design aspects

In Section 5.1 a preliminary analysis is carried out to compare three heat supply systems for the reference neighborhood presented in the previous Chapter (case-study 1): a district heating system with central heat pump and auxiliary gas boiler, a low temperature district heating system with distributed heat pumps and individual gas boilers. Then, the potential of the heat source in different scenarios for the town of Abano Terme is shown. Since the district heating system with booster heat pumps results to be the best one with regard to primary energy consumption and carbon dioxide emissions, in Section 5.2 it is analyzed in detail to find out how the supply and return network temperatures affect the economic balance for the DH utility and, in turn, for the final user. The parametric analysis assumes to recover the heat directly and to have different supply temperatures depending on the temperature of the heat source. In order to extend the validity of the results beyond the aforementioned case-study, a wide range of network supply temperatures was considered, i.e. from 15°C to 45°C. The payback time for the utility was set to a fixed value and the heat price was calculated accordingly. Finally, the levelized cost of heat for different residential users is calculated and compared to that of condensing gas boilers. Conclusions are drawn in Section 5.3.

5.1 Preliminary analysis

5.1.1 Methods

The neighbourhood presented in Section 4.1.4 has been used as a representative residential neighbourhood, as it is wide enough to include buildings of several construction periods. The model presented in Section 3.1 has been used to determine the heat load profiles of the considered district. The archetypes, i.e. the representative envelopes given as inputs to the model, were based on a previous research about the building stock of the Veneto Region [107]. Five age classes have been individuated as explained in Section 4.1. The main sources utilized

were the open-source topographic maps available online on the web-site of the Veneto Region [102]. The simulated neighbourhood consists of 98 buildings, 35 of which were built after the implementation of L.10/1991 [99]. Moreover, among these buildings, 8 are recently constructed (or still in construction) low-energy buildings. More details are given in Section 4.1.4. The model used 1 hour time step and the Test Reference Year of Venice as weather file. The considered heat source was waste water at 41°C –since the study was performed before the measurement campaign presented in Section 4.1.3, a cautionary available temperature was assumed. Once the heat load of the building was calculated, a district heating network was designed for two district heating systems based on two different concepts:

- c-HPDH: DH network supplied by the waste-water through a central heat pump and an auxiliary gas boiler;
- d-HPDH: DH network supplied directly by the waste-water through heat exchangers; in this case, the substations are equipped with booster heat pumps to provide heat at the temperature needed by the building.

The supply temperature has been considered as function of external air temperature. For each age class, the supply temperature was selected in order to be as low as possible throughout the heating season but high enough to provide thermal comfort to the occupants. The supply temperature curves are shown in Fig. 5.1.

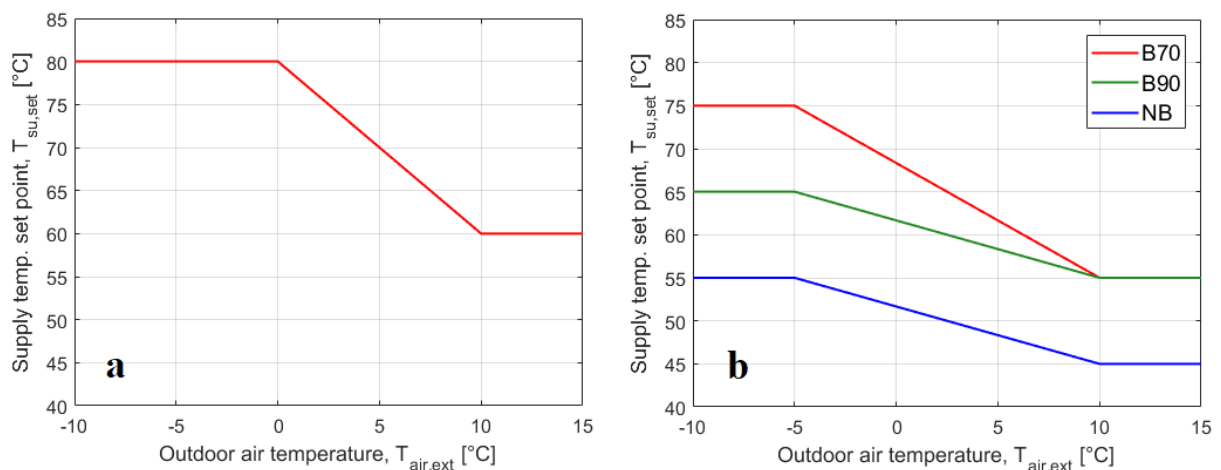


Figure 5.1 - Supply temperature curves of (a) c-HPDH, (b) distributed heat pumps according to the building supplied.

The same tree-shaped network has been adopted for both systems (c-HPDH and d-HPDH). All 98 buildings are assumed to be connected to the DH system. Each building/substation was

given a nominal capacity and a number of equivalent apartments. The design mass flow rate for DHW production was obtained by following the Italian standard UNI 9182 [108] and the design heat load for each substation adds part of the nominal load for DHW to the nominal load for space heating as suggested by [109]. The design heat flow rate for each branch of the network was determined by applying simultaneity factors [110] to the number of equivalent apartments supplied. Figure 5.2 shows the DH network and the buildings of the considered neighbourhood, coloured by age class. As mentioned above, d-HPDH is expected to be more efficient than c-HPDH due to the lower water temperature in the network. This on the one hand reduces heat losses from the heat distribution network, and on the other hand allows heat pumps to deliver water to the temperature required by the supplied customer, thus achieving a higher COP than with a central unit. Moreover, the use of heat pumps can be avoided for those buildings that have radiant surfaces or other low temperature heat emitters. Since in d-HPDH the network supplies the evaporator of the decentralized heat pumps, the substation design heat flow rate must be reduced by the following factor

$$f_{cop} = \left(1 - \frac{1}{COP_{nom}}\right) \quad (5.1)$$

This might lead to the conclusion that pipe diameters in the d-HPDH system can be reduced compared to those of c-HPDH. Nonetheless, this does not necessarily occur because working with a high difference between design network supply and return temperature reduces the COP of the heat pumps. This aspect will be investigated in Section 5.2. In this case, the network capacity has been set to 15 K for c-HPDH system and to 10 K for d-HPDH system.

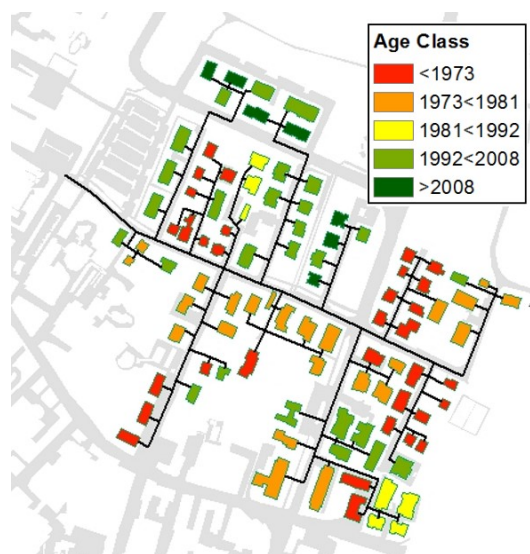


Figure 5.2 - Topology of the district heating network and buildings.

High capacity heat pumps (2-10 MW) require a centrifugal compressor instead of a usual volumetric compressors (scroll or reciprocating) and shell-and-tube heat exchangers instead of brazed plate heat exchangers. Thus, different performance curves are used to calculate the COP of the heat pumps. For the central heat pump of the c-HPDH system, the correlation proposed by [111] was adopted:

$$COP_{pl,c} = \left(0.558 \frac{T_{cd,out} + 273.15 + 4}{(T_{cd,out} + 4) - (T_{ev,out} - 4)} + 1.168 \right) (0.393 x + 0.612) \quad (5.2)$$

Where x is the part load ratio, i.e. the ratio between actual and nominal heat flow rate at the condenser (thermal capacity of the heat pump). For the decentralized units, full load COP values have been obtained by a simple regression of the measurements performed on a real machine with a thermal capacity of 30 kW developed in the labs of a manufacturer –see Section 3.3 for more details. Equation 5.3 is the polynomial for full load COP as function of condenser outlet temperature. Partial load COP was then obtained from as suggested by EN 14825 [112] –see Eq. 5.4.

$$COP_{fl,d} = 0.000366 T_{cd,out}^3 - 0.0723 T_{cd,out}^2 + 4.6046 T_{cd,out} - 89.477 \quad (5.3)$$

$$COP_{pl,d} = COP_{fl,d} \frac{x}{0.1 + 0.9 x} \quad (5.4)$$

Coefficients for primary energy consumption and CO₂ emission are taken from a study of ISPRA [8]. The simulation included only the heating season, from October 15th to March 30th.

5.1.2 Results

Table 5.1 - Summary of the considered buildings and specific consumption.

Age of construction	Buildings [-]	Gross heated volume [m ³]	Reference regulation	Specific consumption [kWh/(m ² y)]	Floor Heating systems [-]
<1973	32	54910	-	125-240	0
1973<1981	23	61865	-	125-240	0
1981<1992	8	15165	L. 373/76	115-180	0
1992<2008	27	57470	L. 10/91	65-95	9
>2008	8	15260	DPR 59/09	40-55	8
TOTAL	98	204670	-	-	17

Although old buildings (built before any regulation on building energy performance) account for 57% of total built volume, they are responsible for 71% of the heat demand. Buildings built after L.10/91 [99] account for 35% of built volume but their heat consumption is only

21% -see pie chart in Fig. 5.3a. The wide range of specific heat consumption for old buildings (see Table 5.1) may be explained by the significant variation in the buildings shape ratios, as shown in Fig. 5.3b.

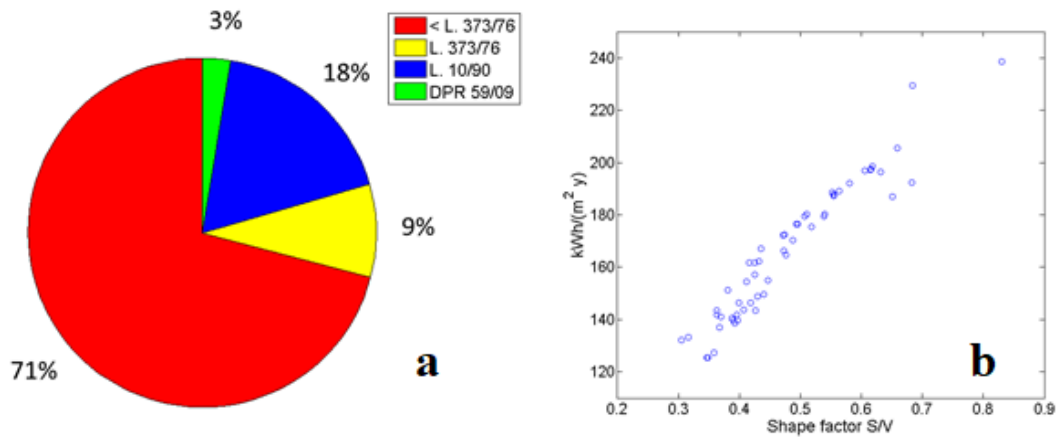


Figure 5.3 - (a) Energy consumption of the neighbourhood by age class; (b) Specific heat consumption vs shape factor for old buildings (< L. 373/76).

Figure 5.4 shows the aggregated heat load profile of the whole district and the profile of the external air temperature with 1-hour resolution during the considered period. Table 5.2 summarizes results for the central and distributed district heating configurations.

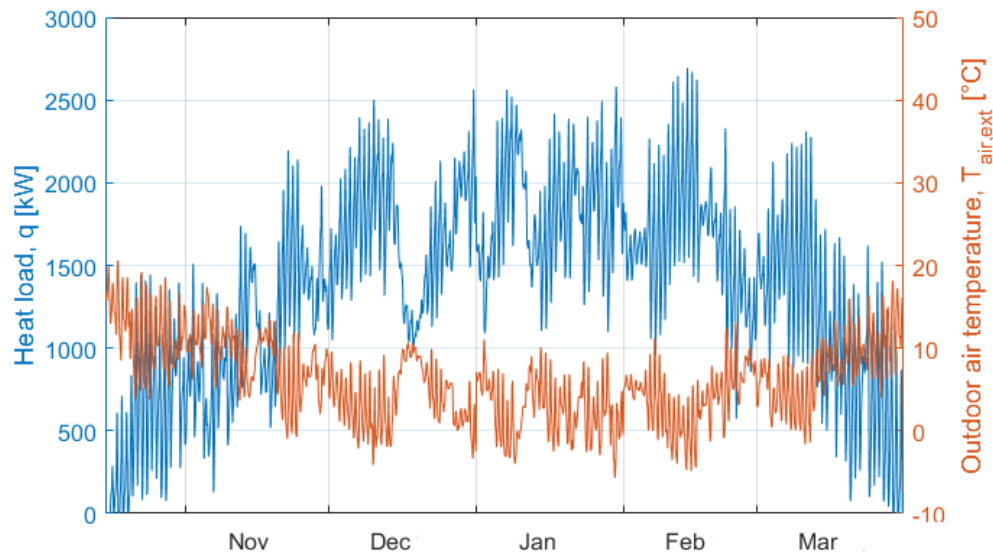


Figure 5.4 - Heat load profile of the reference neighbourhood and outdoor air temperature.

The seasonal COP (SCOP) for the c-HPDH system is the ratio between the heat load of the central heat pump (on the condenser side) and the electrical load of the compressor. The sum

of gas boiler and heat pump load is higher for the c-HPDH system compared to the d-HPDH due to distribution heat losses that amount to about 6.3%. The heat loss in the d-HPDH system amount to 4.4%. However, they have no influence on the amount of electricity needed by the heat pumps, as the heat loss occurs upstream.

Table 5.2 - Summary of energy balance and SCOP.

System	Heat supply condenser(s) [MWh]	Gas boiler heat supply [MWh]	Pumps electricity [MWh]	Compressors electricity [MWh]	SCOP [-]
c-HPDH	5289	683	13	1140	4.64
d-HPDH	5541	-	12	1150 1108	4.82 (on-off) 5.00 (inverter)

The values are rather low compared to heat losses of conventional networks because the simulation included only the heating season. Therefore, heat losses during the summer season were not considered. The expenditure for pumps electricity is almost equal in the two cases. Note that in the d-HPDH system there are 17 buildings with radiant floor (see Table 5.1) that are directly coupled to the low temperature network. Therefore, the SCOP of the d-HPDH system is calculated as the ratio between the sum of the heat load of all the buildings (including those without heat pump) and the electrical consumption of the distributed heat pumps. In the d-HPDH system, the use of variable speed compressors (i.e. compressors with inverter) leads to an increase of the SCOP of about 4%. Figure 5.5 shows the primary energy consumption and the CO₂ emissions of the proposed DH systems compared to the current situation, that assumes that all the buildings are supplied by individual gas boilers with an average efficiency of 90%.

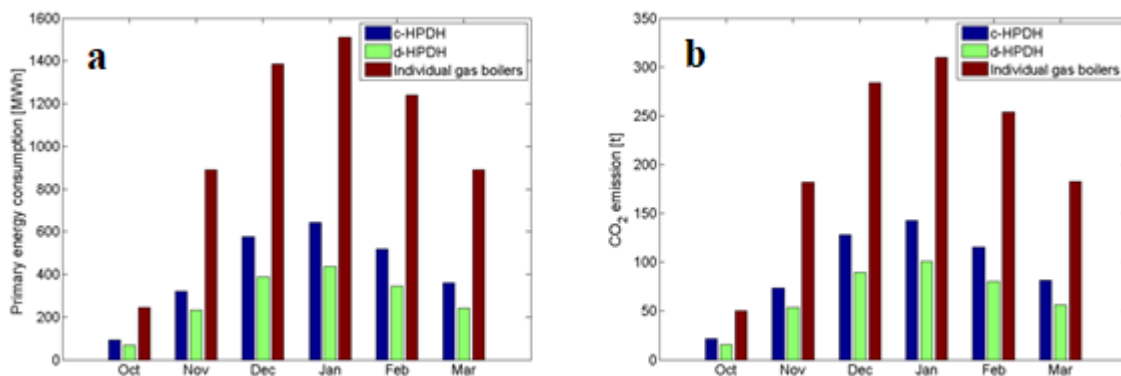


Figure 5.5 - (a) Primary energy consumption and (b) carbon dioxide emissions of c-HPDH, d-HPDH and individual gas boilers.

Both HPDH systems bring a sharp drop in primary energy consumption with regard to the current situation made of individual gas boilers (-60 to -72%). System d-HPDH seems to be preferable in terms of SCOP (+4%), primary energy consumption (-30%) and CO₂ emissions (-30%). If the analysis considered also the warm season, the environmental benefit of the d-HPDH system would probably be even more evident. In fact, the operation of the c-HPDH system during summer months would probably involve an inefficient use of the gas boiler and high heat losses due to the very low heating need of the building, which is limited to that required for DHW preparation. Moreover, the convenience of the d-HPDH system is supposed to increase compared to the c-HPDH system by increasing the share of refurbished and/or new low energy buildings.

5.1.3 Potential for Abano Terme

Although the system with a supply network temperature of 40°C seems to be economically feasible, its practical implementation at urban scale depends on the availability of the heat source. In the following, some scenarios are drawn for the municipality of Abano Terme (case study 1). In order to assess the potential of the wastewater in the heat supply to the buildings, the heat content of the water is calculated and compared to the heat demand of the residential buildings. The latter was derived from Piano Energetico della Provincia di Padova [113]. The heat demand of the residential building stock was evaluated as 129 GWh, 117.4 for space heating and 11.7 for DHW production. Four scenarios for waste water utilization are being envisioned, based on the available mass flow and temperature. Here we call “available temperature” that temperature level that is maintained for the whole year without significant risks of long-lasting temperature drops that could jeopardize the safety of the heat supply. According to the measured data presented in Chapter 4.1, two temperature levels have been individuated: 45°C (worst case, T1) and 55°C (best case, T2). Assuming to cool down the wastewater to 30°C and to supply a district heating network with a supply temperature of 40°C and a return of 25°C, the temperature drop of the wastewater would be 15 K in the worst case scenario and 25 K in the best case scenario. As far as the mass flow rate is considered, the worst case (M1) consists of extracting the amount of water in function of the touristic season, as it happens today. In a scenario where the waste water becomes an energy source, pumping more groundwater during the heating season would make more sense both from an economic and from an energy-oriented perspective. Therefore, in the best case scenario (M2) the amount of thermal water pumped during the heating season is equal to the maximum water withdrawn

nowadays during the peak touristic season. During the other months, the same amount of the worst-case scenario is withdrawn. This corresponds to an annual withdrawal of 8.5 million cubic meters, i.e. only 9% more than the average of period 2006-2013. Table 5.10 explains the four scenarios according to the assumptions on mass flow rate and available temperature. Figure 5.6 shows the monthly values of thermal energy supplied by the wastewater to the network under the four scenarios and the energy needs of the residential building stock of Abano Terme for space heating and DHW production.

Table 5.3 - Assumptions for the waste-water utilization scenarios.

Scenario		Temperatures	
		T1	T2
Mass flow rates	M1	S11	S12
	M2	S21	S22

The heat demand was then spread over the 12 months by using the method of the Degree Days. Results show that in the worst case scenario (S11), the waste water is able to cover 61.5% of the heat demand of the Municipality, whereas in the best case scenario (S22) almost all the heat demand can be covered by low temperature heat. It is interesting to notice that an increase of 10 K of available temperature brings the potential to 86% of the heat demand, while an increase of extracted volumes during the winter period can only improve the coverage factor to 71%. In all the considered scenarios, the waste water is able to cover the heat demand for DHW production during the warm season. Also the heat demand for space heating during October and April can be entirely covered in all the considered cases. During March and November, instead, the heat available is enough to cover the heat demand only if the available temperature is 55°C. In any case, a significant part of the heat demand would be covered by the electricity converted into heat by the heat pump compressors (approximately 80% assuming a global SCOP of 4.5).

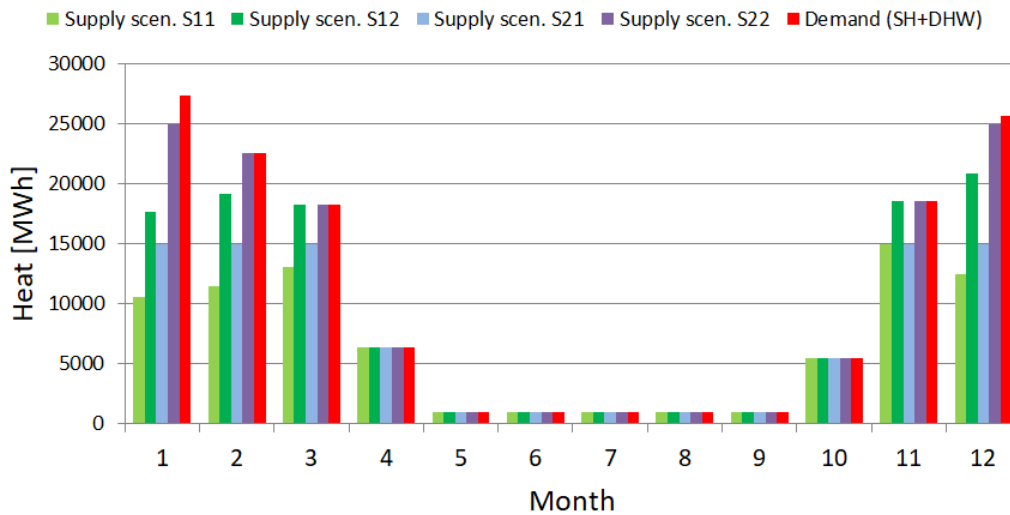


Figure 5.6 - Four scenarios for the use of thermal wastewater in Abano Terme and comparison to the heat demand of the residential building stock.

This means that if the waste water is available at 45°C, the district heating with booster heat pumps would be able to cover from 76% to 88% of the heat demand. With an available temperature of 50°C, the residential heat demand of the town could be entirely covered.

5.2 Techno-economic analysis

In light of the environmental benefit of the d-HPDH system, the attention is focused here on its economic balance.

5.2.1 Methods

This work analyses the economic feasibility of district heating systems with distributed heat pumps considering both the perspective of the district heating utility (also called network manager in the following) and that of the customers. First of all, three reference buildings were simulated with the dynamic simulation software TRNSYS [11] in order to get the heat load profiles for space heating of representative customers. Section 5.2.1.1 describes the reference buildings and the assumptions used in the yearly simulations. The obtained heat load profiles were used as input in the simulation of the district heating substations, including the heat pump and the hot water tank for domestic hot water (DHW) production –Section 5.2.1.2. The load files for DHW consumption were obtained using the free software DHWCalc [114]. After energy simulations, economic evaluations are performed on a district level, considering a small network as a case study. For each case, the DH network is sized and the installation and operative costs are calculated accordingly. Then, the latter are used to find a suitable price

of heat under the constraint of a fixed pay-back time for the DH utility considering two different financial models to sell heat to the buildings (Section 5.2.1.3). Finally, the price of heat calculated in the previous step is used to determine the levelized cost of energy for the aforementioned reference households. The study includes both “cold” water networks with supply temperatures of 15-20°C and low temperature networks with supply temperatures of 40-45°C. Also the cases that lie between these design solutions were considered to give generality to the results.

The reference buildings. The dynamic simulations were performed with the commercial software TRNSYS [11]. A time-step of 5 minutes was used. In order to avoid convergence problems and deal with a simple model, the building and the substation were simulated separately. Thus, the heat load profile of each building was calculated at the beginning and successively used as input in the simulation of the substations. The buildings are multi-family houses of 12 apartments with a modular structure consisting of four blocks. Each block is made up by three floors with one apartment per floor, as shown in Figure 5.7.

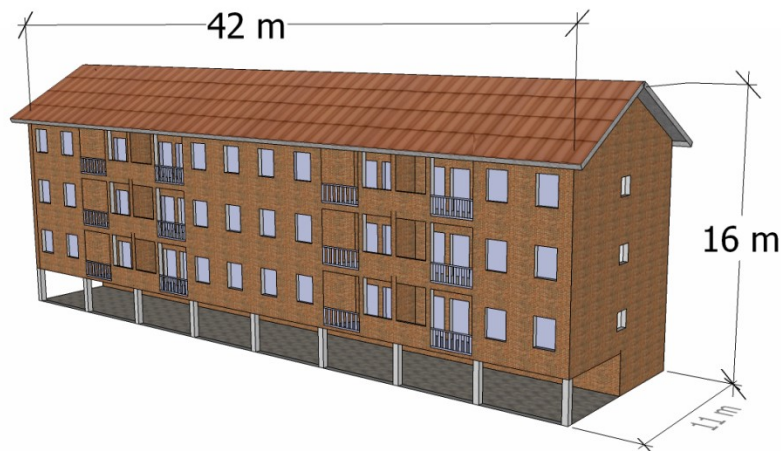


Figure 5.7 - 3D-view of the reference building.

Three reference envelopes with different degrees of thermal insulation were used to represent a significant share of the Italian residential building stock. Each envelope corresponds to the prescriptions of the Italian law at the age of construction: old buildings with low thermal insulations that were typical in the 70s and the 80s built according to L. 373/76 [98] and named here B70, buildings from the 90s i.e. built after L. 10/91 [99] and well insulated buildings constructed after the implementation of the recent EU Directives on building energy performance, i.e. after D.lgs. 192/2005 [100]. More information can be found in the detailed description of the case study –see Section 4.1.4. A constant set point for the indoor air tempera-

ture of 20°C was used to obtain the heat load profiles. Table 5.3 resumes the thermal properties of the simulated buildings. A constant efficiency was used to scale up the heat load of the building in order to account for the heat losses due to emission, regulation and distribution according to Standard UNI/TS 11300-2 [115], as reported in Table 5.3. The DHW load profile was calculated with the free software *DHWCalc* [114] using a time-step of 5 minutes, assuming a mean daily draw-off of 1800 l and a maximum flow rate of 8000 l/hr. The software is based on step functions to calculate the probability of the draw-off during week days and during weekends and uses four categories of draw-off, each with its own probability distribution [114].

The substation model. For each dwelling, the substation was simulated assuming different supply temperatures of the water coming from the network ($T_{net,su}$) and assuming to draw different mass flow rates from the network based on the design network temperature difference ΔT_{net} . The parametric study includes network supply temperatures in a range between 15°C and 45°C with 5 K step and three cases of network temperature difference: 5, 10 and 15 K. The substation model consists of the heat pump and of a hot water storage tank for domestic hot water production, as shown in Figure 5.8. A time step of 5 minutes was used. The heat pump model is thoroughly described in Chapter 3.

Table 5.4 - Synthetic description of the reference buildings.

Properties\building type	B70	B90	NB
<i>External opaque building elements</i>			
<i>Thermal transmittance</i>			
- Ext. walls U (W/(m ² K))	1.295	0.663	0.315
- Ceiling U (W/(m ² K))	2.169	1.969	0.639
- Floor slab U (W/(m ² K))	2.336	1.969	0.639
<i>Areic thermal mass</i>			
- Ext. walls m (kg/m ²)	334	504	576
- Ceiling m (kg/m ²)	528	528	370
- Floor slab m (kg/m ²)	528	528	370
<i>Glazed elements</i>			
- Transmittance, U (W/(m ² K))	5.68	2.83	1.40
- G-value (-)	0.85	0.75	0.59
<i>Ventilation</i>			
- ACH (1/h)	0.50	0.50	0.30
<i>Efficiency</i>			
- Emission	0.920	0.940	0.950
- Regulation	0.970	0.970	0.970
- Distribution	0.917	0.958	0.958

The hot water tank is simulated with TRNSYS Type 4 using 8 nodes. The volume of the tank was set to 1200 l; the sizing was done according to the Italian Standard UNI 9182 [108]. A suitable supply temperature curve was given to each reference building to guarantee the thermal comfort in the heated spaces. The supply temperature curves chosen here are not the same one of the preliminary analysis -they are shown in Figure 5.9b. The mass flow rate of the water drawn from the district heating loop was calculated for each case using the design thermal peak load of the building, the design network temperature difference ΔT_{net} and assuming a COP for the design point –set here to 4 for all cases. The design thermal peak load and a nominal temperature difference of 10 K were used to determine the mass flow rate exiting the condenser.

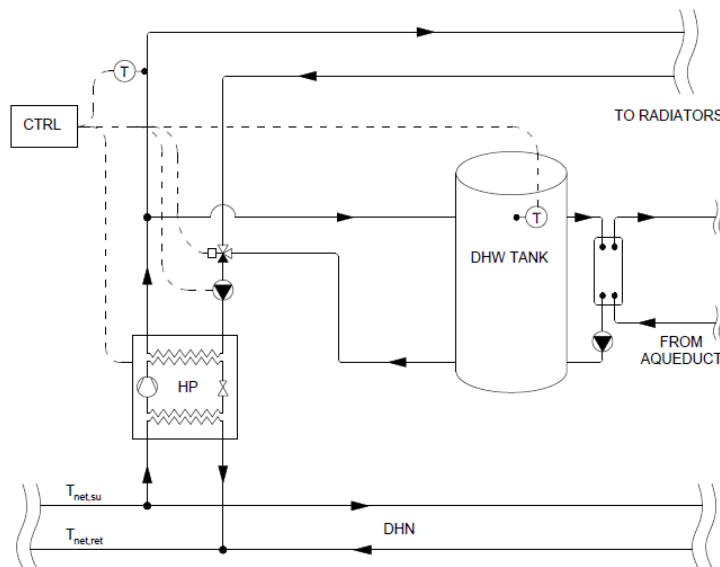


Figure 5.8 - Schematic view of the substation.

Depending on the supply temperature of the network and on the set point temperature needed by the heat emitters of the considered building, a compressor among those available in the market was chosen and its performance map was used by the heat pump model. After a survey of available machines, a scroll compressor designed for R134a and a scroll compressor with vapour injection designed for R407c were selected as candidates for cases with $T_{net,su}$ respectively higher and lower than 30°C. With $T_{net,su} = 30^\circ\text{C}$, the simulation was run with both compressors to evaluate the difference in their performance and consequently choose the best one.

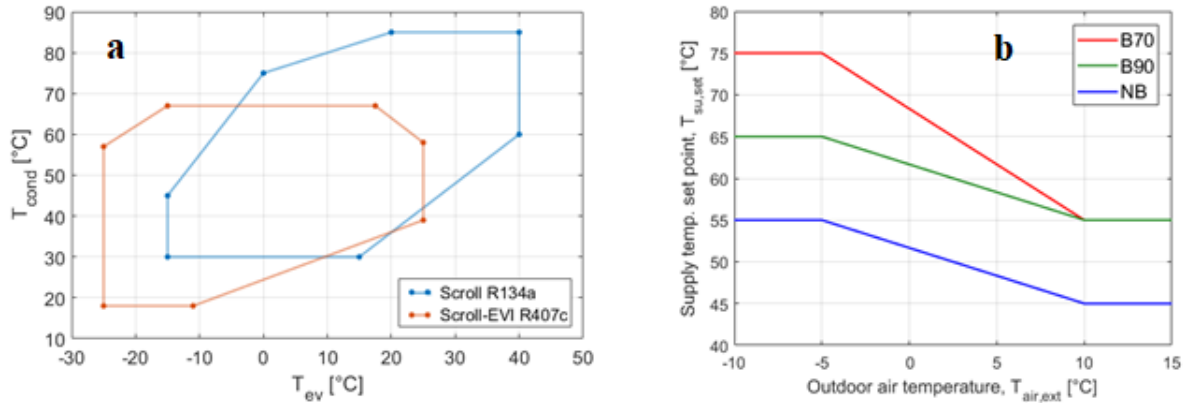


Figure 5.9 - (a) Limits of operative conditions of the selected compressors; (b) supply temperature curves for the reference buildings.

The control system prioritizes the heat supply to the DHW tank to avoid discomfort for the end users. Therefore, when the thermal storage goes below the set point temperature -set to 48°C-, the mass flow exiting the condenser is deviated towards the tank that is charged until the set point is reached again. An hysteresis of $\Delta T_{set} = 2$ K was used to avoid intermittent operation of the heat pump. The measurement point was placed in the middle of the tank. When there is simultaneous demand of heat (for both space heating and DHW production), the thermal energy needed but not given to the building is stored in memory and released afterwards, when the thermal storage has been recharged. This conceptual simplification is practically equal to have a fully mixed thermal buffer that acts as a hydraulic disjunction between the heat pumps and the building, which is a common design choice for multi-family houses. The annual performance of the heat pump that supplies heat to the building of type j is calculated as *seasonal coefficient of performance*.

$$SCOP_j = \frac{\int_0^t Q_{cd} dt}{\int_0^t W_{el,k} dt} \quad (5.5)$$

Economic evaluation. The case study analysed is the same neighbourhood used in the preliminary analysis and described in Section 4.1.4. The price of heat was calculated according to two different business models that are thoroughly described in the following Section. In both cases, the price depends on the initial investment in the infrastructure and on the operational costs of the utility. Here, the analysis includes also the DHW production, and not only the space heating as in the preliminary analysis presented in Section 5.1. The total heated area of the district is about 54000 m², corresponding to a total heat demand equal to 6.09 GWh/y (5.54 GWh for space heating and 0.55 GWh for DHW production). The peak load for the

considered district was estimated to be as high as 2.2 MW. The design thermal capacity of the network was then evaluated using factor $f_{ev,pool}$

$$f_{ev,pool} = \frac{COP_{pool} - 1}{COP_{pool}} \quad (5.6)$$

where COP_{pool} is the average COP expected for the whole pool of heat pumps during the coldest days of the year, which also depends on the network temperature. Conservative values were adopted for COP_{pool} : the latter was assumed to be 3.0 for $T_{net,su} = 15^\circ\text{C}$ and then growing by 0.25 points each 5 K. The network was designed considering a nominal velocity of 1.5 m/s in the pipes, which leads to a head loss included between 100 and 300 Pa/m depending on the considered pipe. The connection of buildings to the network throughout time was assumed to follow an exponential law with 25% of the buildings (in terms of heat demand) connected after 1 year, 75% after 8 years and reaching asymptotically 80% of the heat load of the district. The initial investment of the district heating utility I_{dhs} includes network (pipes, labour, groundworks and project) and other costs for heat exchangers, pumps and control system.

$$I_{dhs,0} = I_{net,mp} + I_{he} + I_{ctr} + I_{pumps} \quad (5.7)$$

Different values of I_{dhs} were found for different design network temperature differences ΔT_{net} (5, 10 and 15 K) because a lower temperature difference leads to higher flow rates and, in turn, higher diameters. Moreover, cold networks reduce the temperature difference between the heat carrier and the ground to a few degrees, so that pipes with a thinner insulation layer can be used thus reducing their cost per unit of length. Here, a simple reduction of -50% on the pipe cost was considered for cases at “neutral” temperature level, those with supply temperature lower than 30°C . The cost of the pipe itself is only a fraction of the overall cost due to the groundworks, that depend on the size of the pipe but also on the urban environment where the district pipes must be installed. The prices used in the current analysis are based on report [116], which distinguishes four categories of urban environment: inner city areas (A), outer city areas (B), parks (C) and extensions of existing networks (D). Here, only categories A and B are considered as they are representative of most situations. Prices from 2007 were updated to current currency (2017) considering an inflation rate of 10%. Figure 5.10 shows the specific costs of the pipes for categories A and B. Only the main pipes are considered in the initial investment ($I_{net,mp}$), while the cost of service pipes $I_{net,sp}$ is distributed throughout

the time as an operational cost because these pipes are normally installed as long as new customers get connected to the network.

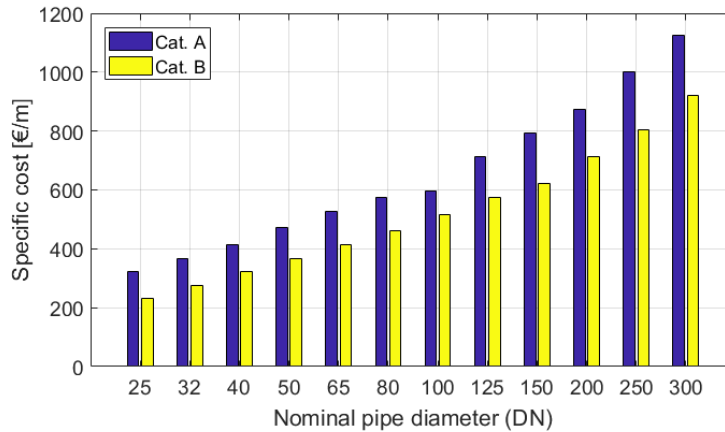


Figure 5.10 - Specific cost of pipelines from [116] updated to current prices.

Two different business models were considered in the economic analysis. In the first one, named *Business-as-Usual* (BaU), the end user invests in the heat pump and pays the electricity bill and the low-temperature heat bill separately. In the second case, named *Investment-on-Utility* (IoU), the utility takes charge of the investment in both infrastructure and heat pumps. In this case, the district heating utility will negotiate the price of electricity with the distribution system operator (DSO) and the user pays only for the consumed heat. Figure 5.11 illustrates the two business models with a conceptual scheme.

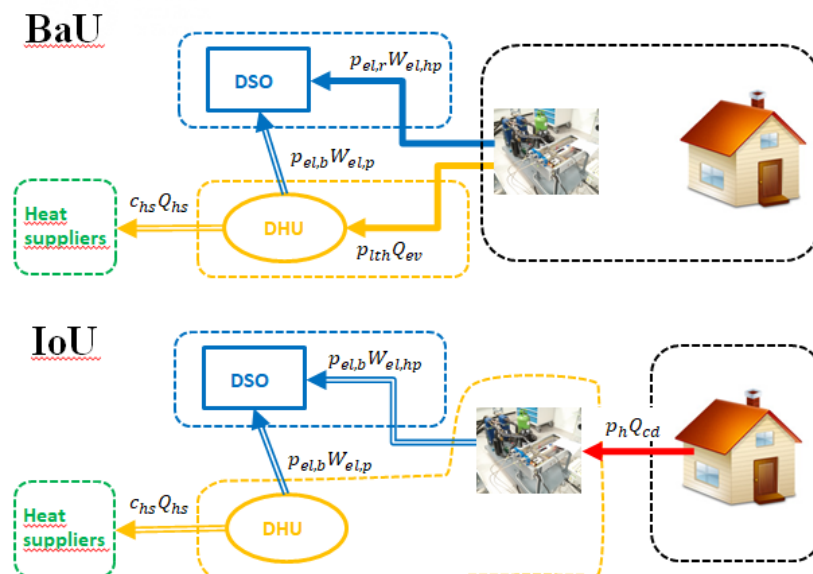


Figure 5.11 - Cash flow in Business-as-Usual (BaU) and Investment-on-Utility (IoU) business models.

The operating costs of the utility are different in the two cases. Both cases include the maintenance costs C_m , the expense for the heat source -Eq. (5.8)- and for the electrical consumption for pumping -Eq. (5.9). In the Business-as-Usual model, the fourth and last term ($I_{dhs,t}$) corresponds to the investment cost for service pipes of users that get connected during the lifetime of the project -Eq. (5.11). In the other business model, $I_{dhs,t}$ includes also the investment for heat pumps of new users -Eq. (5.13). Moreover, the operating costs include also the electricity consumption of the heat pumps, -Eq. (5.14). Finally, Equations (5.10) and (5.12) express the overall yearly operating costs of the district heating system for business models BaU and IoU, respectively.

$$C_{hs}(t) = c_{hs}Q_{hs}(t) \quad (5.8)$$

$$C_{el,p}(t) = p_{el.b}W_{el,p}(t) \quad (5.9)$$

Table 5.5 - Operating costs under BaU and IoU condition.

Business model	Operating costs	Eq.
BaU	$C_{dhs,BaU} = C_m + C_{hs} + C_{el,p} + I_{dhs,t}$	(5.10)
	$I_{dhs,t}(t) = I_{net,sp}(t)$	(5.11)
IoU	$C_{dhs,IoU} = C_m + C_{hs} + C_{el,p} + I_{dhs,t} + C_{el,hp}$	(5.12)
	$I_{dhs,t}(t) = I_{net,sp}(t) + I_{hp}(t)$	(5.13)
	$C_{el,hp}(t) = p_{el.b}W_{el,pool}(t)$	(5.14)

Table 5.6 - Assumptions used for the calculation of heat price.

Cost	Value/Function
Cost of heat exchangers, I_{he}	14 €/kW
Cost of pumps, I_{pumps}	11.5 k€ for $\Delta T_{net} = 5$ K; 8.8 k€ for $\Delta T_{net} = 10$ and 15 K
Cost of control system, I_{ctr}	75 k€
Cost of heat source, c_{hs}	10 €/MWh
Maintenance cost, C_m	$30 + 0.5 \cdot I_{he}$ [k€]
Price of electricity for business client, $p_{el.b}$	190 €/MWh
Specific cost for heat pump installations, I_{hp}	180 €/kW

The assumptions on the specific costs and investment costs are summarized in Table 5.6. In order to evaluate the power consumption of the pool of heat pumps, the SCOP of the whole district has been estimated from the SCOP of the reference buildings -calculated according to Eq. (5.5)- and to the composition of the reference residential neighbourhood presented above.

Here, it was assumed that 60% of the energy consumption comes from old buildings (corresponding to archetype B70), 30% from buildings of type B90 and only 10% from new buildings (NB). The energy consumption from old buildings is slightly decreased compared to that reported in Fig. 5.3 to account for partial refurbishment of the building stock throughout the time. Thus, the SCOP of the pool has been simply calculated with a weighted sum of the SCOP of the reference buildings, as follows:

$$SCOP_{tot} = 0.6 SCOP_{B70} + 0.3 SCOP_{B90} + 0.1 SCOP_{NB} \quad (5.15)$$

Thus, the heat delivered to the heat pumps evaporators Q_{ev} was calculated at each year by multiplying the heat demand of the buildings by factor

$$f_{ev,tot} = \frac{SCOP_{tot} - 1}{SCOP_{tot}} \quad (5.16)$$

The heat recovered from the heat source and supplied to the network Q_{hs} is bigger than the heat delivered to the heat pump evaporators Q_{ev} due to heat losses, that grow with the network temperature. However, as mentioned above, the pipes at low temperature have a lower insulation class thus reducing this gap; in addition due to the low cost of the fuel considered here (low temperature waste heat), a slight increase of heat losses has a very limited impact on the final economic balance. Thus, they were considered equal to 7% regardless of the network temperature.

The price of heat was evaluated as the price that would pay back the initial investment in the infrastructure and the annual running costs of the utility within 15 years, which is a reasonable time frame for district heating networks. The discounted cash flow method with a discount rate of 5% was used –see Equations (5.17) and (5.18). Thus, the payback time for the utility (PBT = 15 years) is used as an equality constraint to fix the heat price to the district heating customers (p_{lth} in the BaU case, p_h in the IoU case).

$$-I_{dhs,0} + \sum_{t=1}^{PBT} \frac{p_{lth} Q_{ev}(t) - C_{dhs,BaU}(t)}{(1+i)^t} = 0 \quad (5.17)$$

$$-I_{dhs,0} + \sum_{t=1}^{PBT} \frac{p_h Q_{cd}(t) - C_{dhs,IoU}(t)}{(1+i)^t} = 0 \quad (5.18)$$

In order to understand if the proposed system is competitive against other heat supply solutions, the levelized cost of energy (LCOE) was evaluated in all cases and compared to that of

an old gas boiler –assumed to be the heat supply system installed in most residential multi-family houses in Northern Italy- and to a condensing boiler, which is the standard solution for new or refurbished buildings. The LCOE is the sum of all costs related to an energy supply system -including both investment and operating costs- divided by the energy supplied over its entire lifetime T considered here as 15 years:

$$LCOE_{BaU} = \left(I_{hp} + \sum_{t=1}^T \frac{p_{el,r} W_{hp}(t) + (p_{lth} - p_{inc}) Q_{ev}(t) - C_{m,sub}(t)}{(1+i)^t} \right) / \sum_{t=1}^T \frac{Q_{cond}(t)}{(1+i)^t} \quad (5.19)$$

$$LCOE_{IoU} = \sum_{t=1}^T \frac{p_h Q_{cd}(t) - p_{inc} Q_{ev}(t) - C_{m,sub}(t)}{(1+i)^t} / \sum_{t=1}^T \frac{Q_{cd}(t)}{(1+i)^t} \quad (5.20)$$

In these Equations, it can be seen that under BaU conditions, both the investment cost in the heat pump and the operating costs (O&M) are accounted. On the other hand, under IoU conditions, the investment in the heat pumps is already included in the operating costs, as explained above. Taxes were considered as high as 10% of the heat sale, entirely on the consumer side.

Table 5.7 - Assumptions used for the calculation of the LCOE.

Cost	Value/Function
Incentive on renewable district heat, p_{inc}	26 €/MWh
Price of electricity for residential client, $p_{el,r}$	190 €/MWh
Investment cost for the heat pumps, I_{hp}	170 €/kW for B70; 250 €/kW for B90; 360 €/kW for NB
Gas price, p_{gas}	75 €/Sm ³
Efficiency of old gas boiler	75%
Efficiency of condensing gas boilers [118]	85% for B70; 87% for B90; 91% for NB
Cost of condensing boiler	100 €/kW
Maintenance cost for the user, $C_{m,sub}$	550 €/year for old GB 300 €/year for new GB 250 year for heat pump

However, in both cases an incentive (p_{inc}) was applied as provided by Italian law to financially support generation of district heat from renewable sources (biomass and geothermal) [117]. Note that the incentive is applied only to the heat delivered to the evaporators and not to the heat purchased to the final user. An annual expense for maintenance of the substation ($C_{m,sub}$) was considered as a further cost for the customers. The specific investment costs for the heat pumps include also installation costs and are different from building to building due to economies of scale. These prices, obtained from a heat pump manufacturer, represent realistic prices of water to water heat pumps for the end user. Table 5.7 summarizes all the assumptions made for the calculation of the levelized cost of energy.

5.2.2 Results

The results are divided into two subsections. The first one summarizes the energy performance of the heat pumps on annual basis in all the considered cases. Then, results concerning the economic evaluation are discussed.

Energy performance. Table 5.8 shows the peak loads and the energy needs of the reference buildings. The values include the efficiency of regulation, distribution and emission system calculated as in the Standard UNI/TS 11300-2 [115]. After having determined the load profiles for space heating through the dynamic simulation of the buildings and the domestic hot water draw-offs, they were used as input to simulate the operation of a water to water heat pump coupled with a hot water tank.

Table 5.8 - Peak loads and specific energy needs of the considered buildings.

Building	Efficiency [%]	Peak load [kW]	Energy need [kWh/(m ² y)]		
			SH	DHW	TOT
B70	0.818	83.5	185.0	23.6	208.6
B90	0.874	45.2	90.8	23.6	114.4
NB	0.883	24.9	38.8	23.6	62.4

The performance of the heat pump depends on the temperature of the water entering the evaporator –i.e. the network supply temperature, $T_{net,su}$ – and on the temperature of the water exiting the condenser. Older buildings need higher supply temperatures in order to guarantee the thermal comfort throughout the cold season –see supply temperature curves in Fig. 5.10. Moreover, a higher temperature drop in the evaporator turns into a lower COP of the heat pumps. All these factors concur to determine the *seasonal coefficient of performance* of the heat pump (SCOP). Therefore in Fig. 5.12 for each building and each network supply temper-

ature three values of SCOP are shown, depending on the nominal temperature drop in the evaporators. The values shown in Figure 5.12 are summarized in Table 5.9. Since the present analysis does not consider retrofit solutions on the building envelope, the study excludes the use of heat pumps for network temperatures lower than 30°C for old buildings of type B70. In fact, this building needs 75°C during the coldest days of the year as shown in Figure 5.9b. Such a high temperature rise requires the use of two heat pumps in series or a two-stage heat pump, which would increase the cost of the system. For the other two buildings (B90 and NB), a different compressor model was selected in order to work closer to the design point of the compressor. The latter works with refrigerant R407c. The old building has the worst performance due to high temperatures needed by the radiators: with a nominal ΔT_{net} of 5 K, the SCOP goes from 4.4 to 6.1. An increase of 5 K of the nominal temperature drop in the evaporator reduces the SCOP of approximately 0.7 points. This trend holds true for the other two buildings when the supply temperature of the network is in the same range (30-50°C). At lower temperatures, instead, the effect of the temperature difference in the evaporator is lower: approximately 0.3 points every 5 K. In these cases the SCOP varies in a limited range: from 3.1 to 4.1 in building B90 and from 3.4 to 4.4 in the new building.

Table 5.9 - SCOP of the buildings for the combined production of space heating and DHW with different heat pumps, supply temperature and mass flow rates to the evaporators.

$T_{net,su}$ [°C]	Compr.	B70			B90			NB		
		ΔT_{net} [K]			ΔT_{net} [K]			ΔT_{net} [K]		
		5	10	15	5	10	15	5	10	15
15	R407c	-	-	-	3.29	3.11	-	3.67	3.42	-
20	R407c	-	-	-	3.65	3.28	3.11	3.88	3.62	3.40
25	R407c	-	-	-	3.89	3.64	3.28	4.15	3.83	3.58
30	R407c	-	-	-	4.15	3.87	3.63	4.43	4.07	3.78
30	R134a	4.41	3.71	3.13	4.54	3.91	3.63	5.51	4.79	4.12
35	R134a	4.82	4.30	3.64	5.22	4.46	3.82	5.97	5.37	4.69
40	R134a	5.65	4.73	4.00	5.74	5.12	4.38	6.53	5.80	5.25
45	R134a	6.11	5.46	4.48	6.46	5.59	5.03	6.90	6.27	5.64

Looking at Figure 5.12c, one may argue that using a R134a-based heat pump also for cases with network supply temperature lower than 30°C would lead to an advantage over the selected machine based on refrigerant R407c. However, according to the performance curves of the selected compressors, this choice would require two compressors in parallel to reach the desired heat output due to the limited thermal capacity of R134a-based compressor at low evaporating temperatures. Therefore, it was decided here to work with only one compressor, thus having limited COP but avoiding excessive investment costs.

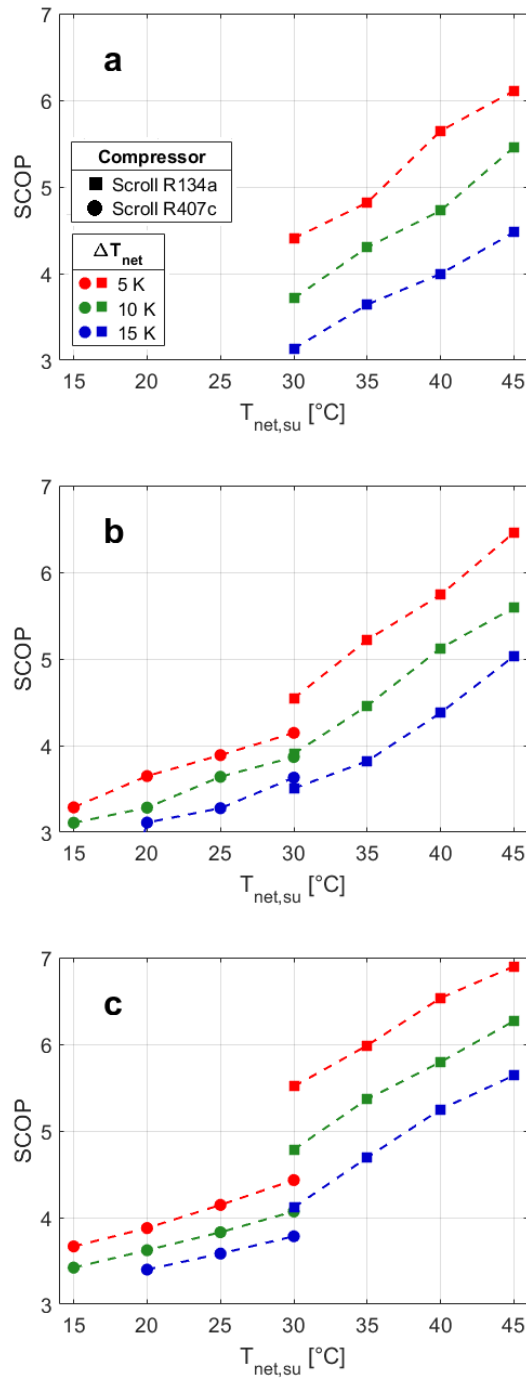


Figure 5.12 - SCOP for buildings (a) B70, (b) B90 and (c) NB.

Economic performance. In the first part of this Section, the results concerning the price of the low-temperature heat p_{lth} and for the all-inclusive tariff p_h are shown for the different business models adopted by the utility to sell the heat. In the following part, the LCOE of the different solutions are compared and the results are discussed.

Tables 5.10 and 5.11 show the low-temperature heat price of the BaU case and the final heat price of the IoU case obtained with the method described above. Different prices were calcu-

lated based on the temperature difference ΔT_{net} used in the network design phase and depending on the area where the network is installed, namely in inner (Category A) or outer (Category B) city areas.

Table 5.10 - Low-temperature heat price p_{lth} [€/MWh] in the BaU case.

$T_{net,su}$ [°C]	$\Delta T_{net} = 5 \text{ K}$		$\Delta T_{net} = 10 \text{ K}$		$\Delta T_{net} = 15 \text{ K}$	
	A	B	A	B	A	B
15	109	95	92	80	-	-
20	105	92	91	78	84	72
25	103	91	88	76	83	71
30	101	88	87	76	84	72
35	97	86	84	73	80	69
40	95	83	82	71	78	67
45	94	83	80	69	76	65

The most evident trend in Table 5.10 is the decrease of the price p_{lth} with increasing network supply temperature. This trend is linked to the different SCOP that the distributed heat pumps yield at different network temperatures. Indeed, when the network has a supply temperature of 15°C the overall SCOP varies between 3.1 and 3.7, whereas it goes from 4.5 to 6.9 when the supply temperature is 45°C, depending on the design temperature difference as discussed in the previous Section. This means that when the network supply temperature is 15°C, the heat pumps need approximately 20% more heat from the network than in the case at 45°C for supplying the same amount of heat to the buildings. This makes it possible to pay back the investment within the same time frame –set here to 15 years- using a lower heat price. Indeed, the price of heat with $T_{net,su} = 45^\circ\text{C}$ is on average 17% lower than with $T_{net,su} = 15^\circ\text{C}$. The second notable fact that emerges from Table 5.10 is that the price of heat decreases with increasing network temperature difference ΔT_{net} . The reason is straightforward: designing the network with a higher ΔT_{net} entails carrying the same amount of heat with lower mass flow rates and, in turn, using smaller pipes. The initial investment is reduced on average by 15% from $\Delta T_{net} = 5 \text{ K}$ to $\Delta T_{net} = 10 \text{ K}$ and a further reduction of -9% occurs from 10 to 15 K. The drop in the price of heat is on average -15% from 5 K to 10 K and around -6% from 10 K to 15 K. Besides the investment costs, also pumping costs are reduced when the district heating network is designed with higher ΔT_{net} . In fact, the share of heat price due to pumping costs is around 13-15% with $\Delta T_{net} = 5 \text{ K}$ and drops to 6-7% with $\Delta T_{net} = 15 \text{ K}$. The trends described above for the BaU model hold true in the IoU case. However, here the different SCOP at different network temperatures affects not only the amount of low-temperature heat delivered to the substations, but also directly affects the amount of electrical energy supplied to the heat

pumps, which is the main operational cost for the utility. Moreover, the latter must also invest in the heat pumps as long as new customers get connected to the network.

Table 5.11 - Heat price p_h [€/MWh] in the IoU case.

$T_{net,su}$ [°C]	$\Delta T_{net} = 5 \text{ K}$		$\Delta T_{net} = 10 \text{ K}$		$\Delta T_{net} = 15 \text{ K}$	
	A	B	A	B	A	B
15	136	128	128	120	-	-
20	132	123	125	117	124	116
25	129	120	121	112	122	113
30	124	116	119	111	122	113
35	119	110	112	104	115	107
40	115	106	108	100	111	102
45	112	103	104	96	106	98

Figure 5.13 sheds light on how the price of heat is formed. The bar charts show the share of investment and operative costs for network installed in inner city areas with supply network temperature of 20°C (a) and 45°C (b). Investment costs are divided into those occurring at time 0 (blue) and those occurring throughout the lifetime of the project, such as the investment for heat pumps and service pipes for new customers (light-blue). The operative costs are divided into “fuel costs” (green), i.e. electricity for pumps and heat pumps and costs for waste heat recovery, and maintenance costs (light-green). Fuel costs are expressed as:

$$C_{dhs,fuel} = C_{hs} + C_{el,p} + C_{el,hp} \quad (5.21)$$

If the supply temperature of the network is 20°C the fuel costs cover approximately 53-57% of the heat price, while this component drops to 43-48% with $T_{net,su} = 45^\circ\text{C}$. The variation with the network temperature difference is not particularly evident because the decrease of SCOP is counteracted by the higher energy needed for circulating the water in the network, as shown in Figures 5.13 for $T_{net,su} = 20^\circ\text{C}$ (c) and $T_{net,su} = 45^\circ\text{C}$ (d). Figure 5.14 compares the levelized cost of energy (LCOE) of the district heating system with booster heat pumps to that of existing and new gas boilers for the end user. The gas boilers are used as benchmark to assess the competitiveness of the proposed system. Each bar chart is referred to one of the reference buildings and to one of the financial models –namely BaU or IoU. Figure 5.14 shows that the three buildings have similar LCOE. This is a trivial fact for the IoU case, where the LCOE coincides to the price of heat for the customers of the district heating utility. On the other hand, in the BaU business model this fact means that the lower consumption does not affect the cost-effectiveness of the system for new buildings, where the specific costs for the heat pumps are higher than for old buildings.

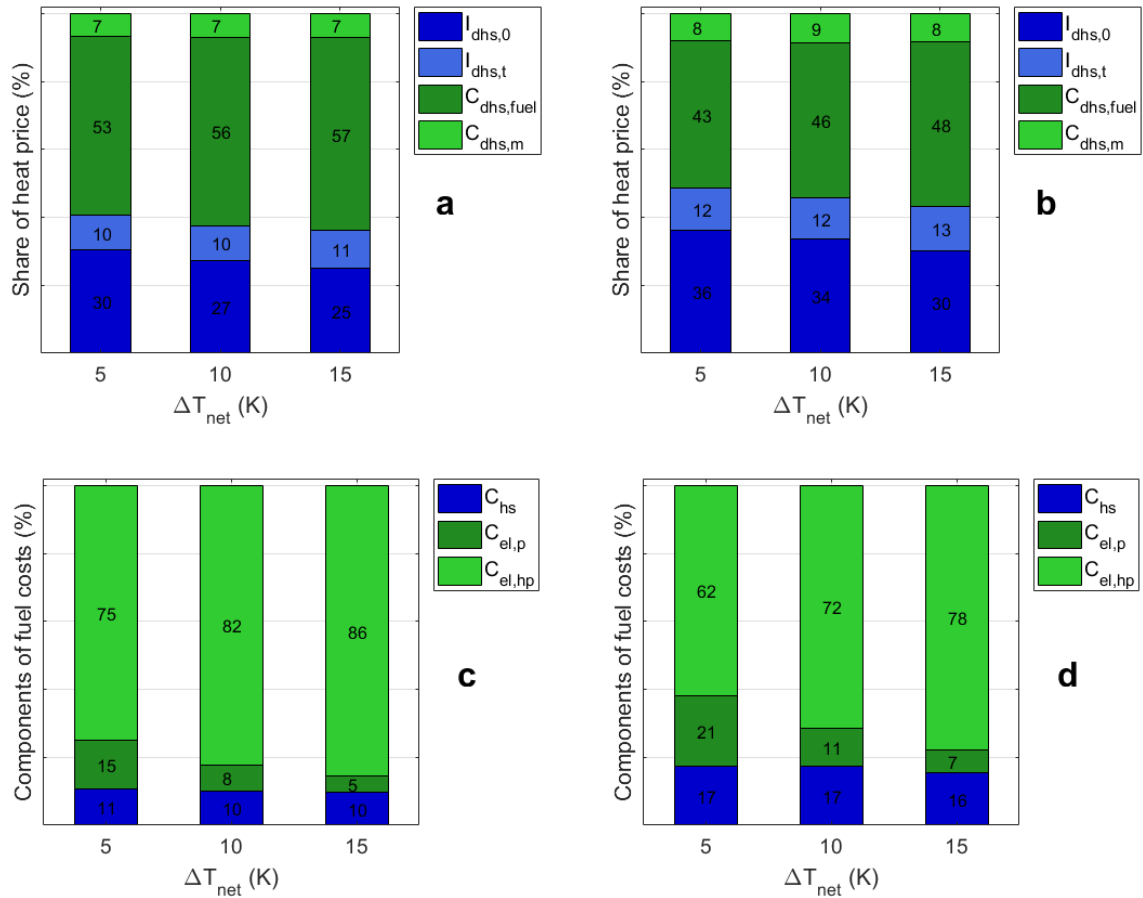


Figure 5.13 - Components of heat price p_h in the IoU case with supply network temperature of (a) 20°C and (b) 45°C; components of fuel costs for (c) 20°C and (d) 45°C.

The higher initial cost is indeed compensated by a higher efficiency of the heat pumps, thus reducing the expense for electricity during the lifetime of the system. The positive effect of higher network temperatures on the COP of the heat pumps does also influence the LCOE of the system because on one hand it increases the amount of heat required by the heat pumps evaporators for a given heat demand of the building, and on the other hand it decreases the amount of electricity needed by the heat pump compressors, as discussed above. When the network supply temperature is 45°C, the LCOE is on average 13-16% lower than with $T_{net,su} = 30^\circ\text{C}$ and 25-27% lower than with $T_{net,su} = 15^\circ\text{C}$. The LCOE is also significantly affected by the design network temperature difference. In the BaU cases, the LCOE of the system designed with $\Delta T_{net} = 5\text{ K}$ is on average 8.1% higher than with 10 K. With $\Delta T_{net} = 15\text{ K}$, the LCOE is higher than with 10 K only for the old building (+2.9%). For building B90 there is no significant variation in LCOE from 10 K to 15 K, and for the new building the LCOE seems to show a decreasing trend (-0.6%). In the IoU cases, the minimum between 5 and 15 K

seems to occur for all the considered buildings, and is more evident in the old building than in the other ones. In fact, the LCOE with $\Delta T_{net} = 5$ K is on average 6.3% higher than with 10 K and with $\Delta T_{net} = 15$ K it increase by 3.8% for building B70 and around 2.4% for the other buildings. A low ΔT_{net} increases the evaporating temperatures of the heat pumps, thus increasing the COP and consequently decreases the operative costs for the consumer. On the other hand, designing the network with a lower temperature difference turns into higher pipe diameters and therefore into higher investment costs for pipelines and higher pumping costs due to higher mass flow rates. Under BaU conditions, the results clearly show such trade-off for the old building with poor insulation, while it is less evident as long as new and refurbished buildings are considered. Under IoU conditions, the trade-off occurs for all the considered buildings. This effect is probably related to the ratio between initial investment and operative costs for the end user. In fact, in the BaU case the end user invests in the heat pump at time 0, which smooths the effect of variations in the operative costs –such as higher expenditure for electricity when the COP is lower. In the IoU case, the end user does not perceive this effect because the investment is made by the utility. Moreover, the compressor of the heat pump is assumed to work with variable speed. This means that at partial loads the evaporating temperature and the COP of the heat pump are higher than with a conventional on/off regulation. Thus, if an on/off regulation were considered, these trends would probably be more marked. In terms of absolute values, the IoU business model seems to be slightly more convenient than the BaU, especially for new buildings. In fact, the LCOE for the end user is on average 5% lower for building NB, and 2.5% lower for building B90. For the old building, this decrease does not seem significant (-0.8%). This is likely due to the effect of the initial investment in the BaU cases, that weighs more on the overall economic balance for low energy buildings than for old ones with poor thermal insulation. If the network supply temperature is 40°C or 45°C, the district heating system with booster heat pumps competes with condensing gas boilers. In fact, at this network temperature the LCOE of the best design solution is always equal or lower than that of individual gas boilers (around 94 €/MWh) under the cost assumptions reported above. At lower network temperatures, the proposed system can compete provided that the electricity is purchased at lower prices. Alternatively, the electricity needed by the heat pumps could be partially self-produced and transported via micro-grid. However, this scenario goes beyond the objectives of the present study and was not analysed here.

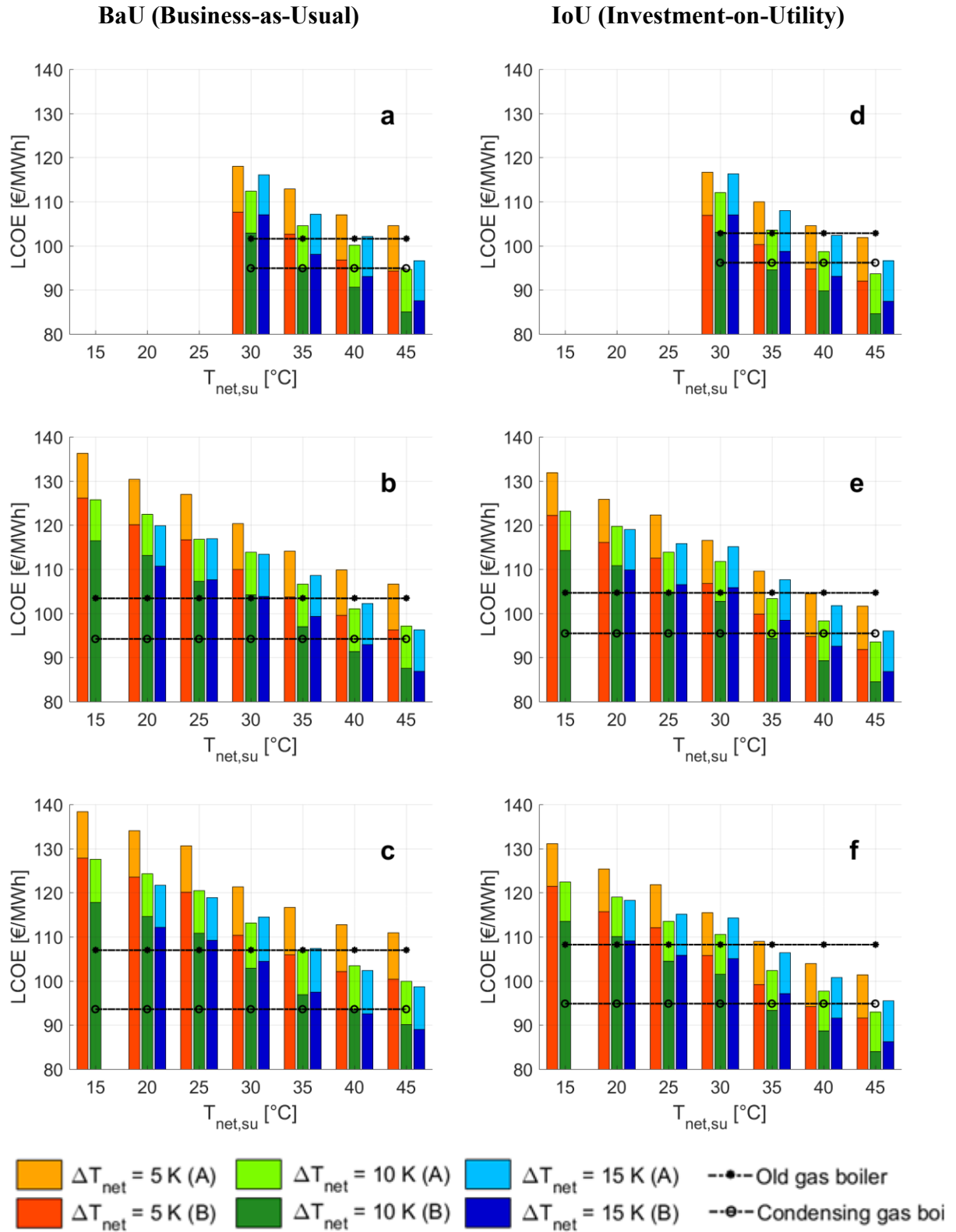


Figure 5.14 - Levelized cost of energy of the d-HPDH system and of gas boiler for multi-family buildings (a,d) B70, (b,e) B90; (c,f) NB with an incentive of 26 €/MWh.

5.3 Conclusions

The present study investigates the suitability of an innovative concept of district heating networks, that allows the utilization of low temperature heat sources (available at temperature $\leq 50^{\circ}\text{C}$) for domestic hot water production and for space heating of new and existing buildings. The proposed system is supplied by the local heat source, distributes heat through the pipes at low temperature (here a range between 15°C and 45°C was considered) and uses distributed heat pumps to raise the temperature level according to the requirements of the supplied building.

A preliminary analysis has shown that this concept performs better than a conventional solution with one centralized heat pump and an auxiliary gas boiler from an environmental point of view. In fact, the use of natural gas can be avoided and the overall performance of the pool of distributed heat pumps is superior to that of a large-size unit equipped with a centrifugal compressor. This occurs because each heat pump adapts the supply temperature according to the building served, while in conventional district heating systems the supply temperature must be high enough to supply the most critical customer. It was calculated that the DH system with booster heat pumps supplied by waste water at 40°C can dramatically reduce carbon dioxide emissions and primary energy consumption of a real neighbourhood –case study 1- compared to the conventional district heating system (around -30%) and to individual gas boilers (around -70%). Four scenarios were then drawn for the Municipality of Abano Terme based on on-field measurement and historical data on thermal water withdrawal and on heat demand. It came out that even with pessimistic assumptions on temperature and mass flow rates, the thermal water released by hotels and thermal spas could cover the heat demand of almost 80% of the residential building stock of the town. With more realistic assumptions, the heat demand could be entirely covered.

A parametric study was then carried out to investigate the economic performance of the proposed system, assuming that the latter is supplied entirely by low temperature heat sources and assuming two different business models for the heat sale of the DH utility. Water-to-water heat pumps already available on the market were selected and simulated with a simplified heat pump model implemented in TRNSYS, assuming to use a hot water tank for DHW production. The simulations showed that the seasonal coefficients of performance (SCOP) vary between 3.1-3.6 when the network supply temperature is 20°C to 4.0-5.8 when the latter reaches 40°C . The wide range depends on the supply temperature curve of the building and on

the network temperature difference between supply and return line. Table 5.9 is a valid reference for those who want to evaluate new projects based on this concept.

Successively, an economic analysis was carried out to evaluate the cost of heat for three multi-family houses in Northern Italy. The payback time for the utility was fixed to 15 years and the levelized cost of energy was calculated adopting two different business models.

In the “Investment-on-Utility” (IoU) model, the DH utility invests in the heat pumps and purchases the electricity, whereas in the “Business-as-Usual” (BaU) solution the DH utility is only responsible for the recovery and distribution of heat and the user pays for the electricity and for the district heat separately. The IoU business model has proved to be more cost-effective as it allows to avoid the financial barrier of the initial investment for the end user, that significantly affects the economic balance especially for new and refurbished buildings. Moreover, a DH utility adopting the IoU business model has more contracting power than single residential users. Therefore, it could probably negotiate with the DSO to get cheaper electricity prices.

Working with high network temperatures allows to achieve two positive effects at the same time: on one hand, the DH utility sells more heat for a given heat demand of the buildings, and on the other hand the electrical expenditure is lower. Therefore, unless the electricity is self-produced (case that was not considered here), it is always convenient to work with the highest possible network supply temperature, according to the local heat source that is available. Given the costs of electricity and of the low temperature heat, the LCOE of the system with a supply network temperature of 40°C is from 15 to 20% lower than with supply temperature of 20°C. In the considered case-study, the DH network with supply temperature of 40°C with the incentive on renewable district heat competes with condensing gas boilers.

The nominal temperature difference between supply and return line (ΔT_{net}) is a key design parameter in low-temperature district heating systems with decentralized heat pumps. Indeed, a low ΔT_{net} increases both the COP of the heat pumps and the investment cost of the network due to higher cross sections of the pipes. A trade-off between low investment costs (high ΔT_{net}) and low operative costs (low ΔT_{net}) must therefore be pursued in the design phase. This trade-off emerges from the comparison of the LCOE corresponding to the three values of ΔT_{net} adopted in the parametric study. Regardless of the adopted business model, designing the network with $\Delta T_{net} = 5$ K always leads to excessive costs. Under the assumptions used in

this study, an optimal mass flow rate seems to occur around $\Delta T_{net} = 10$ K. From the observation of the LCOE of the different buildings it can be inferred that the optimal value will increase with the number of refurbished/new houses connected to the network as a result of a lower ratio between operative costs and initial investment in the infrastructure. These last aspects deserve a more detailed analysis and will be addressed in future research.

5.4 Discussion on the validity of the results

The conclusions achieved so far rely on the following assumptions:

- All the heat provided to the network comes from waste or renewable heat sources that can be recovered at low cost;
- The cost of electricity is much higher than the cost of the recovered heat;
- The supply temperature curves are fixed for each building typology.

The first assumption aims at simplifying the problem, in light of the numerous cases considered in the parametric study. As reported in the literature review, in a previous study [51] it was found out that, according to a First-Principle analysis, the ULTDH system (the district heating system with booster heat pumps) is preferable to the LTDH system only when heat is provided by a central heat pump, and not when heat is supplied by a CHP plant. This occurs because the gain in total efficiency of the CHP is overwhelmed by the higher electricity needed to feed the booster heat pumps. The decrease in the network temperatures brought by the ULTDH system leads to a significant drop in energy consumption when a low temperature heat source is present. This result partially justifies our assumption. However, a more complete analysis should include the comparison between direct heat recovery and use of central heat pumps when the low temperature heat sources are at almost neutral temperatures, i.e. lower than 30°C. The presence of conventional fossil-fuelled plants, such as gas boilers or CHP plants, as well as of central heat pumps, would probably drag the optimal return temperatures to lower values.

As far as the second assumption is concerned, the values of electricity price assumed in the analysis are in line with those one can currently find in the Italian market. A different case would be to self-produce the electricity via local power plants and to distribute it to the heat pumps via a microgrid. In this case, the challenge would probably be to reduce as much as possible the amount of heat purchased by the bulk grid. This introduces control issues that are partially addressed in the next Chapter.

The last assumption reduces the number of considered cases, excluding refurbished buildings from the parametric study. Total or partial refurbishment of the building envelope would in fact allow using lower supply temperatures in existing buildings. Moreover, the supply temperature curves adopted in the study are quite conservative and could probably be lower by extending the operation period of the heat pumps or by tolerating thermal discomfort for a limited number of hour a year. This means that the SCOP could probably be higher than those calculated here.

Chapter 6 System control

6.1 Introduction

This Chapter presents two control strategies to control the central heat supply units (a CHP plant and a GB) of a low temperature DH network with decentralized heat pumps at the customer substations and with a significant share of heat injected from intermittent waste heat substations. The “basic” control logic (BAS) aims to keep the average supply temperature within a small range and thus considers the stability and quality of heat supply as the major priority. The “advanced” control logic (ADV) is instead an economically optimised control solution that is able to cope with the changing electricity and fuel prices and with the varying heat load and waste heat availability to reduce the overall cost for the heat supply.

The case study is thoroughly described in Section 4.2. However, here it is briefly recalled to improve readability. The system consists of a district heating network distributing heat at low temperature (in a range between 20°C and 30°C) to decentralized heat pumps, which have to fulfil the heat demand of the buildings in the given area. The annual heat demand amounts to approximately 20.7 GWh with a peak load around 6.0 MW. The NM of the considered system is responsible for balancing the energy flows and owns the central supply station of the district heating grid that consists of a 2.2 MW gas-fired reciprocating engine that produces combined heat and power (CHP) and a 2.3 MW auxiliary gas boiler (GB) assumed here to have a constant efficiency of 80%. A 330 m³ central storage tank is used to buffer the heat supply by the CHP unit. The NM is also responsible for the power supply to the heat pumps, that is either bought or self-produced with the CHP plant. The water-to-water heat pumps use R407c as refrigerant and provide water to the buildings at 55-65°C. The performance of the heat pumps is affected by the temperature of the water supplied by the DH network. A higher network temperature increases the COP of the heat pumps, which turns into a lower power con-

sumption of the compressors for a given heat demand of the buildings. As long as the power consumption is reduced, a higher amount of heat is extracted from the DH network. Furthermore, two additional substations supply waste heat to the network. In our case-study, two levels of heat source temperature are considered: one at 40-50°C (low-temperature waste heat, LTWH) which is typically the temperature of water coming from condensing units of refrigeration processes and one at 80-90°C (medium-temperature waste heat, MTWH), which corresponds to the waste heat of an industrial process. Note, that the network temperature also influences the heat recovery from these low temperature waste heat substations due to the changing temperature difference between hot and cold fluid. However, the NM does not directly control the two substations and the feed-in occurs as long as waste heat is available.

The control concepts are discussed in Section 6.2 and the used models, including the optimization problem are presented in Section 6.3. The simulation results are discussed in Section 6.5 and, finally, conclusions are drawn in Section 6.6.

6.2 Method

In this Section the basic (“BAS”) and the advanced (“ADV”) control concepts are described. To evaluate their performance, a 2-month simulation of the system was run with both control loops. Both control schemes are compared with respect to their overall operational cost. The latter is defined as the sum of all the costs for the heat supply of the network minus the incomes resulting from the electricity sold to the market. The costs for the heat supply include the gas cost, the running costs for the CHP, the heat purchased to the waste heat substations and the electricity purchased for the heat pumps. Note that part of the electricity produced by the CHP is consumed by the heat pumps. The simulations are carried out in TRNSYS 17 [11].

6.2.1 Basic control

This basic operation mode assumes very limited communication abilities within the network, as only local sensors and actuators are used. It consists of three loops: the supply temperature loop, the pressure loop and the unit commitment. In the first loop, every generation unit is regulated to provide hot water at a given desired temperature allowing the network to run under nominal conditions. Hereby the CHP unit is operated by means of a hysteresis controller to keep a given threshold temperature in the central storage tank and the gas boiler is controlled at a given constant outlet temperature. The pressure is regulated in closed-loop mode and the pump speed is adjusted to maintain a given constant pressure differential on the main

supply node. The set point is chosen to ensure a sufficiently high pressure difference to the most critical consumer. For the unit commitment, a simple algorithm is used that takes the storage, the ambient, the supply and the return temperatures into account. More precisely, the gas boiler is started once the ambient temperature goes below a given threshold and it is switched on if the network return temperature decreases below 5°C and the CS is already releasing the highest possible heat flow as shown in Figure 6.1. The storage itself is discharged as long as the supply line temperature does not reach the given set point of 35°C . Since frequent switching of the units causes unnecessary start-up and shutdown costs, two hysteresis of 5 K are foreseen.

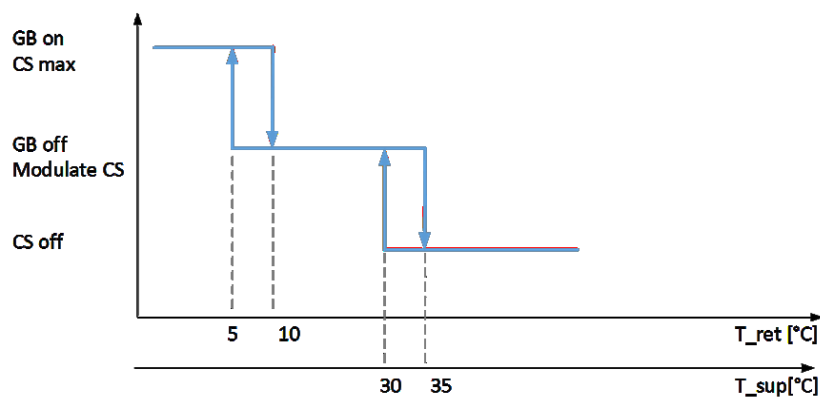


Figure 6.1 - Temperature driven unit commitment of the basic control logic.

6.2.2 Advanced control

The so-called advanced control uses a look-ahead structure based on three consecutive steps: forecast, planning and real-time operation. The planning phase consists of an optimization that uses ideal forecasts of prices and loads (heat demand and waste heat availability) to schedule the operation of the generation units for a time horizon of several hours, set in this case to 12 hours. From this schedule, the values of the first hour are used as targets within the real-time controller (RTC). This controller is meant to react to deviations from the situation assumed in the planning phase, which typically arise in the real system due to the simplifications done in the optimization and, in the real world, due to the uncertainty of predictions. The used targets are three energy values (heat from CHP to CS, heat from CS to the network and heat from GB to the network) and the temperature set point of the network supply lines. The RTC adjusts the mass flow rates of the four pumps and the valve opening of the three-way valve every five minutes, seeking to approach the hourly target within 60 minutes. After each

hour, the above process is repeated. Figure 6.2 provides an overview of this control. The optimization is fully described in the Section 6.3.1.

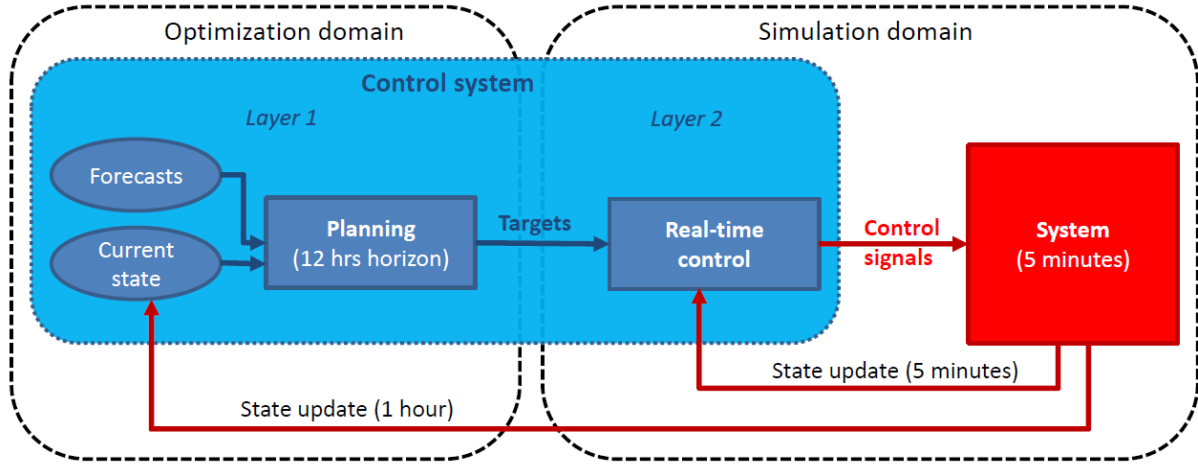


Figure 6.2 - Schematic overview of the advanced control logic.

A TRNSYS 17 simulation is used to reproduce the behaviour of the system with a higher level of detail and to provide the state updates (time-step of 5 minutes within the real-time control) to the optimization (every hour). The Planning and the Real-time control are implemented in MATLAB [5] and linked to TRNSYS 17 via Type 155. The objective of the smart control is to use the central heat storage tank and the water in the pipelines as buffers to optimize the heat production with respect to economic costs. Due to the high gap between selling and purchase price of electricity –see Table 6.1-, the optimization automatically matches the electricity demand of the heat pumps to the electricity produced by the CHP. The price of electricity considered in this study was taken from the German-Austrian spot market price database relative to year 2015 . In Table 6.1 the mean value and the standard deviation are shown for clarity.

Table 6.1 - Economic parameters used in the case-study.

Parameter	Value [€/MWh]
c_{gas}	50
$p_{ee, buy}$	175
$p_{ee, sell}$	$\mu = 32.5, \sigma = 14.4$
c_{wh}	10

Although in this case-study only one storage tank (CS) is used, the proposed method is perfectly suitable for the management of a several decentralized heat storage tanks, positioned for instance in strategic places such as in the WH substations. However, if a high number of

heat storage tanks (in the order of hundreds) would have to be managed, the computational burden might be too high.

6.3 Models

As explained in the previous Chapter, the advanced control strategy includes both a look-ahead planning (indicated in the following also as scheduling or optimization) and the RTC. A detailed simulation model is used, that simulates the physical system with a higher level of detail compared to the simplified model used in the planning phase. The following sections explain the improvement of the detailed simulation model over the simple one.

6.3.1 The optimization problem

The scheduling is formulated as a Mixed Integer Linear Programming (MILP) problem, meaning that all the relations between physical variables (e.g. energy balances) are expressed as linear equality and inequality constraints. These constraints are described in the following. Both the CS and the network are modelled as fully mixed thermal storage systems. Thus, their state of charge is indicated by only one value, which can be interpreted as their average temperature. In the network case, the temperature refers to the supply pipe. This simplification allows to consider the network as a buffer with energy flows in both directions. The values of the variables (state of charge of the buffers $S_{cs,j}$ and $S_{ns,j}$ and status -on or off- of the CHP $x_{1,j}$) are given with one-hour time resolution. Equation (6.1) and (6.2) are the energy balances of the CS tank and of the network. In Equation (6.3), the state of charge of the return pipe is estimated from that of the supply pipe by making the energy balance at the heat pump evaporators. In Equation (6.4), the inverse of the COP is also estimated as a linear function of the return network temperature. In Equations (6.5) and (6.6), the power and the heat output of the CHP are respectively calculated. The index j in the equations refers to the j -th hour. Thus, we have $j = 1, \dots, 12$:

$$S_{cs,j} = S_{cs,j-1} + x_{1,j}Q_{chp,min} + Q_{chp,mod,j} - x_{2,j}Q_{cs} \quad (6.1)$$

$$S_{ns,j} = S_{ns,j-1} + x_{2,j}Q_{cs} - x_{3,j}Q_{gb} + \sum_{p=1}^{NP} Q_{rec,p} - (1 - f_{cop,j}) \sum_{c=1}^{NC} D_c \quad (6.2)$$

$$S_{nr,j} = S_{ns,j} - (1 - f_{cop,j}) \sum_{c=1}^{NC} D_{c,j} \quad (6.3)$$

$$f_{cop,j} = k_{cop,0} + k_{cop,1}S_{nr,j} \quad (6.4)$$

$$W_{chp,j} = k_{chp,a}x_{1,j} + k_{chp,b}(x_{1,j}Q_{chp,min} + Q_{chp,mod,j}) \quad (6.5)$$

$$Q_{chp,in,j} = k_{chp,c}x_{1,j} + k_{chp,d}W_{chp,j} \quad (6.6)$$

Inequality (6.7) expresses that the heat output of the CHP is modulated between $Q_{chp,min}$ and $Q_{chp,max}$ and only if the CHP is on ($x_{1,j}=1$). The inequalities (6.8-10), instead, define the moment when a start-up of the CHP occurs ($x_{su}=1$), which is needed to apply a penalty for an excessive number of start-ups. The inequality (6.11) is a technical constraint used to limit the heat discharge rate of the CS as function of its state of charge.

$$Q_{chp,mod,j} \leq x_{1,j}(Q_{chp,max} - Q_{chp,min}) \quad (6.7)$$

$$x_{su,j} \geq x_{1,j} - x_{1,j-1} \quad (6.8)$$

$$x_{su,j} \leq x_{1,j} \quad (6.9)$$

$$x_{su,j} \leq 1 - x_{1,j-1} \quad (6.10)$$

$$Q_{cs,j} \leq k_{cs,0} + k_{cs,1}S_{cs,j} \quad (6.11)$$

The inequalities (6.13-16) are meant to limit the heat recovered from the WH sources according to the return temperature from the network and to the amount of heat that is actually available. The latter is defined as follows:

$$Q_{av,p} = m_{hs,p}c_p(T_{hs,av,p} - T_{min,p}) \quad (6.12)$$

where $m_{hs,p}$ and $T_{hs,av,p}$ are the mass flow rate and the temperature of the heat carrier of “prosumer” p and $T_{min,p}$ is its minimum return temperature, which is specific to the process of prosumer p . In our case, we set this lower limit to 22°C for the low-temperature heat source and to 50°C for the medium-temperature heat source. Finally, the inequalities (6.17-18) define the maximum amount of self-consumed power at each hour j . Thus, the following holds true for $\forall j=1,\dots,12$:

$$Q_{rec,1,j} \leq Q_{av,1,j}(k_{he1,0} + k_{he1,1}S_{nr,j}) \quad (6.13)$$

$$Q_{rec,2,j} \leq Q_{av,2,j}(k_{he2,0} + k_{he2,1}S_{nr,j}) \quad (6.14)$$

$$Q_{rec,1,j} \leq Q_{av,1,j} \quad (6.15)$$

$$Q_{rec,2,j} \leq Q_{av,2,j} \quad (6.16)$$

$$W_{chp,self,j} \leq W_{chp,j} \quad (6.17)$$

$$W_{chp,self,j} \leq f_{cop,j} \sum_{c=1}^{NC} D_{c,j} \quad (6.18)$$

The problem has 14 “physical” independent variables that are summarized in Table 6.2.

Table 6.2 - Variables used in the optimization

Number	1	2	3	4	5	6	7
Name	S_{cs}	S_{ns}	S_{nr}	x_1	x_2	x_3	$Q_{rec,1}$
Type	real	real	real	int	real	real	real
Number	8	9	10	11	12	13	14
Name	$Q_{rec,2}$	f_{cop}	$Q_{chp,mod}^r$	x_{su}	W_{chp}	$Q_{chp,in}$	$W_{chp,self}$
Type	real	real	real	int	real	real	real

As there is one schedule (12 hourly values) for each “physical” variable, the problem has $14 \cdot 12 = 168$ variables (of which 24 are integer) and $6 \cdot 12 = 72$ equations. Therefore the optimization problem has 96 degrees of freedom, which correspond to the optimal schedules of eight decision variables. The latter are: heat provided by the CHP to the CS specified by an on-off signal (var.4) and a heat flow rate (var.10); normalized heat provided by the CS to the network (var. 5); normalized heat provided by the GB to the network (var.6); state of charge of the network (var.2); heat recovered from the WH sources (vars. 7 and 8) and power used to feed the heat pumps (var.14). The objective function of the optimization aims to minimize the overall operational costs of the system, as given in (6.19).

$$f = c_{gas} Q_{chp,in} - p_{el,sell} (W_{chp} - W_{chp,self}) + x_{su} SUC_{chp} + c_{gas} Q_{gb} + c_{wh} (Q_{rec,1} + Q_{rec,2}) + p_{el,buy} \left(f_{cop} \sum_{c=1}^{NC} D_c - W_{chp,self} \right) \quad (6.19)$$

In conclusion, the optimization problem can be summarized as follows:

$$\min f(x) \quad (6.20)$$

subject to equalities (6.1) – (6.6) and to inequalities (6.7) – (6.18).

6.3.2 Detailed simulation model

The optimal schedule for this MILP for a given 12-hour period is then passed to RTC. This RTC in principle uses only the values of the variables of the first time interval (hour) and sends control signals on a higher time resolution to the different components of the system. The RTC receives feedback signals from the system and recalculates the control signals ac-

cordingly at each time step as briefly described in the ‘Methods’ Section. By simulating the system with a 5-minute time-step, we are able to reproduce the behaviour of the system with an acceptable approximation. There are four points where the detailed simulation brings an actual improvement over the linear model described in the previous section:

- (a) The model *spHeat* based on Finite Element Method is used to reproduce the hydraulic and thermal behaviour of the District Heating system [119].
- (b) Stratification in the central thermal storage system is considered by using TRNSYS Type 4.
- (c) The behaviour of the heat pumps is calculated using a TRNSYS Type described in Section 3.3.
- (d) The heat output and the electrical power output of the CHP are calculated with non-linear performance curves based on data provided with the TRNSYS TESS libraries.

Figure 6.3 shows the topology of the network and the position of the heat suppliers and consumers. The district heating network model used is *spHeat*, that was chosen instead of the model presented in Chapter 3.2 because an interface with the simulation software TRNSYS was already available.

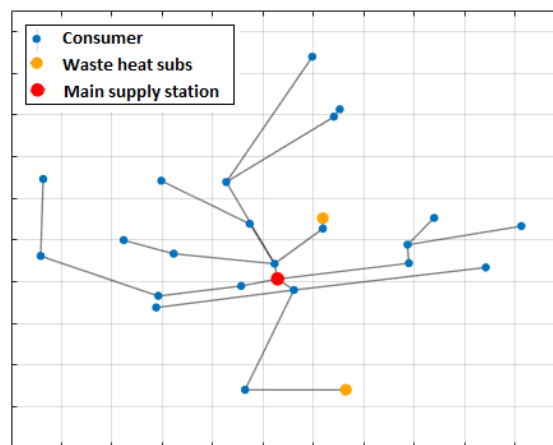


Figure 6.3 - Topology of the considered DH network.

Although these models bring a significant improvement over the linear equations described above, there are still some features that can be improved. Indeed, the typical on-off behaviour of the heat pumps is not considered, as the heat pumps are modelled as variable speed heat pumps under continuous operation. Moreover, each heat pump used in the simulation aggre-

gates a group of buildings. Although the heat pump model would be able to separate between space heating and domestic hot water operation, the latter is not considered here, as the simulation does not include the hot water tanks at the customer substations.

6.4 Results and discussion

In the first section, the strategies adopted by the planning are shown and commented. The second section provides some insights on the limits that arise when implementing the optimization in the –simulated- physical system. In third and last section the comparison between the advanced and the basic control is carried out.

6.4.1 Optimal planning

In this Section the output of the optimization is discussed without considering its implementation in the simulation. Figure 6.4, 6.5 and 6.6 show the forecasts (heat demand, electricity price and waste heat availability) and the schedules calculated by the planning for typical days in winter, summer and middle seasons, respectively.

The first graph of Figure 6.4b shows that the CHP produces around 1100 kW electricity, i.e. it runs at its minimum capacity of 50% in order to supply heat to the network and at the same time cover the power demand of the heat pumps. Due to the low thermal output of the CHP, the CS is discharged during the first 3 hours (see reduced temperature) to allow a higher production during off-peak hours (between hour 6 and 7), when the electricity price is higher and the CHP is running at full capacity. During the first 3 hours there is a significant amount of heat available. Thus, the gas boiler remains off. Then, it is switched on (hour 4) as the waste heat sources are forecasted to inject less heat. From hour 8 to hour 11, the GB lowers its production and now the CS that was charged during off-peak hours by the CHP, delivers thermal energy to the network. Most of the remaining part is covered by the WH sources. The network temperature stays stable at 20°C in order to maximize the share of electricity self-consumption. This allows to maximize the heat recovered by the low temperature waste heat and to minimize the heat demand of the network.

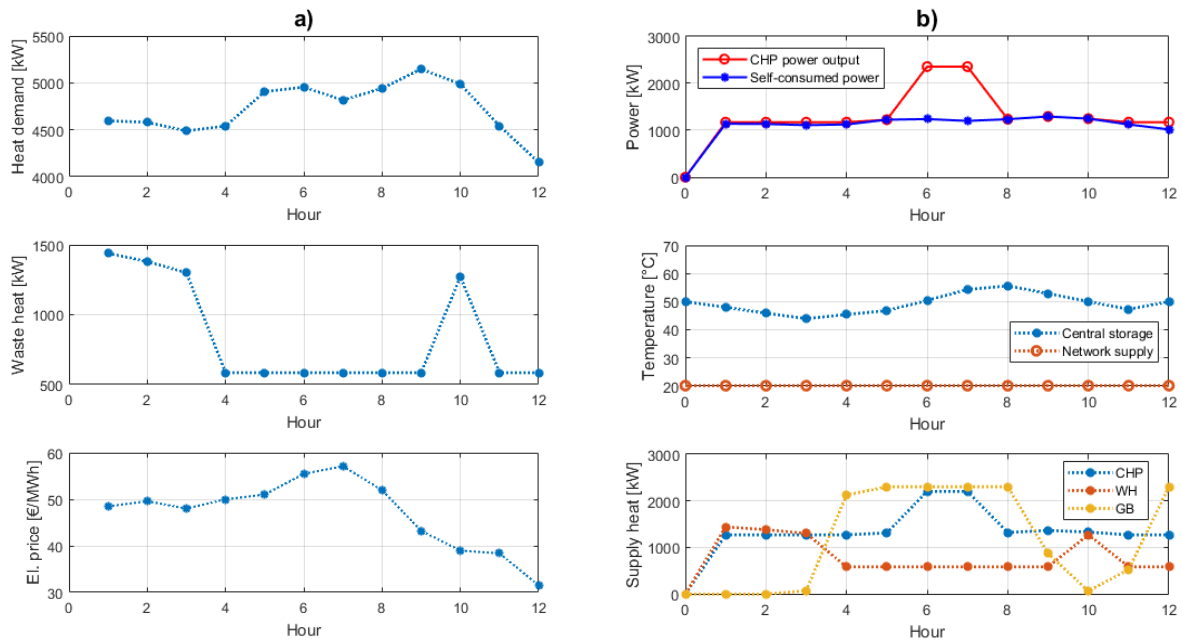


Figure 6.4 - (a) Forecast and (b) optimization output for a typical winter day.

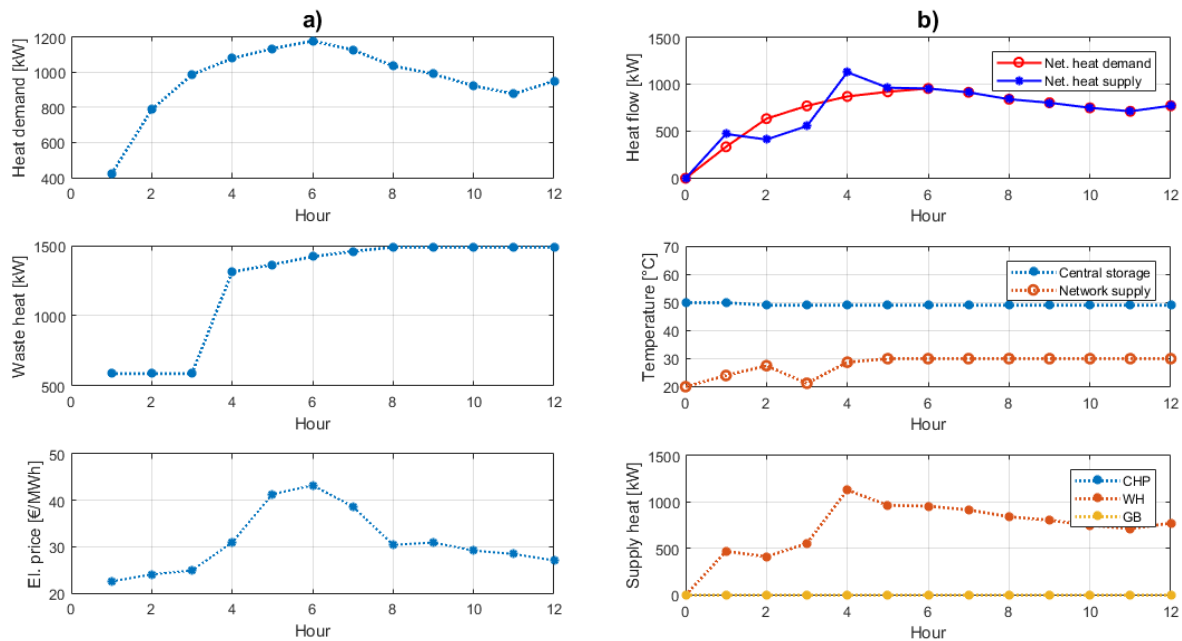


Figure 6.5 - (a) Forecast and (b) optimization output in a typical summer day.

During summer, the policy adopted by the smart controller is completely different as can be seen in Figure 6.5. Due to the low heat demand, the share of electricity self-consumption is not sufficiently high to justify switching on the CHP. If this had done, a great part of the generated electricity would have been sold to the market. Thus, the strategy is to reduce the power

demand further by increasing the network temperature, consequently increasing the COP of the heat pumps. This policy is driven by the high electricity purchase price. As a drawback, a higher heat demand occurs at the network side and the waste heat recovery slightly decreases. Thanks to the high amount of waste heat available from hour 3, this strategy allows to minimize the costs and at the same time to cover all the heat demand forecasted for the next 12 hours by only relying on the low grade heat sources. The thermal inertia of the water in the pipelines is used to match the profiles of supply and demand between hour 1 and hour 5. Other simulations –not shown here- showed that when the waste heat available is not enough to cover the heat demand, also the gas boiler is switched on. During middle seasons, the supply temperature is kept most of the time at 30°C to decrease the power consumption of the heat pumps. The waste heat substations supply the “base load” to the network. If the waste heat is not enough and the electricity price is high enough to justify its operational costs, the CHP is turned on at minimum load. Otherwise, the missing heat is provided by the gas boiler as in summer. When the CHP is turned on at minimum load, the supply temperature is reduced to 20°C to increase the power consumption, with the aim of maximizing the share of self-consumed electrical energy.

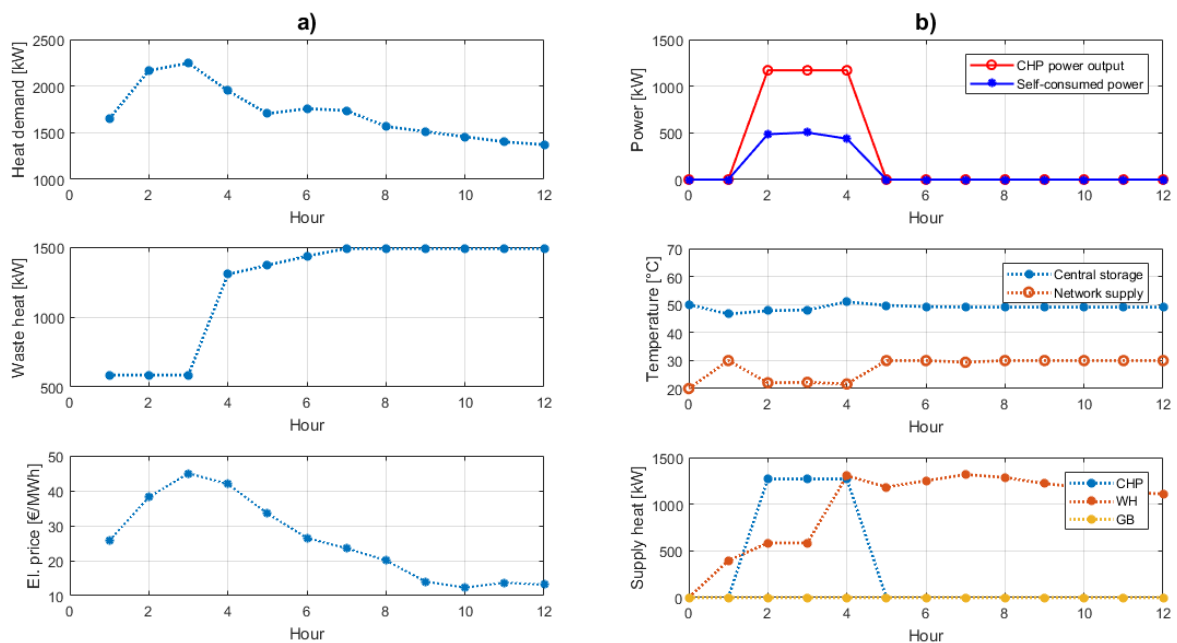


Figure 6.6 - (a) Forecast and (b) optimization output in a typical day of spring/autumn.

6.4.2 TRNSYS Simulations

The optimization discussed above is repeated in a rolling horizon fashion every hour within the advanced control. Thus, every hour the targets of thermal energy and temperatures (see the third section) must be achieved. Nonetheless, the targets are not always met because of the non-linear behaviour of the system and because of effects that are not considered in the optimization. This implies that the states of the buffers deviate from the predicted values calculated during the optimization. In the following, an example of this effects is reported.

In Figure 6.7, the deviations of the network supply temperature from the target values for a specific case are given. It can be noticed that at the central supply station (red dots), the target (blue line) is almost always met, apart from a short period when the supplied temperature is 4-6 K lower than the set point. On the other hand, the average temperature of the supply lines (green dots) is on average 2 K higher than the set point.

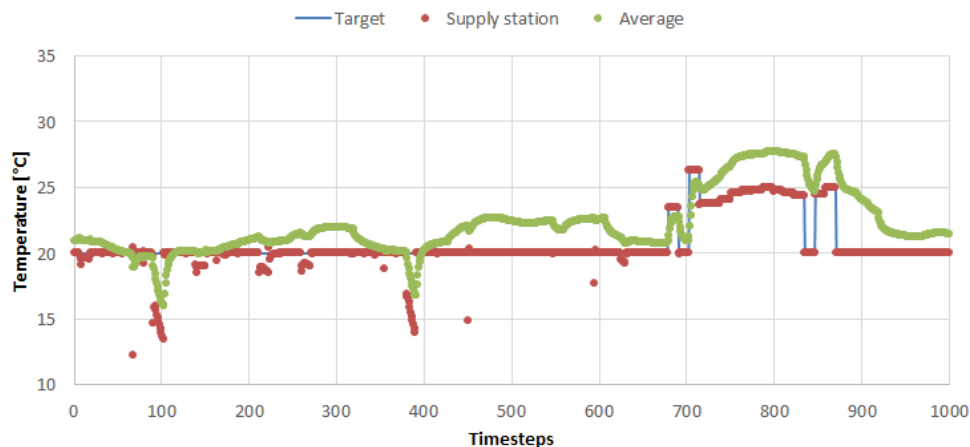


Figure 6.7 - Example of supply network temperature with the advanced control (targets and actual values from simulation).

This deviation arises because a hot temperature wave coming from the WH substations propagates through the network when these stations inject heat. In future work the possibility of imposing an hourly set point temperature to the prosumers to prevent this problem will be investigated. A further problem is that the current layout of the central station (displayed in Fig. 6.1a) is not well suited to the purpose of controlling the heat discharge rate of the CS and the supply network temperature simultaneously. This is due to the disturbance effect of the GB on the return temperature of the cold fluid to the CS. Figure 6.8 shows the target and the actual values of the temperature in the CS. Since stratification occurs in the tank, the state of charge can be obtained by averaging the temperatures measured by sensors placed at different

heights. The red dots represent the average tank temperature, while the green dots are an average of three measurement points coming from sensors placed in the bottom, middle and top of the tank. The average tank temperature has a mean error of 1.4 K compared to the target, whereas the average of the three measurements, that was used to update the state of charge of the CS, shows a negligible mean error. This confirms that the RTC is able to follow the scheduled cycles of charge and discharge of the CS.

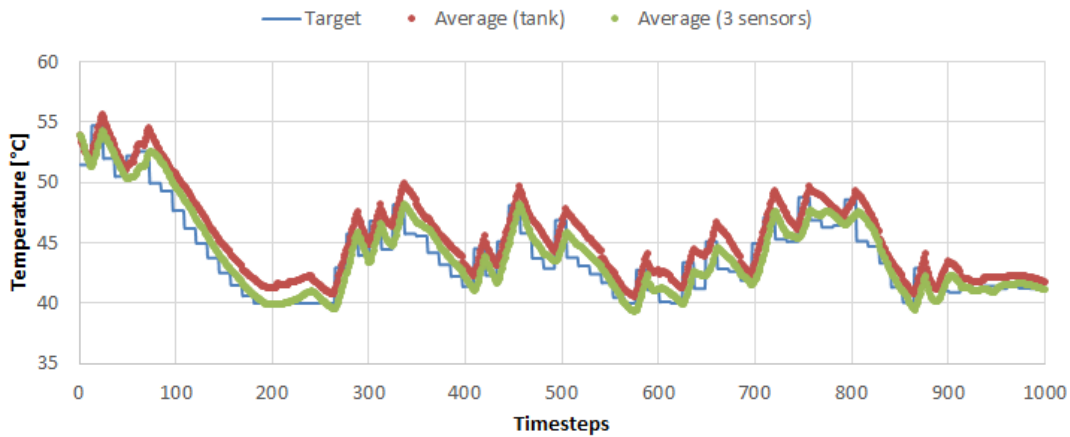


Figure 6.8 - Example of temperatures in the CS tank with the advanced control (targets and actual values from simulation).

Figure 6.9 shows the profile of the power produced by the CHP (orange line), the share of it that is sold to the grid (yellow line) and the corresponding electricity price (blue line) with the advanced control logic during two winter weeks. As mentioned above the CHP is modulated between a minimum and maximum when it is on. Here, due to the high heat demand, the CHP is always on. Apart from a few hours when it runs at partial load, the unit works at full capacity when the electricity price is higher than a certain value (around 53 €/MWh under our assumptions), and at minimum load (50% of the nominal capacity) when the electricity price is below this value. The CS is used as a buffer to store the thermal energy produced during full load operation. Figure 6.10 shows that during the considered winter period the network supply temperature is kept at 20°C for most of the hours, as explained in the previous section. However, a few exceptions seem to occur. In fact, a deviation from the supply temperature set point arises when the CHP works at full load or when the heat demand is low and there is a high availability of waste heat. In the first case, increasing the network temperature decreases the self-consumed power, thus increasing the revenues from electricity sales (see hours 800-850 and 970-1000). In the second case, increasing the network temperature increases the heat

required by the heat pump evaporators (at the price of a lower heat recovery rate), thus exploiting the low-grade heat source instead of using the gas boiler (see hours 700-740).

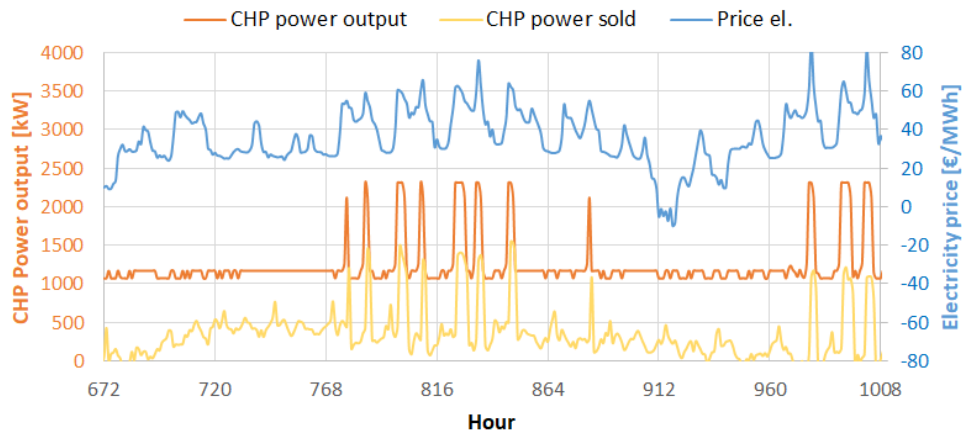


Figure 6.9 - CHP electrical total power output, power sold to the market and price of electricity with the advanced control during two winter weeks.

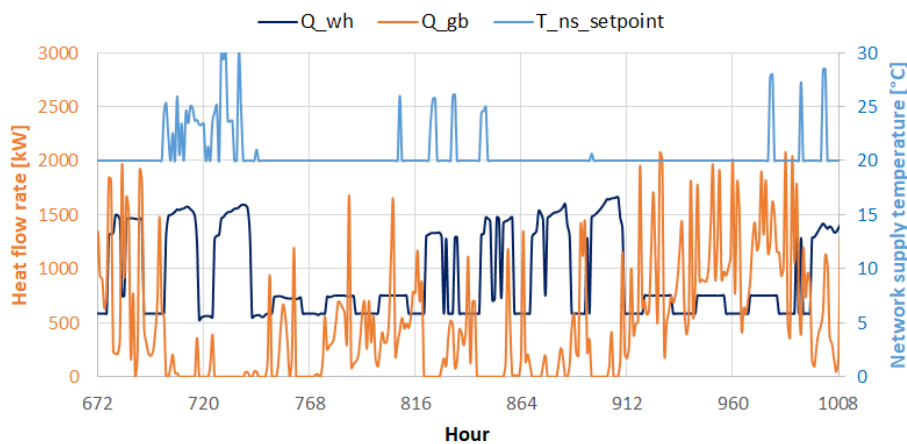


Figure 6.10 - Waste heat recovered, heat from the GB and target (set point) network supply temperature during two winter weeks.

This counterintuitive behaviour is a consequence of the fact that changing the network temperature has a much larger effect on the COP of the heat pumps –thus changing their heat demand- than on the effectiveness of the heat recovery at the waste heat substations.

6.4.3 Comparison between basic and advanced control

In general, the improvement of the advanced control over the basic control depends on the weights given to the objective function. In Table 6.3, the energy share of the different production units and the corresponding costs are summarized. The strategy adopted by the advanced control is to adapt the power production to meet the demand of the heat pumps, and to work at full load only when the price of electricity is higher than a threshold value. The remaining

heat demand is covered by the gas boiler (25.6%) and by the waste heat sources (29.5%). The basic control, on the other hand, is designed to give the priority of heat production to the CHP, and to use the GB as last option. This leads to a much lower share of heat produced by the GB (4.8%). The heat recovered from the WH stations is also slightly lower than with the advanced control, because of a lower network temperature set point (see previous sections for further explanation). As a result, the overall COP of the system (heat supplied to the buildings divided by power consumption of the heat pumps) is higher in the BAS case (4.64) than in the ADV case (4.04). The main difference between the two control strategies can be seen in the ratio between self-consumed power and total power production of the CHP: 39.2% in the BAS case and 79.4% in the ADV case. In the two simulated months, the advanced control system is able to cut the operational costs by almost 11% with respect to the basic control logic.

Table 6.3 - Energy and cost balances of the two-months simulation.

	Energy [MWh]		Cost [k€]	
	BAS	ADV	BAS	ADV
W_{chp}	3143	1726	-	-
self-consumed	1231	1370	-	-
sold	1912	356	60.8	13.1
Q_{chp} (share out of supply mix)	3157 (67.9%)	1994 (45.0%)	-	-
$Q_{chp,in}$	7293	4338	365	217
Q_{gb} (share out of supply mix)	260 (5.6%)	1135 (25.6%)	16.3 (4.8%)	70.9 (23.5%)
$Q_{wh,rec}$ (share out of supply mix)	1231 (26.5%)	1306 (29.5%)	12.3 (3.6%)	13.1 (4.3%)
$W_{el,hp}$ purchased	1262 31	1449 79	- 5.5	- 13.9
Total gas consumption	7618	5757	381	288
Net power production	1881	277	55	-0.7
Overall operational cost	-	-	338	302

6.5 Conclusions

The current paper presents two control systems (basic and advanced) to be used in a district heat system using water between 20 and 30°C as heat carrier and distributed heat pumps at the consumer substations. The system recovers a high share of heat (25-30% during the cold season, more in warmer periods) from locally available low-grade heat sources. The performance of the control systems was tested in 2-months TRNSYS 17 simulations, using a part of Aar-

hus south-west district as a case-study. The objective was to optimally control a CHP unit and a gas boiler to minimize the overall operational costs of the system by using a central storage tank and the network pipelines as thermal buffers under time-varying electricity prices. The study considered the effects of network temperature on both the COP of the heat pumps and on the heat recovery of the heat exchangers in the waste heat substations.

The results show that the advanced control system is capable of self-adapting to the current situation of heat demand, waste heat availability and electricity price, thus matching the power generated by the CHP with that required by the heat pumps and at the same time increasing the share of low-grade heat recovered. The advanced control system allowed a reduction of 11% in the operational costs of the system during the simulated period (January and February) with regard to a conventional rule-based control. The improvement was obtained at the price of increased complexity of the control system. Further simulations are needed to assess the performance of the advanced controller during warm periods and to investigate the impact of forecast uncertainty. Moreover, both the layout of the controlled physical systems and the capability of the RTC to achieve the targets set in the planning phase are aspects that need to be improved, particularly with regard to the stability of the mass flow in the network.

In conclusion, the advanced controller has shown to be a promising technology to allow an efficient management of heat supply plants in district heating systems with decentralized generation.

Chapter 7 Conclusions

7.1 **Original contributions**

Heat sources available at temperatures below 50°C cannot be used directly for space heating of old uninsulated buildings with radiators and for domestic hot water production. Although recent policies have supported the refurbishment of building envelopes, the greatest part of the heating demand in Italy still comes from buildings with poor thermal insulation. This barrier hinders the exploitation of these heat sources, that are ubiquitous in urban areas.

The present thesis investigates the suitability of district heating systems that are able to recover heat directly from low temperature heat sources and to distribute it to both new and existing buildings with different levels of thermal insulation. The system is based on two concepts: low temperature heat distribution and use of booster heat pumps at the customers substations.

After a literature review on the potential of low temperature heat sources and on the expansion potential of district heating systems in Europe, the thesis analysed the proposed system with regard to its environmental, energy and economic performance using an Italian case study where the thermal network is supplied entirely by the low temperature heat source. Then, an advanced control concept was developed and applied to another case study –a district of a Danish city. In both cases, the methodology followed four consecutive steps:

- (a) screening and collection of available data on the case-study;
- (b) development of models;
- (c) detailed simulations;
- (d) analysis of the results.

Starting from the case study of an Italian town with a large potential of thermal water, the thesis investigated the environmental and economic balance of small networks entirely supplied by locally available low temperature heat sources. The available data on the building stock was collected via GIS platform and integrated in a model developed ad-hoc to estimate the heating demand of a reference district. Historical data on thermal water withdrawal and on-field measurements allowed to characterize the low temperature heat source in terms of temperature and mass flow rates.

A preliminary analysis showed that the district heating system with booster heat pumps is superior to a conventional district heating system with central heat pump and auxiliary gas boiler in terms of carbon dioxide emissions and primary energy consumption (-30% for both). Such improvement does not only occur because the use of gas is completely avoided, but also because the heat source is utilized more efficiently. In fact, in the proposed system the temperature rise provided by the distributed heat pumps is tailored on the buildings supplied, instead of being designed for the most critical user, as it happens in conventional district heating systems. This advantage is particularly relevant when the building stock is heterogeneous as in the analysed residential neighbourhood. Based on historical data on thermal water withdrawal and on the measurements of temperature and mass flow rates, four scenarios were drawn for the Municipality of Abano Terme. In worst-case scenarios (available temperature of waste water equal to 45°C) the low temperature heat source is able to cover from 76% to 88% of the heat demand of the district. If the available temperature were 55°C, the entire residential building stock could theoretically be supplied by the waste water. The distributed nature of the heat source and its proximity to the buildings made the district heating system with booster heat pumps worth being further investigated.

The literature review evidenced a lack of studies focusing on the energy and economic performance of these systems. In particular, there is no study specifically focused on the performance of booster heat pumps for different users. All the more so there is no study that links such performance to the competitiveness of the system as a whole from an energy and economic standpoint. This was indeed the objective of the first part of the thesis: understanding how different conditions affect the cost of heat for the final user.

An economic analysis was therefore carried out to find the effect of different factors on the cost of heat for the final user. First of all, different network supply temperatures (from 15 to

45°C) were considered in order to account for heat sources at different temperature levels. In each case, the network was sized using different nominal temperature differences (5, 10 and 15 K). Three representative buildings with different levels of thermal insulation were considered. The payback time for the DH utility was constrained to a constant value (15 years), thus making it possible to compare the cost effectiveness for the final user (measured with the LCOE) without a significant change in the profitability for the DH utility. The economic analysis was carried out according to two different business models. In the first one, named Business-as-Usual (BaU), the end user invests in the heat pump and pays the electricity bill and the low-temperature heat bill separately. In the second case, named Investment-on-Utility (IoU), the utility takes on the responsibility of the investment in both infrastructure and heat pumps. In this case, the district heating utility is also responsible of heat pump operation; as such, it negotiates the price of electricity with the distribution system operator (DSO) and the user pays only for the consumed heat, i.e. the heat delivered from the heat pump condenser. A higher supply temperature decreases significantly the cost of heat for the final user because two positive effects are achieved at the same time: on one hand, the utility sells more heat for a given heat demand of the buildings, and on the other hand the expenditure to supply electricity to the heat pumps compressors is lower. The LCOE of the system with network supply temperature of 40°C was on average 17% lower than that with supply temperature of 20°C. As a further advantage, network supply temperatures equal or above 35°C allow to supply heat directly -without heat pumps- to buildings that have floor heating systems. This advantage contributes to improve the competitiveness of the system as long as the share of new or retrofitted buildings grows. Moreover, different heat pumps were selected based on the network supply temperature, 30°C being again a “threshold”. Above this temperature, machines working with R134a (or alternatively R1234ze) are preferable, whereas working fluids with lower critical temperature such as R407c (or R410a) are better suited below 30°C. In the latter case, old buildings with no thermal insulation would have very low COP with heat pumps based on single stage compressors. For all these reasons, district heating systems designed with supply temperatures of 40°C seem to be more promising than systems working at “neutral temperature”, i.e. below 30°C. Due to their almost null gradient with the surrounding ground, the main advantage of “neutral temperature networks” is to cut the costs for the thermal insulation of pipes. However, the cost of the pipes themselves is only a part of the investment costs for the whole infrastructure, that include groundworks, installation, design etc. In the present analysis, cutting the pipe costs by 50% did not lead to a significant reduction in

the LCOE, such as to justify the neutral temperature network when heat sources are available at higher temperature. Since increasing the heat sales turns into lower costs for heat distribution under the assumption of a given payback time, being able to connect old buildings improves the economic performance of the system. The effects of refurbishment scenarios on the performance of the system are not included in the present work. The IoU business model seems to be more cost-effective than the “business-as-usual” solution when they are compared under the same boundary conditions. In fact, the first solution allows to avoid the financial barrier of the initial investment for the end user, that significantly affects the economic balance especially for new and refurbished buildings. Moreover, a DH utility adopting the IoU business model has more contracting power than single residential users. Furthermore, due to economies of scale the utility can theoretically negotiate with the DSO to get cheaper electricity prices and with heat pump manufacturers to get cheaper heat pumps. In the BaU business model, the LCOE does not show significant variations from the old building to the new one, as the higher specific investment cost and the lower energy needs are compensated by higher SCOP, that reduces the operational costs. The network temperature difference ΔT_{net} chosen in the design phase was found to be an important parameter to improve the cost effectiveness of the system. Increasing the temperature difference allows to reduce the mass flow rates across the network, thus reducing the pipe diameters and, in turn, the system cost. At the same time, the COP of the heat pumps drops due to lower evaporating temperatures. Therefore, in general, a trade-off must be expected between low investment costs (high ΔT_{net}) and low operating costs (low ΔT_{net}). Under our assumptions, the trade-off is evident in the IoU business model, where there are only operating costs for the end user and the LCOE roughly coincides with the price of heat. In this case, an optimal ΔT_{net} arises between 5 K and 15 K from the compromise between low investment costs and low expenditure for the electricity supply. In the BaU business model this trade-off can only be seen for the old building with poor thermal insulation, for which the operating costs are high compared to the initial investment due to high energy consumption and relatively low SCOP. For new and refurbished households, the initial investment in the heat pumps smooths such effect, thus making $\Delta T_{net} = 15$ K more economically convenient –same LCOE for the user, lower initial investment for the utility.

In the second part of the thesis the focus was on the control of district heating systems based on the same concept (low temperature distribution and booster heat pumps), but with the low temperature heat being supplied from uncontrolled, remote substations and with the possibil-

ity to self-produce the electricity needed by the heat pumps compressors. The proposed smart control system was compared to a rule-based control through a two-months-simulation of a DH network specifically designed for a part of the south-west district of Aarhus. Here, it was assumed that the network manager owns and operates a central heat supply station consisting of a gas-fired internal combustion engine and a gas boiler. The engine cogenerates heat and electricity, the latter being either sold to the grid or supplied to the heat pumps via a micro-grid. A central buffer is used to decouple the CHP unit from the network and the thermal inertia of the water in the pipelines is not negligible and can therefore be used as a further buffer to match demand and supply when they don't occur simultaneously. Two waste heat substations recover heat from an industrial process and from the condensing units of a shopping mall and supply it to the low temperature network, operated with a supply temperature in the range between 20 and 30°C. The effects of supply and return network temperatures on the effectiveness of the heat recovery and on the COP of the heat pumps were also considered thanks to the integrated simulation environment. The advanced control system consists of three consecutive steps: forecasts, planning and real-time control. The present work assumed ideal deterministic forecasts of waste heat availability, heat demand and electricity prices. The planning is modelled as a mixed integer linear programming (MILP) optimization problem, which is solved in a rolling horizon scheme. The real-time controller is instead responsible of achieving the targets set in the planning phase by reacting on the deviations that typically occur in the real system, that was reproduced through the detailed dynamic simulation. The results showed that the advanced control system is capable of self-adapting to the current situation of heat demand, waste heat availability and electricity price, thus matching the power generated by the CHP with that required by the heat pumps and at the same time increasing the share of low-grade heat recovered. The advanced control system allowed a reduction of 11% in the operational costs of the system during the simulated period (January and February) compared to a conventional rule-based control. Such improvement was obtained at the price of a higher complexity. Unexpected control logics emerged by the analysis of the results, proving the "smartness" of the control system. However, most of the cost reduction came from simple rules that could be implemented also without a real-time optimization. However, the optimization could be further improved by a better approximation of the physical system, that was only described through linear equations.

The present thesis has also given an original contribution in the field of energy systems models. A tool for the simulation of the thermal behaviour of buildings at district scale was developed. A workflow was established to use GIS data, weather data and building occupancy profiles as inputs for simplified building models based on the electrical analogy. Two lumped capacitance models were presented and their accuracy was quantified in both heating and cooling mode. Then, a district heating network model was developed. The model used the SIMPLE algorithm to find pressures and velocities and the Finite Difference method with the upwind scheme to find the temperatures in the network. The model was thoroughly described and the accuracy of the heat propagation was assessed for different levels of network discretization. Finally, a simplified water-to-water heat pump model was developed and implemented as a Type in the TRNSYS environment.

In conclusion, the present thesis has drawn some patterns to understand the performance of district heating networks with booster heat pumps from different standpoints. Furthermore, useful tools were developed to study the behaviour of energy systems at district scale.

7.2 Future work

The results achieved so far are only a short step towards sustainable heat supply scenarios of buildings and districts. Both design and off-design aspects of the proposed system must be addressed further and tested in a pilot plant. A preliminary study is currently ongoing for the implementation of the proposed system in the Municipality of Montegrotto Terme, the second largest town of the Euganean Geothermal Basin. The impact of building refurbishment on the cost-effectiveness of the system is an issue that must be investigated, as well as the integration of PV in order to self-produce part of the electricity needed by the heat pumps compressors. Installing several heat pumps in the same area could provide flexibility but could also be an issue for the distribution grid operator. Therefore, strategies for Demand Side Management are necessary for instance to reduce peak loads and avoid synchronization issues. As far as the control system is concerned, the stability of the mass flow rate in the network and the approximation of non-linear behaviours are aspects that need to be improved. Its robustness to forecast uncertainty must also be analysed to understand the suitability of the control system for real-world applications.

References

- [1] P. Mancarella, «MES (multi-energy systems): An overview of concepts and evaluation models», *Energy*, vol. 65, n. Supplement C, pagg. 1–17, 2014.
- [2] M. Manfren, P. Caputo, e G. Costa, «Paradigm shift in urban energy systems through distributed generation: Methods and models», *Appl. Energy*, vol. 88, n. 4, pagg. 1032–1048, 2011.
- [3] H. Lund, B. Möller, B. V. Mathiesen, e A. Dyrelund, «The role of district heating in future renewable energy systems», *Energy*, vol. 35, n. 3, pagg. 1381–1390, 2010.
- [4] European Commission, *Directive 2012/27/EU of the European Parliament and of the Council on Energy Efficiency*. 2012.
- [5] D. Connolly, «Heat Roadmap Europe: Quantitative comparison between the electricity, heating, and cooling sectors for different European countries», *Energy*, vol. 139, n. Supplement C, pagg. 580–593, 2017.
- [6] European Commission, *Directive 2010/31/EU of the European Parliament and of the Council on the Energy Performance of Buildings*. 2010.
- [7] U. Persson e S. Werner, «Heat distribution and the future competitiveness of district heating», *Appl. Energy*, vol. 88, n. 3, pagg. 568–576, 2011.
- [8] H. Lund *et al.*, «4th Generation District Heating (4GDH): Integrating smart thermal grids into future sustainable energy systems», *Energy*, vol. 68, n. Supplement C, pagg. 1–11, 2014.
- [9] A. D. Rosa e J. E. Christensen, «Low-energy district heating in energy-efficient building areas», *Energy*, vol. 36, n. 12, pagg. 6890–6899, 2011.
- [10] Klein, S.A. et al, *TRNSYS 17: A Transient System Simulation Program*. Solar Energy Laboratory, University of Wisconsin, Madison, USA., 2017.
- [11] Jensen L.L. et al, «FLEXYNETS D3.1 - Analysis of Network Layouts in Selected Urban Contexts», dic. 2016.

- [12] European Commission, *Communication from the Commission to the European Parliament, the Council, the European Economic and Social Committee and the Committee of the Regions. An EU Strategy on Heating and Cooling*. 2016.
- [13] D. Connolly *et al.*, «Heat Roadmap Europe: Combining district heating with heat savings to decarbonise the EU energy system», *Energy Policy*, vol. 65, n. Supplement C, pagg. 475–489, feb. 2014.
- [14] European Commission, *Communication from the Commission to the European Parliament, the Council, the European Economic and Social Committee and the Committee of the Regions. Energy Roadmap 2050*. 2011.
- [15] Capros *et al.*, «EU Reference Scenario 2016 (REF2016). Energy, transport and GHG emissions trends to 2050», European Commission, 2016.
- [16] A. Colmenar-Santos, E. Rosales-Asensio, D. Borge-Diez, e J.-J. Blanes-Peiró, «District heating and cogeneration in the EU-28: Current situation, potential and proposed energy strategy for its generalisation», *Renew. Sustain. Energy Rev.*, vol. 62, n. Supplement C, pagg. 621–639, 2016.
- [17] Werner S. *et al.*, «ECOHEATCOOL WP4, Final Report. Possibilities with more district heating in Europe.», 2006.
- [18] Connolly *et al.*, «STRATEGO, Enhanced heating and cooling plans to quantify the impact of increased energy efficiency in EU Member States. WP2, Main report: Executive summary.», 2015.
- [19] International Energy Agency (IEA), «Energy Technology Perspectives 2016. Towards Sustainable Urban Energy Systems. Executive summary.», 2016.
- [20] Andrews D., Riekkola A.K., Tzimas E., Serpa E. *et al.*, «Background Report on EU-27 District Heating and Cooling Potentials, Barriers, Best Practice and Measures of Promotion», 2012.
- [21] Persson U., «Realise the potential! Cost effective and energy efficient district heating in urban areas.», Thesis for the Degree of Licentiate in Engineering, Chalmers University of Technology, Gothenburg, Sweden, 2011.
- [22] European Commission, *Directive 2009/28/EC of the European Parliament and of the Council on the promotion of the use of energy from renewable sources*. 2008.
- [23] U. Persson e M. Münster, «Current and future prospects for heat recovery from waste in European district heating systems: A literature and data review», *Energy*, vol. 110, n. Supplement C, pagg. 116–128, 2016.
- [24] Geological and Geophysical Institute of Hungary (MFGI), «Geothermal District Heating, GeoDH Europe. Web Map Viewer (WMV)», 2014.
- [25] European Geothermal Energy Council (EGEC), «Geothermal District Heating, GeoDH Europe. Executive summary», 2014.
- [26] European Geothermal Energy Council (EGEC), «Geothermal District Heating, GeoDH Europe. Executive summary», 2016.

- [27] AEBIOM., «AEBIOM Statistical Report, European bioenergy outlook (2016) Key findings.», 2016.
- [28] European Commission, *Directive 2009/28/EC of the European Parliament and of the Council on the promotion of the use of energy from renewable sources*. 2009.
- [29] Elbersen B, Startisky I, Hengeveld G, Schelhaas MJ et al., «Atlas of EU biomass potentials. Deliverable 3.3: Spatially detailed and quantified overview of EU biomass potential taking into account the main criteria determining biomass availability from different sources. Biomass Futures (2012)», 2012.
- [30] L. Miró, S. Brückner, e L. F. Cabeza, «Mapping and discussing Industrial Waste Heat (IWH) potentials for different countries», *Renew. Sustain. Energy Rev.*, vol. 51, n. Supplement C, pagg. 847–855, 2015.
- [31] Berthou M. e Bory D., «Overview of waste heat in the industry in France. ECEEE Summer study on energy efficiency in industry.», 2012.
- [32] ENOVA, «Utnyttelse av spillvarme fra norksindustri – en potensial studie (2009) (in Swedish)», 2009.
- [33] Cronholm L., Groenkvist S., e Saxe M., «Spillvarme fran industrier – och vaermeatervinning fran lokaler Svensk Fyaerrvarme. (in Swedish)», 2009.
- [34] S. Broberg, S. Backlund, M. Karlsson, e P. Thollander, «Industrial excess heat deliveries to Swedish district heating networks: Drop it like it's hot», *Energy Policy*, vol. 51, n. Supplement C, pagg. 332–339, 2012.
- [35] Pehnt M. e Bödeker J., «Die Nutzung industrieller Abwärme – technisch wirtschaftliche Potenziale und energie politische Umsetzung (in German)», 2010.
- [36] Dalenbäck J.O. e Werner S., «Market for solar district heating. WP2 – European market study. Deliverable 2.3.», 2012.
- [37] Mauthner F. e Herkel S., «IEA-SHC Task 52. Solar Heat and Energy Economics in Urban Environment. Technology and Demonstrators. Technical Report Subtask C - Part C1.», gen. 2016.
- [38] R. Lund e U. Persson, «Mapping of potential heat sources for heat pumps for district heating in Denmark», *Energy*, vol. 110, n. Supplement C, pagg. 129–138, 2016.
- [39] Li, H. *et al.*, «Technological Issues to Supply Low Temperature District Heating», presentato al The 15 th International Symposium on District Heating and Cooling, Seoul (South Korea), 2016.
- [40] M. Wahlroos, M. Pärssinen, J. Manner, e S. Syri, «Utilizing data center waste heat in district heating – Impacts on energy efficiency and prospects for low-temperature district heating networks», *Energy*, vol. 140, n. Part 1, pagg. 1228–1238, 2017.
- [41] Zhang M., «Energy Analysis of Various Supermarket Refrigeration Systems», in *R062*, 2006.
- [42] M. Brand e S. Svendsen, «Renewable-based low-temperature district heating for existing buildings in various stages of refurbishment», *Energy*, vol. 62, n. Supplement C, pagg. 311–319, 2013.

- [43] L. Brange, J. Englund, e P. Lauenburg, «Prosumers in district heating networks – A Swedish case study», *Appl. Energy*, vol. 164, n. Supplement C, pagg. 492–500, 2016.
- [44] E. Zvingilaite, T. Ommen, B. Elmegaard, e M.L. Franck, «Low temperature DH consumer unit with micro heat pump for DHW preparation», presentato al 13th International Symposium on District Heating and Cooling DHC13, Copenhagen, Denmark, 2012.
- [45] D. Schmidt *et al.*, «Development of an Innovative Heat Supply Concept for a New Housing Area», presentato al 12th REHVA World Congress CLIMA 2016, Aalborg, Denmark, 2016.
- [46] T. Schluck, P. Kräuchi, e M. Sulzer, «Non-Linear Thermal Networks – How Can a Meshed Network Improve Energy Efficiency?», presentato al CISBAT 2017, 2017.
- [47] Pietruschka D. et al, *Vision 2020. Die Plusenergiegemeinde Wüstenrot*. Bonn: Fraunhofer IRB Verlag, 2016.
- [48] Tarantino P., «Teleriscaldamento Freddo. Infrastruttura a rete alimentata da fonti rinnovabili ed assimilate al servizio di pompe di calore per la riqualifica energetica del patrimonio edilizio esistente», presentato al Retrofitting impianti di teleriscaldamento: Evolvere al passo con il tempo utilizzando le risorse locali, Milano, 2017.
- [49] S. Henchoz, P. Chatelan, F. Maréchal, e D. Favrat, «Key energy and technological aspects of three innovative concepts of district energy networks», *Energy*, vol. 117, n. Part 2, pagg. 465–477, 2016.
- [50] P. A. Østergaard e A. N. Andersen, «Booster heat pumps and central heat pumps in district heating», *Appl. Energy*, vol. 184, pagg. 1374–1388, dic. 2016.
- [51] T. Ommen, J. E. Thorsen, W. B. Markussen, e B. Elmegaard, «Performance of ultra low temperature district heating systems with utility plant and booster heat pumps», *Energy*, vol. 137, pagg. 544–555, ott. 2017.
- [52] J. Fink, R. P. van Leeuwen, J. L. Hurink, e G. J. M. Smit, «Linear programming control of a group of heat pumps», *Energy Sustain. Soc.*, vol. 5, n. 1, dic. 2015.
- [53] F. Verrilli *et al.*, «Model Predictive Control-Based Optimal Operations of District Heating System With Thermal Energy Storage and Flexible Loads», *IEEE Trans. Autom. Sci. Eng.*, vol. 14, n. 2, pagg. 547–557, apr. 2017.
- [54] L. Giraud, M. Merabet, R. Baviere, e M. Vallée, «Optimal Control of District Heating Systems using Dynamic Simulation and Mixed Integer Linear Programming», 2017, pagg. 141–150.
- [55] Cozzini M., D'Antoni M., Buffa S., e Fedrizzi R., «Pricing strategies for neutral-temperature district heating and cooling networks based on heat pumps», presentato al 12th IEA Heat Pump Conference, Rotterdam (NL), 2017.
- [56] H. Madsen e J. Holst, «Estimation of continuous-time models for the heat dynamics of a building», *Energy Build.*, vol. 22, n. 1, pagg. 67–79, 1995.
- [57] International Organization for Standardization, *ISO 13790: Energy performance of buildings: calculation of energy use for space heating and cooling*. 2008.

- [58] V. Corrado e E. Fabrizio, «Assessment of building cooling energy need through a quasi-steady state model: Simplified correlation for gain-loss mismatch», *Energy Build.*, vol. 39, n. 5, pagg. 569–579, 2007.
- [59] D. B. Crawley *et al.*, «EnergyPlus: creating a new-generation building energy simulation program», *Energy Build.*, vol. 33, n. 4, pagg. 319–331, 2001.
- [60] University of Strathclyde, Energy Systems Research Unit, *ESP-r*. Glasgow, 2003.
- [61] Clarke J., *Energy Simulation in Building Design*. Oxford: Butterworth-Heinemann, 2001.
- [62] Stephenson D.G. e Mitalas G.P., «Calculation of heat conduction transfer functions for multi-layer slabs.», *ASHRAE Trans.*, vol. 77, n. 2, pag. 117–26., 1971.
- [63] Stephenson D.G. e Mitalas G.P., «Room thermal response factors.», *ASHRAE Trans.*, vol. 73, n. 2, pag. III.2.1–III.2.10, 1967.
- [64] Milbank N.O. e Harrington-Lynn J., «Thermal response and the admittance procedure.», *Build. Serv Eng Res Technol.*, vol. 42, pagg. 38–47, 1974.
- [65] Underwood C.P. e Yik F.W.H., *Modelling Methods for Energy in Buildings*. Oxford: Blackwell, 2004.
- [66] M. M. Gouda, S. Danaher, e C. P. Underwood, «Building thermal model reduction using non-linear constrained optimization», *Build. Environ.*, vol. 37, n. 12, pagg. 1255–1265, 2002.
- [67] F. Déqué, F. Ollivier, e A. Poblador, «Grey boxes used to represent buildings with a minimum number of geometric and thermal parameters», *Energy Build.*, vol. 31, n. 1, pagg. 29–35, 2000.
- [68] J. Vivian, A. Zarrella, G. Emmi, e M. D. Carli, «An evaluation of the suitability of lumped-capacitance models in calculating energy needs and thermal behaviour of buildings», *Energy Build.*, vol. 150, n. Supplement C, pagg. 447–465, 2017.
- [69] L. Rouvel e F. Zimmermann, «Berechnung des instationären thermischen Gebäudeverhaltens.», *HLH*, vol. 55, n. 3, pagg. 39–46, 2004.
- [70] Rouvel L., «Thermische Gebäudesimulation GEBSIMU- Berechnungsverfahren zum instationären thermischen Gebäudeverhalten», 2015.
- [71] European Committee for Standardization, *BS EN 15265: Energy performance of buildings. Calculation of energy needs for space heating and cooling using dynamic methods. General criteria and validation procedures*. 2007.
- [72] International Organization for Standardization, *ISO 13791: Thermal performance of buildings — Calculation of internal temperatures of a room in summer without mechanical cooling — General criteria and validation procedures*. 2012.
- [73] International Organization for Standardization., *ISO 13792: Thermal performance of buildings -- Calculation of internal temperatures of a room in summer without mechanical cooling - Simplified methods*. 2012.

- [74] German Association of Engineers, *Calculation of transient thermal response of rooms and buildings -modelling of rooms (VDI 6007-1)*. 2012.
- [75] M. A. Lefsky, W. B. Cohen, G. G. Parker, e D. J. Harding, «Lidar Remote Sensing for Ecosystem Studies», *BioScience*, vol. 52, n. 1, pag. 19, 2002.
- [76] M. Lauster, J. Teichmann, M. Fuchs, R. Streblow, e D. Mueller, «Low order thermal network models for dynamic simulations of buildings on city district scale», *Build. Environ.*, vol. 73, n. Supplement C, pagg. 223–231, 2014.
- [77] L. G. Swan e V. I. Ugursal, «Modeling of end-use energy consumption in the residential sector: A review of modeling techniques», *Renew. Sustain. Energy Rev.*, vol. 13, n. 8, pagg. 1819–1835, Ottobre 2009.
- [78] Crabb J.A., Murdoch N., e Penman J.M., «A simplified thermal response model.», *Build. Serv Eng Res Technol.*, vol. 8, pagg. 13–19, 1987.
- [79] P. Michalak, «The simple hourly method of EN ISO 13790 standard in Matlab/Simulink: A comparative study for the climatic conditions of Poland», *Energy*, vol. 75, n. Supplement C, pagg. 568–578, 2014.
- [80] Guelpa E., Sciacovelli A., e Verda V., «Thermo-fluid dynamic model of complex district heating networks for the analysis of peak load reductions in the thermal plants», in *IMECE2015-52315*, Houston, Texas, 2015.
- [81] Patankar, S. V. e Spalding, D.B., «A calculation procedure for heat, mass and momentum transfer in three-dimensional parabolic flows», *Int J. Heat Mass Transf.*, vol. 15, n. 10, pagg. 1787–1806, ott. 1972.
- [82] Grosswindhager S., Voigt A., e Kozek M., «Linear Finite-Difference Schemes for Energy Transport in District Heating Networks», presentato al Proceeding of the 2nd International Conference on Computer Modelling and Simulation CSSim 2011, Brno, Czech Republic, 2011.
- [83] The MathWorks Inc, *MATLAB*. Natick, Massachusetts, 2010.
- [84] Ciuprinskas, K. e Narbutis, B., «Experiments on Heat Losses from District Heating Pipelines», *Energetika*, vol. 2, pagg. 35–40, 1999.
- [85] I. Gabrielaitiene, B. Bøhm, e B. Sunden, «Evaluation of Approaches for Modeling Temperature Wave Propagation in District Heating Pipelines», *Heat Transf. Eng.*, vol. 29, n. 1, pagg. 45–56, gen. 2008.
- [86] L. Giraud, R. Baviere, M. Vallée, e C. Paulus, «Presentation, Validation and Application of the DistrictHeating Modelica Library», 2015, pagg. 79–88.
- [87] D. Tenchine e P. Gauthé, «Occurrence of thermal stratification in sodium cooled fast reactor piping», *Nucl. Eng. Des.*, vol. 274, pagg. 1–9, lug. 2014.
- [88] M. Scarpa, G. Emmi, e M. D. Carli, «Validation of a numerical model aimed at the estimation of performance of vapor compression based heat pumps», *Energy Build.*, vol. 47, n. Supplement C, pagg. 411–420, 2012.

- [89] Frisiero A.O., «Progettazione ed analisi di pompe di calore acqua/acqua per il recupero di cascami termici da acque termali reflue ed Abano terme.», MSc Energy Engineering, Università degli Studi di Padova, Padova, 2015.
- [90] P. Fabbri e S. Trevisani, «Spatial distribution of temperature in the low-temperature geothermal Euganean field (NE Italy): a simulated annealing approach», *Geothermics*, vol. 34, n. 5, pagg. 617–631, 2005.
- [91] Piccoli G. *et al.*, «Contributo alla conoscenza del sistema idrotermale Euganeo-Berico.», presentato al Atti Acc. Naz. Lincei, Roma, 1973, vol. XI, pagg. 103–131.
- [92] F. Gherardi, C. Panichi, S. Caliro, G. Magro, e M. Pennisi, «Water and gas geochemistry of the Euganean and Berician thermal district (Italy)», *Appl. Geochem.*, vol. 15, n. 4, pagg. 455–474, 2000.
- [93] A. Galgaro, G. Emmi, A. Zarrella, e M. D. Carli, «Possible applications of ground coupled heat pumps in high geothermal gradient zones», *Energy Build.*, vol. 79, n. Supplement C, pagg. 12–22, 2014.
- [94] Gottardi G., Previatello P., e Simonini P., «An extensive investigation of land subsidence in the Euganean geothermal basin, Italy», in *Land Subsidence*, The Hague (NL), 1995, vol. 234.
- [95] Ballestrazzi, P., Brighenti, G., Ciancabilla, F., Dainese, A., e Schiesaro, G., «Ricerca sulla subsidenza nell'area termale di Abano Terme (PD).», Parma, 1991.
- [96] Carbognin, L., Rizzetto, F., Teatini, P., Tosi, L., e Strozzi, T., «La subsidenza della pianura costiera veneta. Indagini e risultati recenti.»
- [97] Regione Veneto, *Provvedimento del Consiglio Regionale del 23 aprile 1980 n.1111- Piano di Utilizzazione della Risorsa Termale (P.U.R.T.)*. .
- [98] M. Centini, M. R. Tredici, N. Biondi, A. Buonocore, R. Maffei Facino, e C. Anselmi, «Thermal mud maturation: organic matter and biological activity», *Int. J. Cosmet. Sci.*, vol. 37, n. 3, pagg. 339–347, giu. 2015.
- [99] *L. 30 aprile 1976 n. 373 in materia di «Norme per il contenimento del consumo energetico per usi termici negli edifici»*. 1976.
- [100] *L. 9 gennaio 1991 n. 10 in materia di «Norme per l'attuazione del Piano energetico nazionale in materia di uso razionale dell'energia, di risparmio energetico e di sviluppo delle fonti rinnovabili di energia»*. 1991.
- [101] *Decreto Legislativo 19 agosto 2005, n. 192 «Attuazione della direttiva 2002/91/CE relativa al rendimento energetico nell'edilizia»*. 2005.
- [102] European Commission, *Directive 2002/91/EC of the European Parliament and of the Council on the Energy Performance of Buildings (EPBD)*. 2002.
- [103] Segreteria regionale per le Infrastrutture - Unità di Progetto per il Sistema Informativo Territoriale e la Cartografia, «Carta Tecnica Regionale (Regione Veneto)».

- [104] S. N. Petrovic e K. B. Karlsson, «Danish heat atlas as a support tool for energy system models», *Energy Convers. Manag.*, vol. 87, n. Supplement C, pagg. 1063–1076, 2014.
- [105] *Termis District Energy Management - User Guide*. Schneider Electric, 2012.
- [106] Harald Schönberger, Jose Luis Galvez Martos, e David Styles, «Best Environmental Management Practice in the Retail Trade Sector.», 2013.
- [107] Ivan Korolija et al., «Reemain. Resource and Energy Efficient Manufacturing. Deliverable D4.1 Efficiency analysis methodology.», D4.1, 2015.
- [108] F. Peron, P. Romagnoni, A. Righi, e M. Turvani, «Analisi integrata di scenari di miglioramento dell'efficienza energetica del settore civile e commerciale della regione Veneto», in *Atti 6° Congresso AIGE*, Ferrara, 2012, pagg. 39–44.
- [109] Ente Nazionale Italiano di Unificazione (UNI), *UNI 9182. Impianti di alimentazione e distribuzione d'acqua fredda e calda - Criteri di progettazione, collaudo e gestione*. 2010.
- [110] J.E. Thorsen e H. Kristjansson, «Cost considerations on storage tank versus heat exchanger for hot water preparation.», in *10th International symposium District Heating and Cooling*, Hanover, Germany, 2006.
- [111] W. Winter, T. Haslauer, e I. Obernberger, «Untersuchungen der Gleichzeitigkeit in kleinen und mittleren Nahwärmenetzen.», presentato al Euroheat & Power, 2001, vol. 9, pagg. 53–57.
- [112] F. Li, G. Zheng, e Z. Tian, «Optimal operation strategy of the hybrid heating system composed of centrifugal heat pumps and gas boilers», *Energy Build.*, vol. 58, n. Supplement C, pagg. 27–36, 2013.
- [113] European Committee for Standardization (CEN), *EN 14825:2012, Air conditioners, liquid chilling packages and heat pumps, with electrically driven compressors, for space heating and cooling. Testing and rating at part load conditions and calculation of seasonal performance*. 2012.
- [114] Michele De Carli et al., «Piano Energetico Ambientale della Provincia di Padova», University of Padova, 2010.
- [115] U. Jordan e K. Vajen, «DHWcalc: Program to generate domestic hot water profiles with statistical means for user defines conditions.», in *Proc. ISES Solar World Congress*, Orlando (US), 2005.
- [116] Ente Nazionale Italiano di Unificazione (UNI), *UNI/TS 11300-2:2008 Prestazioni energetiche degli edifici – Determinazione del fabbisogno di energia primaria e dei rendimenti per la climatizzazione invernale e per la produzione di acqua calda sanitaria*. 2008.
- [117] Svensk Fjärrvarme, «Kulvertkostnadskatalog», Rapport 2007:1, 2007.
- [118] *L. 22 dicembre 2008, n. 203 in materia di «Disposizioni per la formazione del bilancio annuale e pluriennale dello Stato (legge finanziaria 2009)»*. 2008.
- [119] G. Orr, T. Lelyveld, e Burton S., «Final Report: In-situ monitoring of efficiencies of condensing boilers and use of secondary heating», Department of Energy & Climate Change (UK), 2009.

[120] I. B. Hassine e U. Eicker, «Impact of load structure variation and solar thermal energy integration on an existing district heating network», *Appl. Therm. Eng.*, vol. 50, n. 2, pagg. 1437–1446, 2013.